

Instituto Tecnológico de Costa Rica

Electronics Engineering School

Master of Science in Electronics

Embedded Systems



Electrical Impedance Tomography (EIT)

Image reconstruction for the Human Forearm

Master's thesis presented in partial fulfillment of the requirements to obtain the degree of Master of Science in Electronics – Embedded Systems Major

David Canales Vásquez

Cartago May, 2016

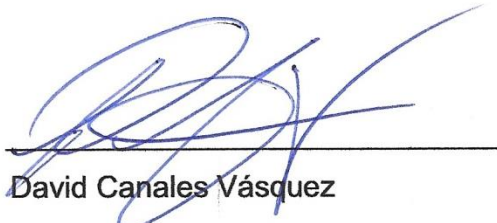


Creative Commons License

This work is licensed under a Creative Commons Attribution-NonCommercial-ShareAlike 4.0 International License.

I declare that this thesis document has been made entirely by me, using and applying literature about the topic and introducing my own knowledge and experimental results.

In cases in which I have used references, I proceed to indicate the sources from corresponding references. Therefore, I assume full responsibility for the thesis work done and for the contents on this document.

A handwritten signature in blue ink, appearing to read 'David Canales Vásquez', is written over a horizontal line.

David Canales Vásquez

Cartago, May, 2016

ID: 1-1199-0633

Instituto Tecnológico de Costa Rica
Escuela de Ingeniería Electrónica
Tesis de Maestría
Tribunal evaluador

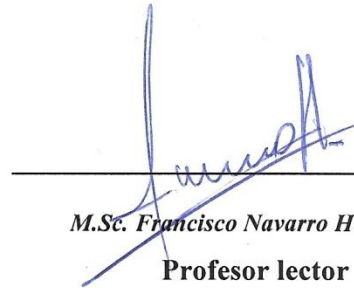
Tesis de maestría defendida ante el presente Tribunal Evaluador como requisito para optar por el grado académico de maestría, del Instituto Tecnológico de Costa Rica.

Miembros del Tribunal



M.Sc. Marta Vilchez Monge

Profesor lector



M.Sc. Francisco Navarro Henríquez

Profesor lector



Dr-Ing. Renato Rímolo Donadío

Profesor asesor

Los miembros de este Tribunal dan fe de que el presente trabajo de graduación ha sido aprobado y cumple con las normas establecidas por la Escuela de Ingeniería Electrónica

Lunes 02 de mayo de 2016

Abstract

This thesis addresses the principles and algorithms of image reconstruction used in electrical impedance tomography (EIT). It is a low cost, portable and non-invasive medical imaging technique.

In this development EIT is used for the nerve location in the human forearm. The work addresses the current injection and voltage acquisition methods, geometry definitions and the finite element method for meshing and impedance map reconstruction.

In order to analyze different features, a software tool kit called EIDORS was used for the target application of EIT applied for human forearm tomography.

This thesis most important contribution is the development of an EIT methodology for image reconstruction from the impedance map of a human forearm using EIDORS.

Different image reconstruction algorithms and prior information methods are evaluated and analyzed to solve the EIT inverse problem for the human forearm. It was found that although the methodology could be successfully implemented, the desired resolution for the precise identification of nerves was not sufficient for practical configurations.

Keywords: EIT, Impedance, Conductivity, Finite Element Method, Constant Current, SNR, Inverse Problem, Forward Problem, EIDORS.

Resumen

Esta tesis aborda los principios y los algoritmos de reconstrucción de imágenes utilizados en la tomografía por impedancia eléctrica (TIE). Esta es una técnica de bajo costo, portable y no invasiva de imágenes médicas.

En esta investigación TIE es utilizada en la localización de los nervios del antebrazo humano. Este trabajo aborda la inyección de corriente y la adquisición de voltaje, la definición de la geometría del sujeto bajo prueba y el método de elementos finitos para el mallado y la reconstrucción del mapa de impedancia.

El conjunto de herramientas de software llamado EIDORS se utilizó en la aplicación objetivo de TIE, se aplicó en la tomografía del antebrazo humano, analizando diferentes características.

La contribución más importante de esta tesis es el desarrollo de la metodología de reconstrucción de imagen para el TIE del mapa de impedancia del antebrazo humano utilizando EIDORS.

Diferentes algoritmos para resolver el problema inverso de reconstrucción de imágenes y métodos de información previa se evalúan y analizan para resolver el problema inverso para el antebrazo humano. Se encontró que, aunque la metodología podría ser implementada con éxito, la resolución deseada para la identificación precisa de los nervios no era suficiente para las configuraciones prácticas.

Palabras clave: TIE, Impedancia, Conductividad, Método de Elementos Finitos, Corriente Constante, SNR, Problema Inverso, Problema Directo, EIDORS.

Acknowledgment

I would like to express my gratitude to:

- Dr. Renato Rímolo Donadio, for being my advisor and MSc. Marta Eugenia Vílchez Monge, both professors of Instituto Tecnológico de Costa Rica. I appreciate very much all your advices and your guidance during this research work.
- Victor Bermudez, Michael Martinez and the whole team in Camtronics S.A/ Canam Technology, Inc. for their support and solidarity in this project.
- CONICIT "Consejo Nacional para Investigaciones Científicas y Tecnológicas" and MICITT "Ministerio de Ciencia, Tecnología y Telecomunicaciones" for the economical support during my master degree studies.

Also I would like to thank Mercedes Canales, Fernando Quirós, Hellen Corrales and Carlos Sánchez for all the support provided during the first stage of my academic life.

A special thanks to my family, for all the understanding and support during all these long years; specially to my parents David Canales Berríos and Dina Vásquez Cambroneró.

Last but not least, I would like to be grateful with my lovely Mariana Alvarenga López and my dear daughter Valeria Canales Alvarenga, both of you have been my biggest motivation and inspiration over the years.

David Canales Vásquez, May, 2016

"Life is too short to learn EIT"

Richard Porson

Table of Contents

ABSTRACT	4
RESUMEN	5
ACKNOWLEDGMENT	6
TABLE OF CONTENTS	8
LIST OF TABLES	10
LIST OF FIGURES	11
LIST OF ACRONYMS	14
CHAPTER 1 INTRODUCTION	15
1.1 MOTIVATION AND PREVIOUS WORK	15
1.2 OBJECTIVES.....	16
1.2.1 <i>General objective</i>	16
1.2.2 <i>Specific objectives</i>	16
1.3 DOCUMENT STRUCTURE.....	18
1.4 RESEARCH ACHIEVEMENTS OF EIT IMAGE RECONSTRUCTION FOR HUMAN FOREARM.....	19
CHAPTER 2 OVERVIEW OF EIT	20
2.5 ELECTRICAL IMPEDANCE TOMOGRAPHY (EIT) REVIEW	20
2.6 CURRENT DRIVE AND VOLTAGE ACQUISITION METHODS.....	22
2.6.1 <i>Adjacent neighboring method</i>	22
2.6.2 <i>Opposite or polar method</i>	23
2.7 IMAGE RECONSTRUCTION.....	24
2.7.1 <i>Forward problem</i>	25
2.7.2 <i>Inverse problem</i>	26
2.8 GEOMETRY AND FINITE ELEMENT METHOD DEFINITION USING FOURIER DESCRIPTORS	28
2.8.1 <i>Fourier descriptors used for geometry components definition</i>	30
2.9 EIT IMAGE RECONSTRUCTION ALGORITHMS.....	32
2.9.1 <i>Sheffield back-projection algorithm</i>	32
2.9.2 <i>Gauss Newton algorithm</i>	36
2.9.3 <i>Gauss Newton priors regularization methods</i>	38
2.10 UNDER-FITTING AND OVER-FITTING.....	40
2.11 COMPARISON OF 2D ALGORITHMS IN EIT	42
2.12 HUMAN FOREARM MODEL.....	43
CHAPTER 3 EIT IMAGE RECONSTRUCTION METHODOLOGY	45
3.13 GENERAL EIT IMAGE RECONSTRUCTION METHODOLOGY.....	45
3.13.1 <i>High level mathematical programming tool</i>	46
3.13.2 <i>EIDORS toolkit</i>	47

3.13.3	<i>Human forearm Image reconstruction methodology flow diagram using EIDORS</i>	48
CHAPTER 4 ANALYSIS AND VALIDATION OF EIT IMAGE RECONSTRUCTION METHODOLOGY FOR HUMAN FOREARM		55
4.14	HUMAN FOREARM GEOMETRY.....	55
4.14.1	<i>Fourier descriptors</i>	57
4.14.2	<i>Geometry with tissue conductivities</i>	59
4.14.3	<i>Finite Element Method (FEM)</i>	60
4.15	CURRENT INJECTION AND VOLTAGE ACQUISITION METHOD	61
4.16	CURRENT LINES.....	64
4.17	IMAGE RECONSTRUCTION.....	65
4.17.1	<i>Hyperparameter selection</i>	65
4.17.2	<i>Current level</i>	68
4.18	EIT ALGORITHM AND PRIOR INFORMATION METHODS	69
4.18.1	<i>Noise effect</i>	71
4.19	VALIDATION AND EVALUATION OF HUMAN FOREARM EIT METHODOLOGY	75
4.19.1	<i>Feasibility of EIT image reconstruction for nerve identification based on EIDORS toolkit</i> .	75
4.19.2	<i>Effect of increasing the electrode number</i>	76
4.19.3	<i>Effect of filtering the EIT output image</i>	77
4.19.4	<i>Effect of a current value over the safety range</i>	78
4.20	OPTIMAL SETUP FOR HUMAN FOREARM EIT IMAGE RECONSTRUCTION	81
4.20.1	<i>Forearm geometry and reconstructed image area comparison</i>	84
4.20.2	<i>Error calculation in reconstructed image</i>	86
CHAPTER 5 CONCLUSIONS AND RECOMMENDATIONS		87
5.1	CONCLUSIONS.....	87
5.2	RECOMMENDATIONS.....	89
BIBLIOGRAPHY		90
GLOSSARY		92
APPENDIX A EIDORS QUICK START GUIDE		93
A.1	INSTALLING EIDORS.....	93
A.2	EIDORS SIMULATION GUIDE	94
A.2.1	<i>Geometry definition</i>	94
A.2.2	<i>Model creation</i>	95
A.2.3	<i>Stimulus definition</i>	96
A.2.4	<i>Forward solver used to calculate V_h and V_i</i>	96
A.2.5	<i>Noise addition</i>	97
A.2.6	<i>Inverse solver configuration</i>	98
A.2.7	<i>Conductivity distribution map</i>	98
APPENDIX B EIDORS SOURCE CODE		99

List of Tables

<i>Table 2-1. Comparison of actual and reconstructed impurity size.</i>	<i>43</i>
<i>Table 2-2. Theoretical values of conductivity and relative permittivity for different tissues in the human forearm [1].....</i>	<i>44</i>
<i>Table 3-1. Image Reconstruction software tool features</i>	<i>47</i>
<i>Table 4-1. Best setup for human forearm EIT reconstruction image.</i>	<i>81</i>
<i>Table 4-2. Comparison the area of reference geometry and reconstructed image for tissues conductivities higher than 0.05 S/m.....</i>	<i>86</i>

List of Figures

Figure 2-1. Main components for electrical impedance tomography process	21
Figure 2-2. Adjacent method for a cylindrical volume conductor and 16 equally spaced electrodes:	23
Figure 2-3. Opposite or polar method representation [4].....	24
Figure 2-4. Block diagram of EIT reconstruction algorithm [8].....	25
Figure 2-5. Graphical representation of forward problem.....	25
Figure 2-6. Graphical representation of inverse problem.	27
Figure 2-7. Graphical representation of the general EIT image reconstruction.	27
Figure 2-8. Finite element model representation.	29
Figure 2-9.(a) Geometry approximation error (b) line element error [14].	30
Figure 2-10. Examples using Fourier descriptors: (a) the original edge image with 1024 edge pixels, (b) 3 Fourier coefficients, (c) 21 Fourier coefficients, (d) 61 Fourier coefficients, (e) 201 Fourier coefficients, and (f) 401 Fourier coefficients [16].	31
Figure 2-11.(a) Coordinates (X5,X6) and (b) coordinates (X3,X4).....	34
Figure 2-12. Step by step example. A) Profiles of voltage deviations in the presence of a regional increase of impedance. B) Successive superposition of the 16 voltage profiles [19].	35
Figure 2-13. Resulting image after selective boundary filtering [19].	36
Figure 2-14. Gauss-Newton algorithm flow diagram.	37
Figure 2-15. Diagram contrasts the probability density functions of the normal distribution and the Laplace distribution [25].	40
Figure 2-16. Under-fitting vs over-fitting results [27].	41
Figure 2-17. Scheme for the error of prediction depending on the size and quality of the calibration data set, which influence the estimation error [28].	41
Figure 2-18. 2D algorithm comparison results : (a) Clay cylinder kept near electrodes 4 and 5 and (b) Non conducting impurity near 4, 5 using back-projection without filter.[20].	42
Figure 2-19. 2D algorithm comparison results : (c) GN algorithm with Tikhonov prior, (d) GN algorithm with NOSER prior, (e) GN algorithm with Laplace prior and (f) Total Variation prior [20].	42
Figure 2-20. Forearm geometry used as reference in this thesis (geometry was reproduced from [1]).	44
Figure 3-1. EIT image reconstruction general methodology.	45
Figure 3-2. EIDORS Image reconstruction flow diagram.....	49
Figure 4-1. Forearm geometry and FEM used in COMSOL.....	55
Figure 4-2. Geometry plotted using Microsoft excel and (X,Y) coordinates extracted from COMSOL file..	56
Figure 4-3. Forearm boundary and the ulna bone (object one) generated in the FEM.....	57
Figure 4-4. Object one model using different (x,y) samples and Fourier descriptors samples: (a) 31 Samples FD=47 and (b) 16 Samples FD= 47.....	57

Figure 4-5. Object one model using different (x,y) samples and Fourier descriptors samples: (c) 11 Samples FD=47, (d) 6 Samples FD = 47 (e) 31 Samples FD=10 and (f) 31 Samples FD=70.....	58
Figure 4-6. Object one model using 310 (x,y) samples and 20 Fourier descriptors samples and reference.	58
Figure 4-7. Human forearm geometry with conductivities definition.	59
Figure 4-8. Human forearm FEM with maximum mesh size of 0.11.....	60
Figure 4-9. Human forearm FEM with maximum mesh size of 0.05 cm.	61
Figure 4-10.FEM with two objects, used as reference for evaluation of injection and acquisition methods.	62
Figure 4-11. Current injection and voltage acquisition patterns: (a) Opposite method and (b) Neighboring method.....	62
Figure 4-12.Current injection pattern for neighboring method.	63
Figure 4-13. Homogeneous voltages (V_h) [Left-Top], Inhomogeneous voltages (V_i) [Right-Top], their difference ($V_i - V_h$) [Left-Bottom] and finally all plots in the same image [Right-Bottom].....	63
Figure 4-14. Current lines generated during injection in electrode 1 and 2.	64
Figure 4-15. Detailed view of current lines focus in electrode 1 and 2.	65
Figure 4-16. Image reconstructions using different hyperparameters: (a) hyperparameter = 3, (b) hyperparameter = 1, (c) hyperparameter = 0.1 and (d) hyperparameter = $2 \cdot 10^{-2}$. (1-2).....	66
Figure 4-17. Image reconstructions using different hyperparameters: (f) hyperparameter = $3 \cdot 10^{-3}$, (g) hyperparameter = $2 \cdot 10^{-3}$, (h) hyperparameter = $1.5 \cdot 10^{-3}$, (i) hyperparameter = $1 \cdot 10^{-3}$ and (j) hyperparameter = $5 \cdot 10^{-4}$. (2-2).....	67
Figure 4-18. Image reconstructions using different current levels in injection: (a) 0.1mA, (b) 0.5mA, (c) 1mA, (d) 2mA and (e) 5mA.....	68
Figure 4-19. Image reconstructions using different prior information methods: (a) Default, (b) Default with 25dB SNR, (c) Tikhonov prior and (d) Tikhonov prior with 25dB SNR.	69
Figure 4-20. Image reconstructions using different prior information methods: (e) NOSER prior, (f) NOSER prior with 25dB SNR, (g) Laplace prior, (h) Laplace prior with 25dB SNR, (i) Total Variation prior and (j) Total Variation prior with 25dB SNR.	70
Figure 4-21. Image reconstructions using different signal to noise values with default and Laplace priors: (a) Default with SNR = 40dB, (b) Laplace with SNR = 40dB, (c) Default with SNR = 35dB, (d) Laplace with SNR = 35dB. (1-3).....	72
Figure 4-22. Image reconstructions using different signal to noise values with default and Laplace priors: (e) Default with SNR = 30dB, (f) Laplace with SNR = 30dB, (g) Default with SNR = 25dB, (h) Laplace with SNR = 25dB, (i) Default with SNR = 20dB and (j) Laplace with SNR = 20dB. (2-3).....	73
Figure 4-23. Image reconstructions using different signal to noise values with default and Laplace priors: (k) Default with SNR = 15dB, (l) Laplace with SNR = 15dB, (m) Default with SNR = 10dB, (n) Laplace with SNR = 10dB, (o) Default with SNR = 5dB and (p) Laplace with SNR = 5dB. (3-3).....	74

Figure 4-24. Human forearm EIT image reconstruction using the recommended parameters according with previous sections; (a) Image without noise, (b) Image with 30dB SNR, (c) human forearm reference image and (d) reconstructed image with forearm reference image superimposed.75

Figure 4-25. Human forearm EIT Image reconstruction using different electrode quantity in electrode array; (a) 16 electrodes and (b) 32 electrodes.76

Figure 4-26. Human forearm EIT Image reconstruction using an image filter centered in -10 ± 1 ; (a) Injection current of 4mA using 16 electrodes, (b) Injection current of 5mA using 16 electrodes, (c) Injection current of 2mA using 32 electrodes, (d) Injection current of 5mA using 32 electrodes.....78

Figure 4-27. Human forearm EIT Image reconstruction using different currents; (a) Current of 3 mA, (b) Current of 10mA and (c) Current of 50mA79

Figure 4-28. Tissue conductivity representation and filter threshold for filtering.81

Figure 4-29. Human forearm EIT Image reconstruction; (a) 30 dB SNR, (b) without noise.82

Figure 4-30. Human forearm EIT Image reconstruction with the geometry superimposed; (a) 30 dB SNR, (b) without noise.....82

Figure 4-31. Human forearm EIT Image reconstruction with filtering; (a) 30 dB SNR, (b) without noise.83

Figure 4-32. Human forearm EIT Image reconstruction with filtering and the geometry superimposed; (a) 30 dB SNR, (b) without noise.....84

Figure 4-33. Forearm dimension image using the AutoCAD software.84

Figure 4-34. Human forearm geometry with tissues colored according to their conductivity (a) complex geometry , (b) simplified geometry.....85

Figure 4-35. Human forearm simplified geometry with reconstructed image super imposed (a) with 30 dB SNR , (b) without noise.85

Figure A-1. EIDORS output when startup script is executed.93

Figure A-2. EIDORS workspace.....94

Figure A-3. FEM with homogeneous conductivities.95

Figure A-4. FEM with inhomogeneous conductivities.97

Figure A-5. Forearm reconstructed image (a) without filter and (b) with filter.98

List of Acronyms

<i>Acronyms</i>	<i>Definition</i>
AC	Alternating current
BestRes	Best resolution
CAD	Computer-Aided Design
CEM	Complete Electrode Model
COMSOL	COMSOL Multiphysics ® software
DOF	Degrees of Freedom
ECAD	Electronic Computer-Aided Design
EIDORS	Electrical Impedance Tomography and Diffuse Optical Tomography
EIT	Electrical Impedance Tomography
FD	Fourier Descriptor
FEM	Finite element Method
FoM	Figure of Merit
GmbH	In German Gesellschaft mit beschränkter Haftung translated as 'company with limited liability'.
GN	Gauss Newton
GNU	Gnu's Not Unix
GPL	General Public License
GREIT	Graz consensus Reconstruction Algorithm for EIT
ITCR	Instituto Tecnológico de Costa Rica
MATLAB	MATLAB ® software
MEF	Método de elementos finitos
MSE	Mean Squared Error
NOSER	Newton's One-Step Error Reconstructor
NR	Newton Raphson
oEIT	Open EIT Data Format
ROI	Region of Interest
SNR	Signal to noise ratio
TIE	Tomografía por impedancia eléctrica
TES	Transcutaneous Electrical Stimulation
TUHH	Technische Universität Hamburg-Harburg

Chapter 1 Introduction

1.1 Motivation and previous work

The Technische Universität Hamburg-Harburg (TUHH) has been conducting research in areas related to handling of patients with tractable injuries using neuromuscular electrical stimulation. For this purpose, a method to determine the location of some specific nerves, tissues, and muscles is required in order to apply the appropriate current levels at the right positions during the therapy. Within this scope, a research initiative between the Instituto Tecnológico de Costa Rica (ITCR) and TUHH is exploring the feasibility to develop an Electrical Impedance Tomography (EIT) system for the human forearm, as a useful, non-intrusive, portable and low cost solution to assist therapy studies.

In this regard, two methods can be employed for electrical stimulation, namely percutaneous and transcutaneous electrical stimulations. The percutaneous method requires surgeries to implant the electrodes around the nerves; while the transcutaneous method provides the stimulation through the skin surface using electrodes. Transcutaneous Electrical Stimulation (TES) systems are preferred due to the simple removal at the completion of a rehabilitation program and the low infection risk. TES requires the deep knowledge of the specific tissue electrical response; it was performed in [1] a previous work dealing with the human forearm tissue behavior, where the creation of the geometrical model of the human forearm was necessary for the analysis and simulation. This previous work is based on the forward solution solved by numerical methods, essentially using the finite element method (FEM), where the electrical behaviors for the tissues are characterized in the human forearm.

In this work [1], the basis for the analysis of the electrical response was established from calculated data for the inhomogeneous conductivities with the complex structural geometry of a subject's forearm when a small stimulation is applied, as well as the voltage surface distribution in forearm.

Based on the human forearm previous work, where EIT forward problem was implemented, simulated and modeled, this thesis research objective is to define an accurate methodology and the corresponding benchmark to evaluate the required parameters to setup the EIT image reconstruction for human forearm with enough precision to detect nerves.

Different algorithms and injection methods have been evaluated to compare their performance regarding the image resolution in order to select the optimal image reconstruction results. Best results are used to investigate the feasibility of implementing EIT medical technique to identify nerves in human forearm for the target application of TES.

1.2 Objectives

1.2.1 General objective

Develop a suitable image reconstruction methodology for the human forearm using the electrical impedance tomography (EIT) technique.

1.2.2 Specific objectives

- Select a suitable platform for EIT image reconstruction.
- Define the corresponding methodology to execute the human forearm image reconstruction using the medical imaging technique EIT.
- Define a benchmark to analyze the methodology, parameters and algorithms for human forearm EIT image reconstruction.
- Evaluate different algorithms for image reconstruction and define the performance according to its feasibility and degree of suitability based on the benchmark case defined.

- Determine the achievable EIT resolution in order to evaluate the feasibility of this technique in order to determine the location of nerves, bones and muscles in human forearm.

1.3 Document structure

This thesis is divided in 5 chapters. A brief summary of each chapter is presented below:

Chapter 2 presents an overview of electrical impedance tomography technique, introducing its fundamental concepts, advantages and components. In this chapter, the adjacent and the opposite current drive and voltage acquisition methods are explained, as well the forward and inverse problem applied in the EIT image reconstruction, based in FEM using the geometry definition and Fourier descriptors. Additionally, algorithms and prior regularization methods for Gauss Newton algorithm are described and evaluated using a simple example as reference. The under-fitting and over-fitting concept is illustrated for hyperparameter definition in the regularization method. Human forearm cross section with the corresponding tissues and conductivities is presented.

Chapter 3 describes the EIT image reconstruction methodology. It introduces and explains the available software tools and platforms for EIT and the evaluation considering its advantages and disadvantages. The chapter presents EIDORS as the selected toolkit for the human forearm EIT image reconstruction methodology. The justification, features, and most relevant functions will be explained, as well a detailed flow diagram for final implementation in order to validate and analyze the EIT image reconstruction results.

Chapter 4 shows the application, validation, and analysis of EIT image reconstruction methodology for human forearm is addressed; different parameters are evaluated, showing its results and analysis in order to recommend the best setup for human forearm EIT image reconstruction.

Chapter 5 summarizes the technical contribution of this thesis on EIT image reconstruction for human forearm methodology based in EIDORS and provides some recommendations for future work.

1.4 Research achievements of EIT image reconstruction for human forearm

The most important achievement of this thesis is the methodology definition for image reconstruction in order to generate the impedance map for the human forearm based on the electrical impedance tomography (EIT) technique using the EIDORS toolkit.

In order to perform the EIT image reconstruction, the (x, y) coordinates extracted from the complex human forearm geometry, developed with the COMSOL platform [1], are organized to create the EIDORS finite element model. It is important to note that the defined geometry is complex and contains 36 objects, whereas most of EIT implementations found in the literature are much simpler and use a much lower number of components.

Through this research, relevant parameters for EIT image reconstruction were evaluated after observing and analyzing its effects in the reconstructed image. Allowing the definition of limits such as the signal to noise ratio (SNR), these evaluations have defined the appropriated values for human forearm image reconstruction setup. There, the minimal SNR acceptable is 30dB for reconstructing a useful image using measurements with background noise according to the simulated values.

In addition, the controlled setup enables the evaluation of the EIT human forearm image reconstruction resolution in the output image, as well different image reconstruction algorithms and regularization methods with their prior information calculated with simulated data, instead of having a subject for testing during fine tune adjustment.

According to obtained results, it is concluded that EIT methodology can be applied to the human forearm, however it was not possible to achieve the resolution to identify nerves in human forearm using up to 32 electrodes and the adjacent method for injection and acquisition based on the EIDORS tool kit. However, several other forearm elements such as bones, fat, and muscles can be identified.

Chapter 2 Overview of EIT

This chapter presents an overview of electrical impedance tomography technique introducing its fundamental concepts, advantages, and components. In this chapter, the adjacent and the opposite current drive and voltage acquisition methods are also explained. The forward and inverse problem applied in the EIT image reconstruction are also addressed, based in FEM using the geometry definition and Fourier descriptors. Additionally, algorithms and prior regularization methods for Gauss Newton algorithm are described and evaluated by means of examples. The under-fitting and over-fitting concepts are illustrated for hyperparameter definition in the regularization method. In the last part, human forearm cross section is presented with the corresponding tissues and conductivities.

2.5 Electrical impedance tomography (EIT) review

Electrical impedance tomography (EIT) is a low cost, portable, non-invasive, and non-radiating general-purpose technique for imaging reconstruction used to obtain images for medical imaging, geological exploration, industrial application and environmental sciences [2].

EIT image reconstruction is used in medical imaging to generate an impedance map of a body part using the electrical conductivity distribution formed from current injection and voltage data measured using a specific pattern over electrode measuring points. The first EIT device used for medical imaging research purposes, named the Sheffield Mark I, was developed by David C. Barber and Brian H. in the early 1980s.

Hereafter, several possible applications in medicine were suggested, ranging from gastric emptying to brain function monitoring and from breast imaging to lung function assessment [3].

The main components required for the EIT image reconstruction process are shown in Figure 2-1 and described below:

1. An electrode array for current injection and data acquisition.
2. Electronic instrumentation for multiplexing, current injection, and data acquisition.
3. Computing system running image reconstruction algorithms to create the impedance map (output image).
4. Subject under test.

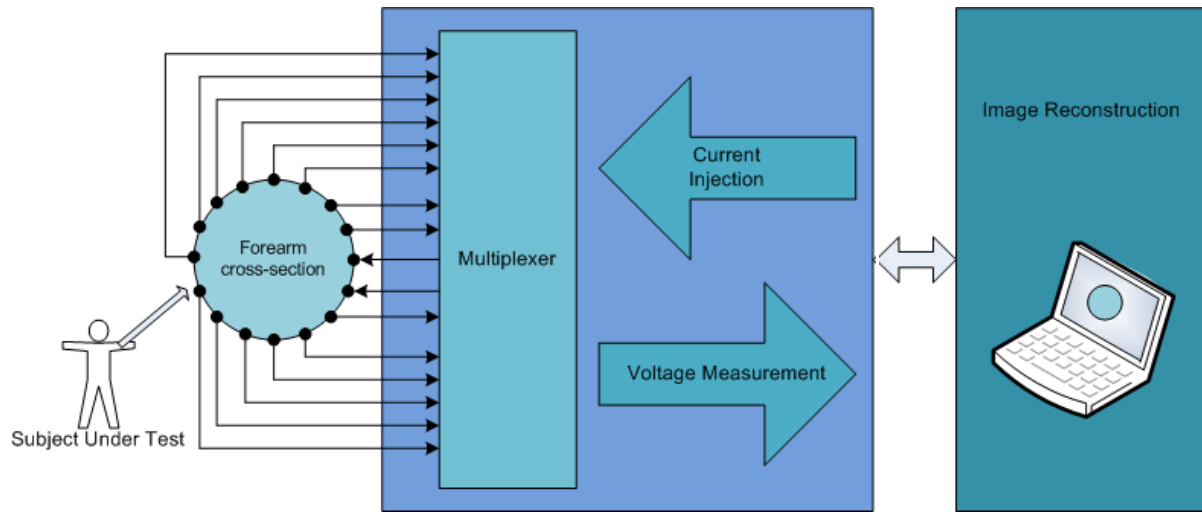


Figure 2-1. Main components for electrical impedance tomography process.

The electrode array is placed around the area of interest for cross section imaging of the subject or object under test. Electronic instrumentation consists in a current injector used to inject a low frequency and magnitude current to subject under test through a pair of electrodes. Although the data acquisition system collects the voltage measurements in the other electrodes, a multiplexer is required to switch the electrodes pairs for injecting the current and measuring the voltages. The image reconstruction algorithm generates the image of internal electrical impedance using the voltages measurements acquired from the electrode array.

The EIT image reconstruction approach that use the surface current and voltage measurements to calculate the impedance map is known as the inverse problem, where the measure voltage is used to predict the base model. To solve the inverse problem, it is necessary to solve the forward problem first. The forward problem requires knowing the conductivity base model as well current pulses of the medium to predict the electric

field inside of it. Therefore, it is necessary to implement the finite element method using a predefined geometry.

2.6 Current drive and voltage acquisition methods

In order to avoid the error due to the contact impedance, in EIT is required to inject the current and measure the voltage through different pairs of electrodes. This document describes two patterns for current drive and voltage measurements used in EIT image reconstruction, although several other types can be found in the literature [4].

2.6.1 Adjacent neighboring method

For this method, proposed by Brown and Segar in 1987, the current is applied to a pair of electrodes and voltage, which is measured from other noncurrent pair of electrodes [5]. As explained in [6], for a 16 electrode array the distribution of internal bioimpedance is determined by applying a known alternating current “I” to a first pair of electrodes and by measuring the resulting surface potentials “ V_n ” at the remaining 13 electrode pairs without the pairs containing one or both the current electrodes [7]. All these 13 measurements are independent.

Subsequently, the current through neighbored electrodes is injected and voltage is measured at the remaining electrodes. By using a system of 16 electrodes, it is possible to collect 208 different voltage measurements (16x13). The measurements in which the current electrodes and voltage electrodes are interchanged must have identical measurement results. Therefore, only 104 measurements are independent.

The current density is highest between the pair of electrodes where the current is injected and decreases rapidly as a function of the distance. Therefore, the measured voltage is maximum with adjacent electrode pairs. With opposite electrode pairs, the voltage is only about 2.5% of that [4].

Figure 2-2 shows an application example of this method for a cylindrical volume conductor with 16 equally spaced electrodes.

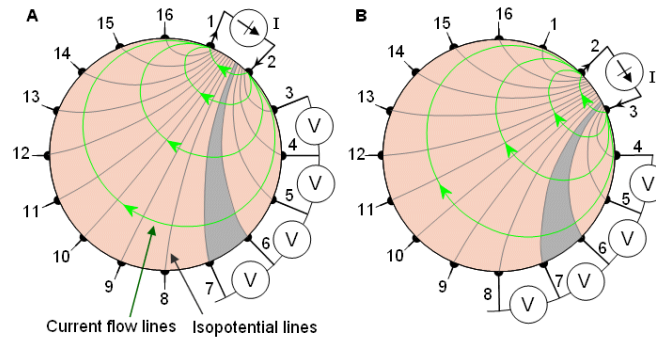


Figure 2-2. Adjacent method for a cylindrical volume conductor and 16 equally spaced electrodes:
 (a) The first four voltage measurements for the set of 13 measurements.
 (b) Another set of 13 measurements is obtained by changing the current feeding electrodes [4].

Figure 2-2 (A) depicts the first four voltage measurements for the set of 13 measurements. The impedance between the equipotential lines intersecting the measurement electrodes is indicated with shading for the voltage measurement between electrodes 6 and 7. Figure 2-2 (B) shows the behavior when moving current injection to electrodes 2 and 3.

2.6.2 Opposite or polar method

This measurement method was also proposed by Hua, Webster, and Tompkins in 1987 [1]. In this method, the current is injected through a pair of opposite electrodes. The voltage differences are measured on the remaining electrodes with respect to the voltage reference electrode that corresponds adjacent to the current-injecting electrode. This process is repeated until current has been injected between all pairs of electrodes. For a system with 16 electrodes there are 8 opposite pairs, and for each pair there are 13 remaining electrodes; then, 104 (8x13) different voltage measurements are produced.

This method offers a better distribution of the sensitivity, as the current travels with greater uniformity through the imaged body being less sensitive to conductivity changes at the boundary [7].

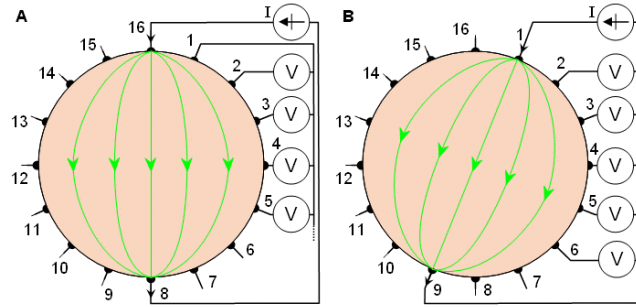


Figure 2-3. Opposite or polar method representation [4].

2.7 Image reconstruction

Image reconstruction in EIT is the stage of the process where an image with the conductivity distribution of the subject under test is generated. In this process the voltages measured from electrodes during the current injection are used to calculate the conductivities values, keeping the error as smaller as possible between the calculate voltage and the measured voltage. The measured voltage is affected by the tissue conductivity between the injection electrode and the detector electrode, a change in the conductivity influence on every single voltage measured at the boundary [8].

Figure 2-4. shows a block diagram of the process to calculate the conductivity distribution image. Measurements are extracted from patient, then the simulated data for constructing the Jacobian matrix is generated using the finite element model. Using this data, the reconstruction smoothness parameters are set up to get the best tradeoff between output image and iterations. Finally, the output of equation (2.4), as described in following sections, corresponds the EIT reconstructed image.

Image reconstruction in EIT is an ill-posed problem because there is not a unique solution. Due to this behavior, it is necessary to implement the forward problem and the inverse problem to create the impedance map These concepts will be explained in detail in the following sections.

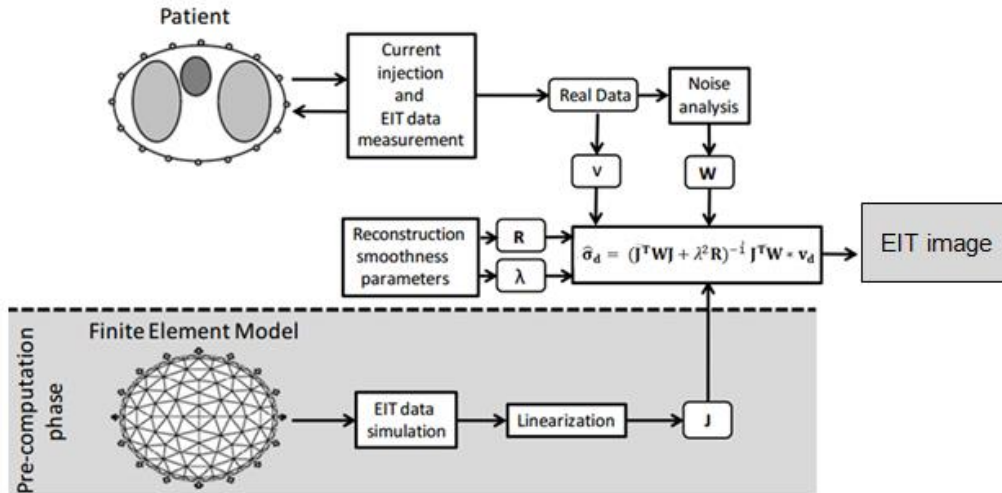


Figure 2-4. Block diagram of EIT reconstruction algorithm [8].

2.7.1 Forward problem

The forward problem is defined as the mathematical prediction of the output data or model behavior based on some physical or mathematical model with a set of data and parameters as represented in Figure 2-5. In EIT the forward problem is used to develop the sensitivity or Jacobian Matrix J, used in the inverse problem solution.

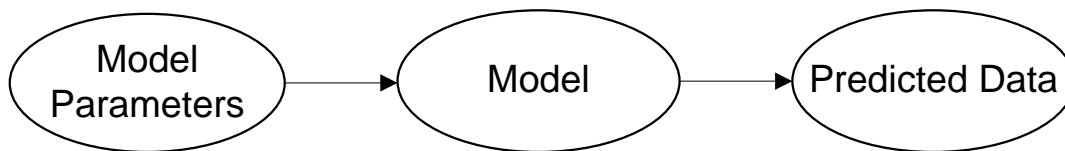


Figure 2-5. Graphical representation of forward problem.

According to [9], the Jacobian matrix describes the change in measurements due to a deformation in the boundary. It is calculated using perturbation techniques by introducing small model deformations and repeatedly solving the forward problem. It is slow and it becomes inaccurate for large finite element models. For this reason, algorithms have been developed mainly for 2D problems.

In electrical impedance tomography (EIT), for a given conductivity distribution and current injection values, the forward problem corresponds to the prediction of the voltages on electrodes and the physics of the problem based on Maxwell's equations.

As mentioned in [10], the EIT forward solver is normally based on the conventional finite element method (FEM). Due the level of noise present in real data the accuracy to detect very small anomalies is affected, usually is needed a mesh with large number of nodes and elements to accurately simulate the forward solution with the FEM. In the case of objects that have not standard geometries as forearm, thorax or brain, it is a common practice to approximate them as spheres or triangles [11].

Using the voltage measurements ($\mathbf{v} \in \mathbb{R}^{n_M}$), subject conductivity ($\hat{\sigma} \in \mathbb{R}^{n_N}$) could be estimated by minimizing the least-squared error:

$$\hat{\sigma} = \arg_{\sigma} \min \|\mathbf{v} - f(\sigma)\|^2, \text{ with: } f(\sigma): D \subset \mathbb{R}^{n_N} \rightarrow \mathbb{R}^{n_M} \quad (2.1)$$

Function $f(\sigma)$ estimates boundary voltages measured at electrodes for a given conductivity distribution ($\sigma \in \mathbb{R}^{n_N}$) this function is known as the forward problem.

In EIT image reconstruction, the function $f(\sigma)$ is linearized in its current operating point σ_0 . to simplify the forward problem.

$$f(\sigma) \approx f(\sigma_0) + \mathbf{J}(\sigma - \sigma_0), \text{ with } \mathbf{J}_{ij} = \left. \frac{\partial v_i}{\partial \sigma_j} \right|_{\sigma_0} \quad (2.2)$$

Despite the simplifications (linearization, differential EIT), the problem remains ill-conditioned and the image reconstruction is not possible. In order to reconstruct the conductivity distribution image, it is necessary to solve the inverse problem.

2.7.2 Inverse problem

Opposite to forward problem, the inverse problem is defined as the prediction of the model parameters based on the model and a known set of data, schematically shown in Figure 2-6. In electrical impedance tomography the inverse problem corresponds to the prediction of the internal conductivity distribution for given set of the voltage measurements on the surface, injection values and the geometry of the domain;

minimizing the difference between the measured and predicted voltages using the forward problem solution[11].

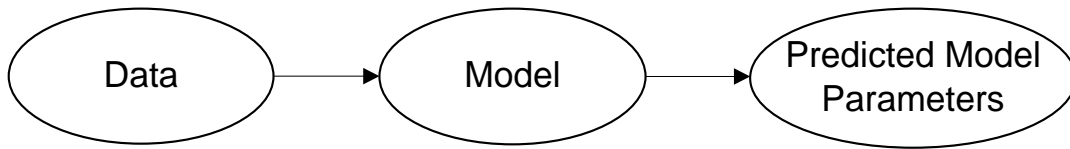


Figure 2-6. Graphical representation of inverse problem.

According to [12] EIT image reconstruction generally consists of both, an inverse problem and a forward problem. The inverse problem relates the measurements to the model and as explained above, the forward problem is used to develop the sensitivity matrix, which is used for solving the inverse problem. A generalized graphical representation of EIT image reconstruction is illustrated in Figure 2-7.

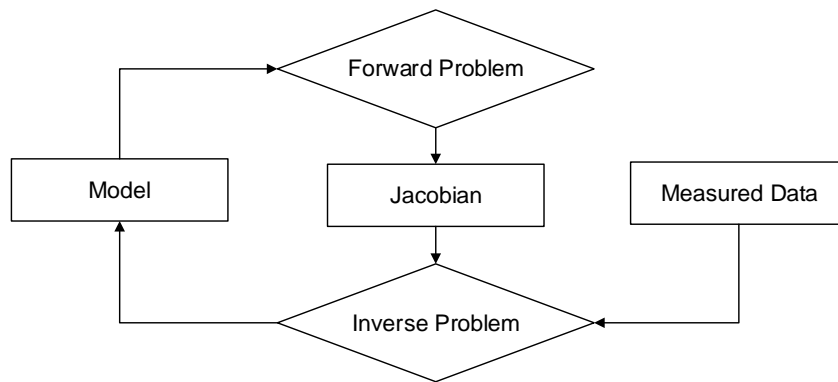


Figure 2-7. Graphical representation of the general EIT image reconstruction.

The inverse problem in EIT is identified as an ill-conditioned problem because it can have two or more solution or the solution procedure is unstable. It can be converted to a well-posed problem, which have a unique and continuously data dependant solution, if some priori information is available.

A problem is called well-posed in the sense of Hadamard, according to [13], For all admissible data, a solution exists and the solution is unique and depends continuously on the data. Due to the ill-conditioned problem, nature of inverse problem in EIT, the obtained reconstructed image requires the application of regularization techniques to eliminated undesirable results.

The regularization is a technique used in mathematics, statistics and particularly in the fields of machine learning and also inverse problems to convert the ill-posed problem into a well-posed problem by the introduction of a regularization term controlled by the hyperparameter (λ). Applying the regularization, the subject conductivity equation is reformulated as follow:

$$\hat{\sigma}_d = \arg_{\sigma_d} \min\{\|\mathbf{v}_d - \mathbf{J}\sigma_d\|^2 \mathbf{W} + \lambda^2 \|\sigma_d\|^2 \mathbf{R}\} \quad (2.3)$$

where:

- \mathbf{W} is the weighting matrix used to attenuate voltage measurements that are classified as unreliable (too noisy).
- λ is the hyperparameter that controls the trade-off between regularization and noise. A high hyperparameter results in a smooth image with lots of noise attenuation whereas a small hyperparameter yields to a noisier image with better spatial resolution as explained in [8].
- \mathbf{R} corresponds to the regularization and can be chosen in various ways:
 - a) When set equals to the identity matrix ($\mathbf{R} = \mathbf{I}$), zeroth-order Tikhonov regularization is used. This simply penalized for too high amplitudes of σ_d .
 - b) Setting \mathbf{R} based on edge-sensitive spatial filters (e.g. Laplacian) The reconstructed image is penalized for sharp edges and forced to smoothness.

The equation (2.3) can be converted for final EIT reconstruction to perform only one matrix multiplication in equation (2.4). It is also known as the one-step Gauss-Newton (GN) reconstruction illustrated in Figure 2-4.

$$\hat{\sigma}_d = (\mathbf{J}^T \mathbf{W} \mathbf{J} + \lambda^2 \mathbf{R})^{-1} \mathbf{J}^T \mathbf{W} * \mathbf{v}_d \quad (2.4)$$

2.8 Geometry and finite element method definition using Fourier descriptors

As explained in [14], the Finite Element Method (FEM) provides a numerical solution for field problems. FEM requires dividing the structure into several elements and then reconnects all of them at “nodes”, holding the elements together and defining a set of simultaneous algebraic equations. The boundary of each component is associated with the geometry under study as shown in Figure 2-8, in the left image is the solid sphere, in the center is the sphere sub-divided and in the right image are the elements(triangles) connected by nodes.

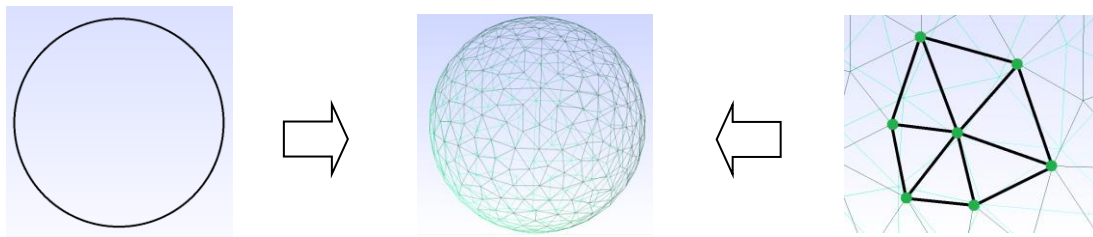


Figure 2-8. Finite element model representation.

This mathematical model is defined to predict the behavior of a determined system under different conditions. Then, the results produced by this model are physically re-interpreted only under modeling conditions. As described in [15], the response of each element is expressed in terms of a finite number of degrees of freedom characterized as the value of an unknown function, or functions, at a set of nodal points. The response of the mathematical model is then considered to be approximated by the discrete model obtained by connecting or assembling the collection of all elements. Finite elements do not overlap, that is known as support or local support.

As shown in Figure 2-9, the most common errors in FEM formulation are the following:

1. Simplification of geometry, the approximated domain loses detail from original.
2. Field quantity is assumed to be a polynomial over an element, which is not true.

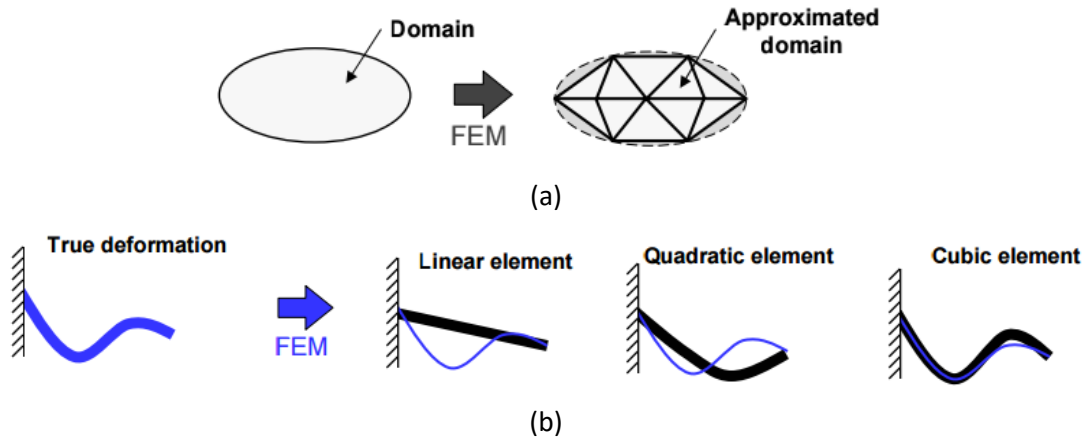


Figure 2-9.(a) Geometry approximation error (b) line element error [14].

Among the main advantages of FEM are the simplification of very complex geometries for their analysis and evaluation and the help for solving indeterminate structures with complex restraints. Its main disadvantages are that the obtained solutions are just an approximation and inherent errors are present in its formulation.

2.8.1 Fourier descriptors used for geometry components definition

For generating the geometry under study for this thesis, it is required to interpolate points in order to define the structure boundaries. Those points are defined by the Fourier descriptors implementation.

The Fourier descriptors are used to encode the shape of a two-dimensional object by taking the Fourier transform of the boundary and by mapping every (x, y) point on the boundary to a complex number $x + iy$.

The original component shape can be recovered from the inverse Fourier transform. The boundary can be smoothed or filtered by using just few terms of the inverse Fourier transform. A highly simplified shape can be obtained when using few descriptors, but the shape can converge to its original form as the quantity of descriptors increases.

Due to Fourier descriptors contains all the information about the shape, it can be reconstructed by setting all the terms that correspond to value above a determinate

frequency to zero, creating a low-pass filtering effect that allows to smooth the shape boundary. Figure 2-10 shows some reconstructed images when different numbers of coefficients are used.

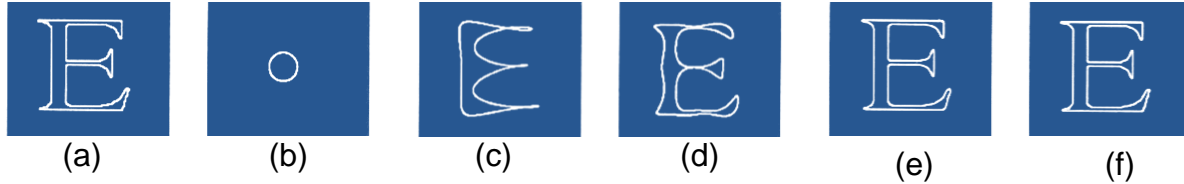


Figure 2-10. Examples using Fourier descriptors: (a) the original edge image with 1024 edge pixels, (b) 3 Fourier coefficients, (c) 21 Fourier coefficients, (d) 61 Fourier coefficients, (e) 201 Fourier coefficients, and (f) 401 Fourier coefficients [16].

As explained in [17], if the boundary of a shape has N pixels numbered from 0 to $N-1$ and the k^{th} pixel along the contour has position (x^k, y^k) the contour can be described with the following two parametric equations:

$$x(k) = x_k \quad (2.5)$$

$$y(k) = y_k \quad (2.6)$$

The Fourier Transform of each function two frequency spectra are gotten. These spectra are known as Fourier descriptors.

$$a_x(v) = F(x(k)) \quad (2.7)$$

$$a_y(v) = F(y(k)) \quad (2.8)$$

The Discrete Fourier Transform can be employed for finite number of discrete pixels and it treats the signal as periodic. Then, the Cartesian coordinates (x, y) points must be considered as a complex number $x + iy$ in the complex plane.

$$s(k) = x(k) + iy(k) \quad (2.9)$$

And finally, the single Fourier descriptor is the transform of the complex function as it is shown in equation (2.10).

$$a(v) = F(s(k)) = F(x(k) + iy(k)) \quad (2.10)$$

Some Fourier transform properties for periodic signals as translation invariance, scaling and rotation and starting point also apply to Fourier descriptors.

1. Translation invariance: Independently where the shape is located in the image, the Fourier descriptors remain the same.
2. Scaling: If the shape is scaled by a factor, the Fourier descriptors are scaled by that same factor.
3. Rotation and starting point: Rotating the shape or selecting a different starting point only affects the phase of the descriptors. Rotation in the complex plane by angle θ is multiplication by $e^{i\theta}$.

2.9 EIT image reconstruction algorithms

In this section Sheffield back-projection and Gauss-Newton image reconstruction algorithms will be explained, as well the different types prior information used in the regularization technique for GN algorithm to minimize the error between the predicted and measured voltage.

2.9.1 Sheffield back-projection algorithm

The Sheffield back-projection algorithm was proposed in 1983 by Barber and Brown. It is one of the most well-known image reconstruction algorithm developed for Electrical Impedance Tomography due its efficiency and relative low power cost.

As explained in [18], the Sheffield back-projection algorithm is a two dimensional reconstruction algorithm initially restricted to a circular domain. Then, a pre-processing procedure denominated filtered back-projection based on first derivative of the FEM of the object under study. It was developed to improve the spatial and the conductivity resolution by pre-processing the electric potential data before the use of the back-projection algorithm.

According to [18], the mathematical representation of the problem is:

$$\nabla \cdot (\sigma \nabla U) = 0 \text{ in } \Omega \quad (2.11)$$

$$\sigma \frac{\partial U}{\partial n} = J \text{ on } \partial \Omega \quad (2.12)$$

Where σ corresponds to conductivity; U , the electrical potential; J , the current density in the boundary; and Ω , the domain of interest.

Then, replacing σ and U for their first variation of the conductivity $\delta\sigma$ and the electric potential δU , respectively in (2.11) and (2.12), results:

$$\nabla \cdot [(\sigma \nabla \delta U) + \nabla \cdot (\delta \sigma \nabla U)] = 0 \text{ in } \Omega \quad (2.13)$$

$$\sigma \frac{\partial (\delta U)}{\partial n} + \delta \sigma \frac{\partial U}{\partial n} = J \text{ on } \partial \Omega \quad (2.14)$$

Using the following hypotheses:

1. Ω is the unit two dimensional ball;
2. the conductivity is unitary $\sigma = 1$;
3. $\delta\sigma = 0$ near the dipole.

the linearized problem reduces to:

$$\nabla^2 \cdot \delta U = -\nabla(\delta\sigma) \cdot \nabla U \text{ in } \Omega \quad (2.15)$$

$$\frac{\partial (\delta U)}{\partial n} = 0 \text{ on } \partial \Omega \quad (2.16)$$

The linearized inverse problem associated with (2.15) and (2.16) becomes: given a variation of electric potential along the boundary, $\delta U|_{\partial\Omega}$, for various choices of dipole positions along the boundary, determine a consistent increment $\delta\sigma$.

To solve this problem, Barber and Brown used a change of variables that mapped the circular domain into a rectangular domain.

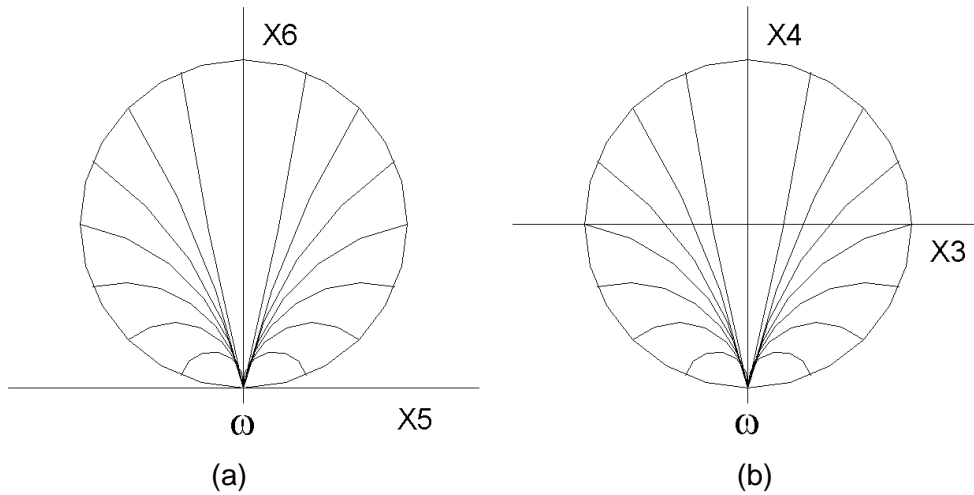


Figure 2-11.(a) Coordinates (X5,X6) and (b) coordinates (X3,X4).

Using as reference frame shown in Figure 2-11.(a), where ω represents the position of current injecting dipole, which is located between two electrodes, the equation for the equipotential lines are:

$$U = \frac{x_5}{x_5^2 + x_6^2} \quad (2.17)$$

$$V = \frac{x_6}{x_5^2 + x_6^2} \quad (2.18)$$

And, translating the reference frame as in Figure 2-11.(b), the equations above correspond to:

$$U = \frac{x_3}{x_3^2 + (x_4 + 1)^2} \quad (2.19)$$

$$V = \frac{(x_4 + 1)}{x_3^2 + (x_4 + 1)^2} \quad (2.20)$$

Based on (2.19) and (2.20), the domain Ω can be mapped to the upper half plane P defined by the rectangular region where $V > 1/2$.

Now, (2.15) and (2.16) can be simplified by using the new coordinates (U, V), to:

$$\nabla^2 \delta U = - \frac{\partial(\delta \sigma)}{\partial U} in P \quad (2.21)$$

$$\frac{\partial(\delta U)}{\partial V} = 0 \text{ on } \partial P = \left\{ V > \frac{1}{2} \right\} \quad (2.22)$$

Barber and Brown suggest the average in (2.23) as the discrete solution for $\delta\sigma$.

$$\delta\sigma = \frac{1}{m} \sum_{j=1}^m W(s, \omega_j) |_{s=U(s, \omega_j)} (2V(x, \omega_j) - 1) \quad (2.23)$$

where m corresponds to the number of the electrodes; W , to the voltage measurement on the boundary; ω , to the position of the electrode; and V , to the current intensity function.

In order to obtain a normalized conductivity, the voltage measurements are normalized as suggested by Barber and Brown. Therefore, the Sheffield back-projection algorithm assumes that the region between two adjacent potential lines has the same voltage measurement. Rotating the position of the current injection dipole, m sets of voltage measurements are obtained. These sets of electric potential measurements, previously normalized, adjusted by the corresponding weight which is $2V - 1$, is the desired normalized conductivity.

The Figure 2-12 is a step by step example showing the profiles of voltage deviations in the presence of a regional increase of impedance and the successive superposition of the 16 voltage profiles.

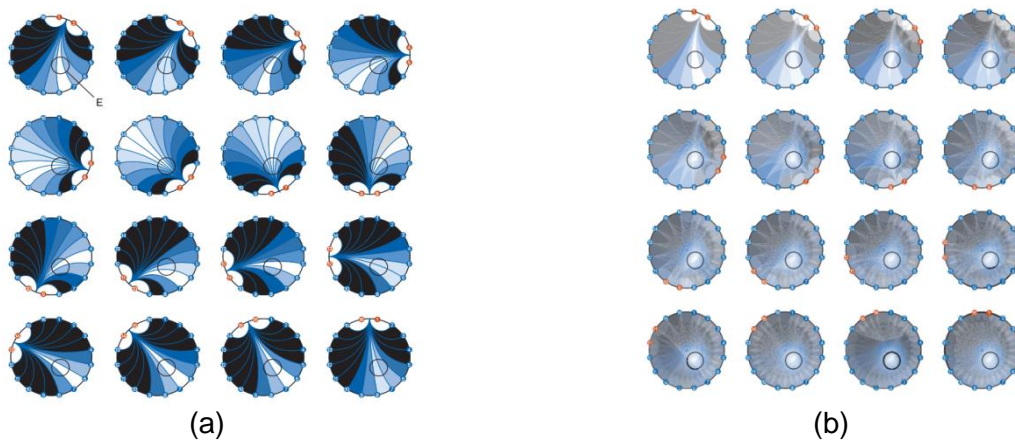


Figure 2-12. Step by step example. A) Profiles of voltage deviations in the presence of a regional increase of impedance. B) Successive superposition of the 16 voltage profiles [19].

In Figure 2-12.(a), white and light blue depict deviations of the voltage distribution in an inhomogeneous medium; the black corresponds to voltages without deviation. Figure 2-13. corresponds to the resulting image after selective boundary filtering explained above.

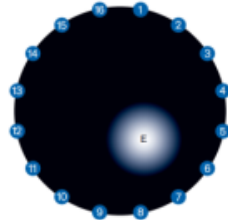


Figure 2-13.Resulting image after selective boundary filtering [19].

2.9.2 Gauss Newton algorithm

As exposed in [14], the EIT image reconstruction is a non-linear inverse problem that is highly affected by errors in measurements, large changes in impedance imply only small changes in surface potentials. Therefore, minimization algorithms are required to approximate the results, reducing the differences between the voltages predicted with forward solvers and the voltages measured.

The GN algorithm is used to find the square solution of the minimized object function $s(\sigma)$. Supposing that V_m is a matrix containing measured voltages and V_c is a matrix for calculated voltages, $s(\sigma)$ can be expressed as:

$$s(\sigma) = \frac{1}{2} \|V_m - V_c\|^2 = \frac{1}{2} \|(V_m - V_c)^T (V_m - V_c)\| \quad (2.24)$$

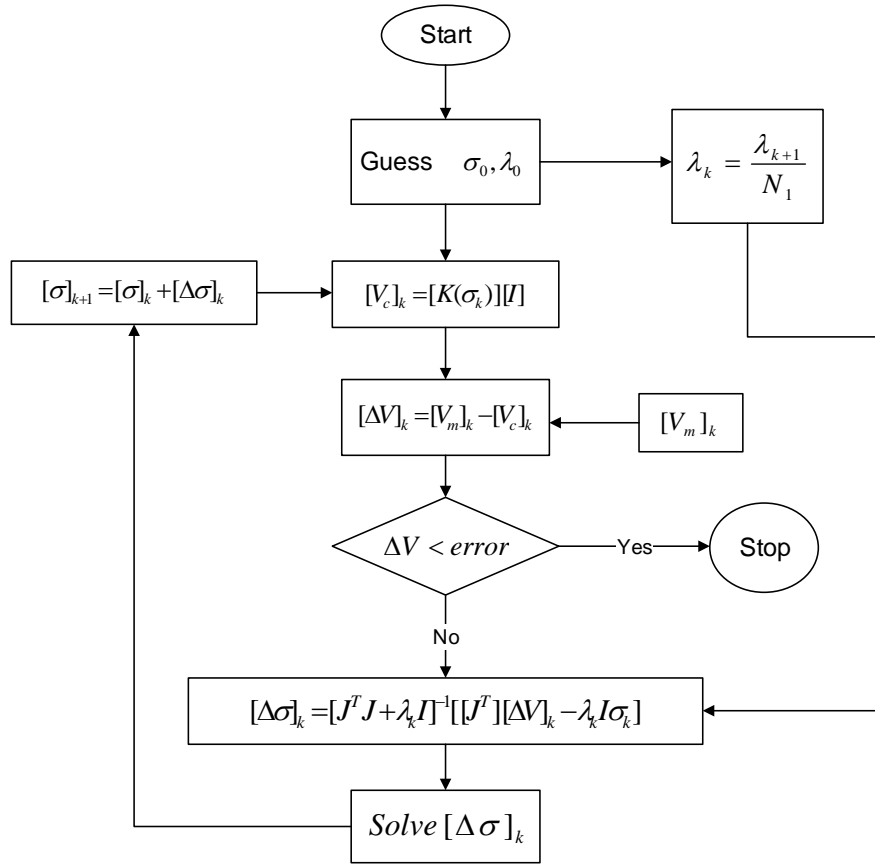


Figure 2-14.Gauss-Newton algorithm flow diagram.

The flow diagram shown in Figure 2-14 describes the GN algorithm. As explained in [20], the GN algorithm requires an initial conductivity (σ_0) value to be started. The voltages are calculated and then compared with the measured potential for obtaining the Jacobian (J) matrix, $\Delta\sigma$ is then updated and σ_{k+1} is calculated using σ_k . The loop is repeated until the specification error limit ε is reached. Symbol λ is the regularization parameter which is updated in each iteration.

The GN algorithm is useful to find images of conductivity by employing different prior regularization methods.

2.9.3 Gauss Newton priors regularization methods

The solution of impedance distribution in electrical impedance tomography requires the use of a regularization methods to convert the ill-posed problem into a well-posed problem using a suitable regularization parameter as is mentioned in [21].

Besides to reduce the ill-posed characteristics of the problems, the regularization and its hyperparameter definition helps to prevent over and under-fitting, allowing to reconstruct images with a better quality and convergence to a model that matches the data observed for inverse problem. Under-fitting and over-fitting concept is explained in section 2.10.

Tikhonov prior

The simplest regularization technique is the standard Tikhonov, in which the regularization matrix is proportional to identity. Since the physical attenuation phenomena responsible for the ill-posed nature of the EIT problem is not taken into account, the standard Tikhonov regularization cannot provide a satisfactory solution in image reconstruction for EIT [3].

The Tikhonov-regularized versions of the EIT inverse problem can be written in the form:

$$\min_{\rho} \{ \|V - U(\rho)\|^2 + \alpha \|L_{\rho}\|^2 \} \quad (2.25)$$

where ρ is the resistivity distribution; $U(\rho)$, the resistivity to potential mapping, that is, the potentials obtained from the model with known ρ ; V , the measured potentials; L , a so-called regularization matrix; and α , a regularization parameter [22].

NOSER prior

The Newton's One-Step Error Reconstructor (NOSER), is a linearization-based algorithm which takes one step of Newton's Method using the best constant conductivity approximation from the measured data as an initial guess.

The reconstruction is done with a particular mesh; the conductivity is assumed to be constant on each mesh element. According to [23], mathematically this can be expressed as:

$$\sigma(\vec{p}) = \sum_{n=1}^N \sigma_n X_n(\vec{p}) \quad (2.26)$$

Where $X_n(\vec{p})$ is the characteristic function that is 1 for \vec{p} contained in the n th mesh element or zero otherwise.

Laplace prior

Laplace prior is a regularization which regression estimates the median, while Normal distribution refers to ordinary least squares. Laplace is based off the prior belief that most coefficients must be close to zero as it is shown in Laplace probability distribution function [24] represented in equation (2.27):

$$p(x; a) = \frac{a}{2} e^{-a|x|} \quad (2.27)$$

Laplace prior reduces the number of predictors in a generalized linear model, identifies important predictors, selects among redundant predictors and produces shrinkage estimates with potentially lower predictive errors than ordinary least squares.

In Figure 2-15. is shown the diagram contrasting the probability density functions of Normal and Laplace distributions, where the second one assigns a higher density to a neighborhood of zero, also Laplace has fatter tails than the Normal distribution.

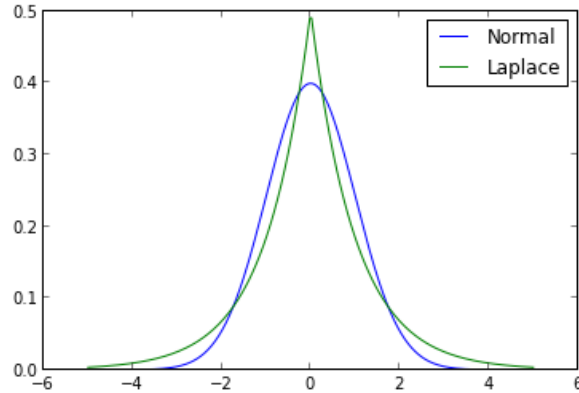


Figure 2-15.Diagram contrasts the probability density functions of the normal distribution and the Laplace distribution [25].

Total Variation

Total variation regularization is mainly used in digital image processing for noise removal. It is based on the principle that signals with excessive and possibly spurious detail have high total variation. According to this, reducing the total variation of the signal subject to a close match of the original signal, removes unwanted detail preserving important details such as edges.

The advantages of this technique over others techniques such as linear smoothing or median filtering, which reduces noise but at the same time smooth away edges to a greater or lesser degree, is the contrasting. Total variation noise removal is effective while preserving the important changes even at low signal-to-noise ratios. According to [26], the total variation is represented by the equation (2.28)

$$TV(u) = \int_{\Omega} |\nabla u| dx \quad (2.28)$$

2.10 Under-fitting and over-fitting

In EIT image reconstruction, the main idea is to define the conductivity distribution model from measured voltage, under-fitting and over-fitting may occur when linear regression is used with polynomial features to approximate nonlinear functions.

The function used for the example shown in [27] is a part of the cosine function, the plots in Figure 2-16 shows the function, the samples from the real function and the approximations of different models. Figure 2-16.(a), corresponds to an under-fitting result, where the linear function is not sufficient to fit the training samples. In the other case Figure 2-16.(b) shows the result where the function is approximated to the true function almost perfectly. Finally, the plot in Figure 2-16.(c) is an over-fitting result due to the use of higher degrees in polynomial equations where the model over-fit the training data.

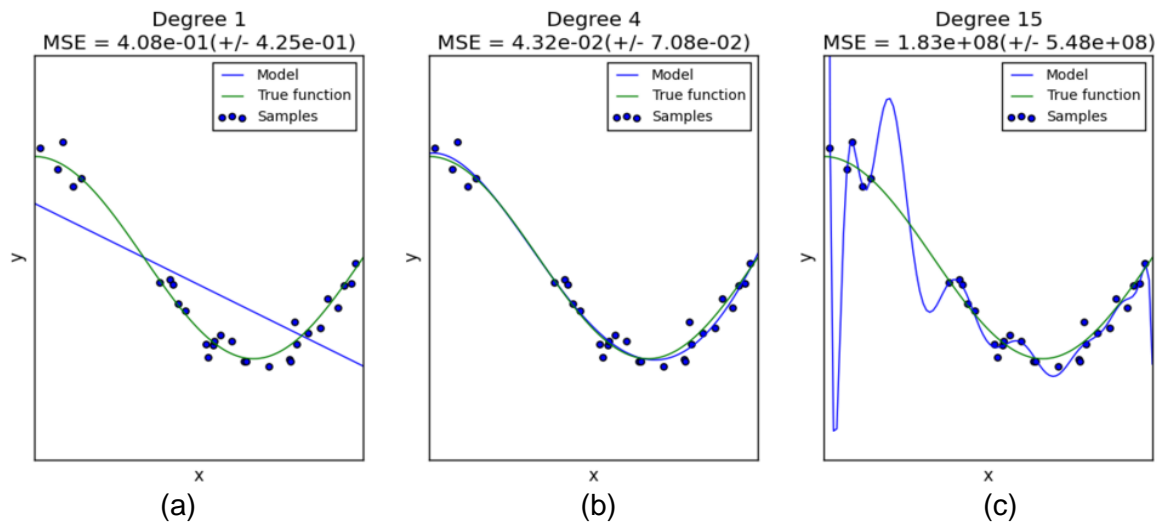


Figure 2-16. Under-fitting vs over-fitting results [27].

Figure 2-17 shows a scheme for the error of prediction depending on the size and quality of the calibration data set, which influence the estimation error. The best predictive and fitted model would be where the validation error has its global minimum.

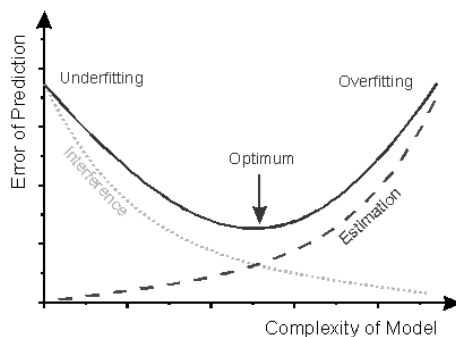


Figure 2-17. Scheme for the error of prediction depending on the size and quality of the calibration data set, which influence the estimation error [28].

Over-fitting/over-training is an employed supervised learning. If the validation error increases (positive slope) while the training error steadily decreases (negative slope) then a situation of over-fitting may have occurred.

2.11 Comparison of 2D algorithms in EIT

In order to select the best algorithm for image reconstruction using EIT technique, the previous work in [20] is used as reference with a simple test bench, a tank and one object, the results are shown in Figure 2-18 and Figure 2-19. These results are very significant to improve knowledge and use better criteria when defining the environment setup for the human forearm.

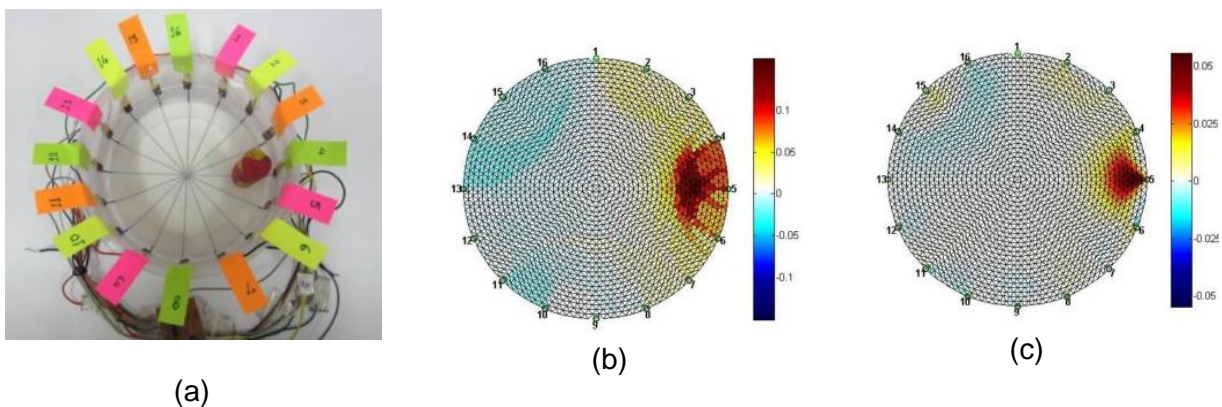


Figure 2-18.2D algorithm comparison results : (a) Clay cylinder kept near electrodes 4 and 5 and (b) Non conducting impurity near 4, 5 using back-projection without filter.[20].

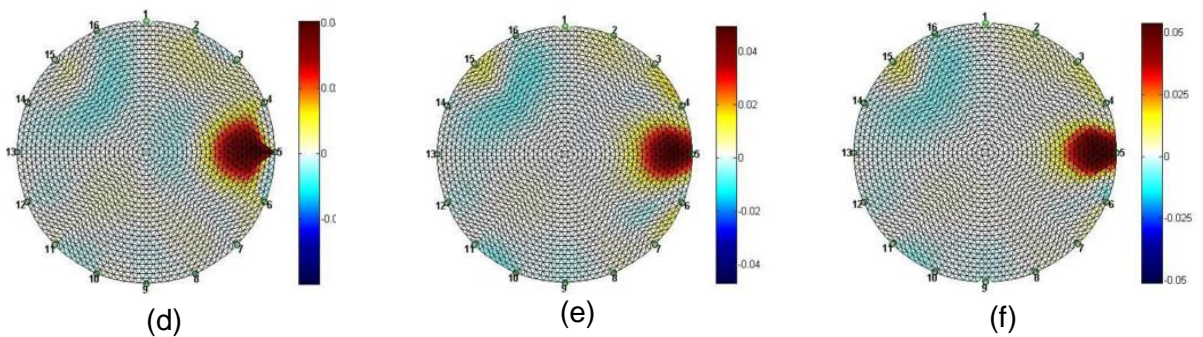


Figure 2-19.2D algorithm comparison results : (c) GN algorithm with Tikhonov prior, (d) GN algorithm with NOSER prior, (e) GN algorithm with Laplace prior and (f) Total Variation prior [20].

Results are summarized in Table 2-1, where the performance of prior information methods is calculated using the error between the current size of 4.5599 cm² and the reconstructed impurity size. According to the results, the best performance is obtained when using total variation prior information.

Table 2-1. Comparison of actual and reconstructed impurity size.

Impurity (Clay cylinder)	Size (cm ²)	$Error(\%) = \frac{4.5599 * -reconstructed}{4.5599 *}$
Reconstructed image using Tikhonov prior	3.619	20.63
Reconstructed image using NOSER prior	5.2285	14.66
Reconstructed image using Laplace prior	4.84946	6.35
Reconstructed image using total variation prior	4.7047	3.175

*Actual size of clay cylinder is 4.5599 cm²

2.12 Human forearm model

As described in [29], the forearm extends from the elbow joint to the hand and is compound by the lower half of the arm. The forearm has two long bones, the ulna and the radius, forming a rotational joint which allows the forearm to turn so that the palm of the hand faces up or down. The forearm skin provides a sensory function and typically its top features more follicles than the underside.

The forearm has two arteries, the radial and ulnar, which follow a course close to the bones of similar name. These arteries are branched into lesser arteries, servicing the forearm's musculature. It has also four nerves, the volar antebrachial interosseous, radial, ulnar, and median; that innervate most of the forearm components.

Figure 2-20 represents a cross section image of the human forearm tissues. Different tissues, as well different conductivities, are remarked using the different colors.

For this thesis purposes, the most important tissues to identify in the image reconstruction are the nerves, which are marked in white.

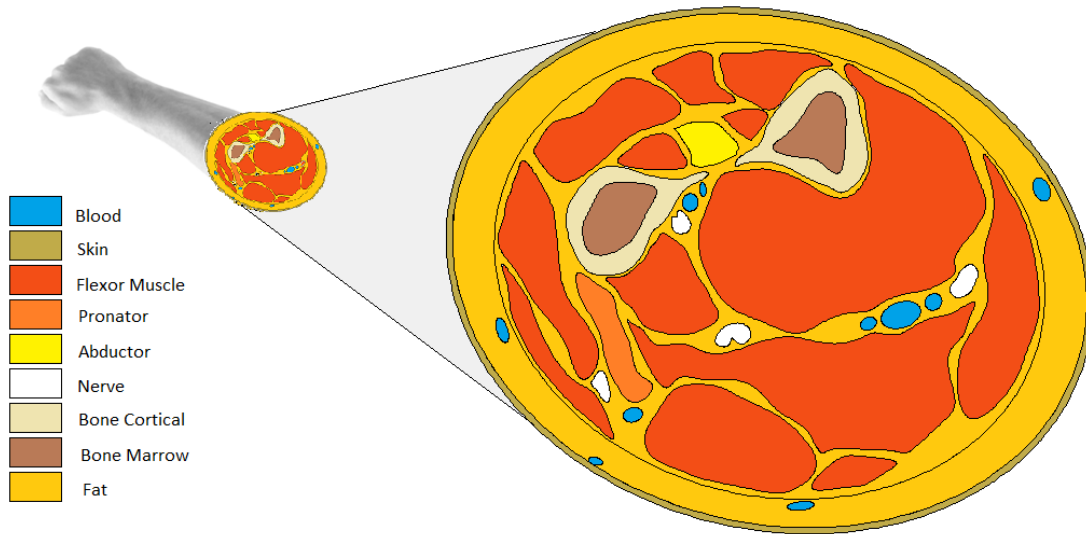


Figure 2-20.Forearm geometry used as reference in this thesis (geometry was reproduced from [1]).

In Table 2-2 are shown the theoretical values of forearm conductivity that are being used for this thesis purposes [1].

Table 2-2.Theoretical values of conductivity and relative permittivity for different tissues in the human forearm [1].

Tissue	Conductivity* (S/m)	Rel. Permittivity**
Fat ¹	0.03	5×10^6
Muscle ¹	--	
Transversal	0.09	2×10^7
Longitudinal	0.55	3.3×10^6
Skin ¹	0.1135	6×10^5
Bone		
Cortical ¹	0.03	5.2×10^5
Marrow ²	0.002	45520
Blood ¹	0.7	3×10^3
Nerve ²	0.028	5.89×10^6

Chapter 3 EIT image reconstruction methodology

This chapter explains the EIT image reconstruction methodology including a detailed flow diagram for final implementation in order to validate and analyze the results. Available software tools and platforms for EIT are also evaluated considering its advantages and disadvantages. For the human forearm EIT image reconstruction methodology, the selected toolkit is EIDORS. The reason of its selection, features and most relevant functions will be explained.

3.13 General EIT image reconstruction methodology

Figure 3-1 summarizes the general procedure to reconstruct the EIT image. At first, model geometry must be defined; then the current injection and voltage acquisition patterns in the electrodes array are simulated; Finally, conductivity distribution of the subject under test is calculated using the forward and inverse solvers.

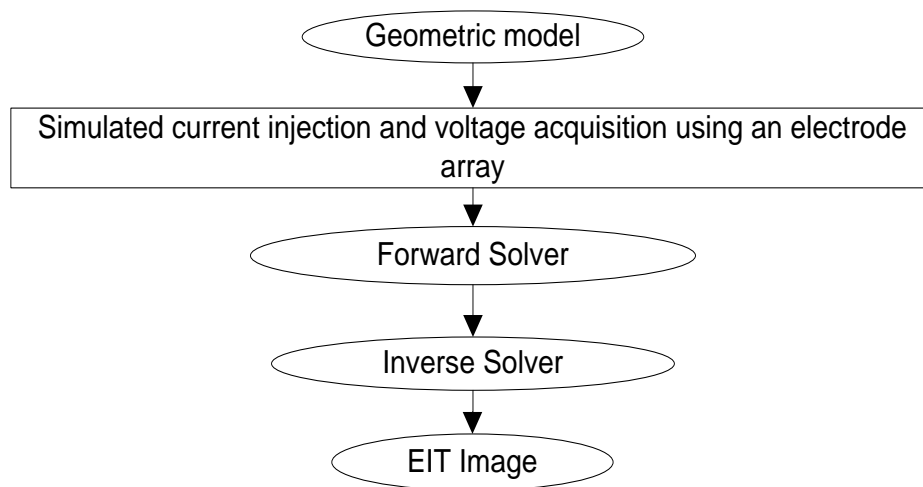


Figure 3-1. EIT image reconstruction general methodology.

To perform the EIT image reconstruction, a finite element model based on the object geometry is required in order to solve the forward problem. For the inverse solver, several forward problem solver iterations are required previously to compare the data and minimize the prediction error.

The inhomogeneous data used for image reconstruction algorithms could be acquired from real electrodes or from simulated values. For this thesis, the image reconstruction algorithms are applied using simulated data generated using the adjacent injection pattern. The measured data from virtual electrodes is merged with Gaussian noise in order to evaluate the image reconstruction within a realistic environment. Once the set of input data is available, the forward and inverse solvers are executed with the corresponding hyperparameters to obtain the EIT reconstructed image of the conductivity distribution.

The selection of the appropriate software tool to implement the image reconstruction from the voltage measurements is one of the specific objectives of this thesis. EIT implementation requires a computer and specialized software in order to process all the mathematical model information. At the time of this research, only two software options were found to implement the EIT image reconstruction methodology: a generic numeric solver or a high level mathematical programming tool, and EIDORS [30], an open source tool kit that works linked with Matlab. In the following section, the features of each option and their main advantages are described in order to justify the selection of the best alternative to develop the human forearm image reconstruction methodology.

3.13.1 High level mathematical programming tool

Application structure, algorithms, and implementation shall be developed by the researcher as well all required optimizations, increasing the development effort, cost, and time. The development of an EIT implementation from scratch is a very complex task.

General purpose software tools or physics solvers are expensive and their use could be justified depending of the model complexity and spatial resolution required. However, they are also not customized for EIT; therefore, the development effort would be high. For this research, these options are discarded because of the price, license terms, and development time limitations.

3.13.2 EIDORS toolkit

The name of EIDORS stands for Electrical Impedance Tomography and Diffuse Optical Tomography Reconstruction Software [13]. EIDORS is used for EIT image reconstruction and modeling for medical and industrial applications. According to [31], the project is currently supported by William R.B. Lionheart and Andy Adler, from University of Manchester (U.K.) and University of Ottawa (Canada), respectively.

The latest release of EIDORS is version 3.8 (available at www.eidors.org licensed under the GNU GPLv2 (or GPLv3)). It has a strong basis with several built-in reconstruction algorithms. Also, as mentioned in [28], adds and improves many important aspects in EIT field like speed optimizations: improved Jacobian calculation, faster cache handling, and faster forward solutions.

EIDORS performs an iterative absolute inverse solver for Gauss-Newton and Conjugate-Gradient; as well as some speed optimizations in Jacobian calculation, faster cache handling, and faster forward solutions. EIDORS toolkit offers four primary objects represented by a structure with its own properties, name, and type. These four objects are the data, image, fwd model, inv model. The name is arbitrary and it is displayed by the graphical functions, being useful to distinguish objects in a user specified function during the development.

EIDORS have been used and supported by strong commercial brands like Dräger and Swisstom, supporting their file formats. More details about EIDORS could be found in [30]. The following table shows a summary of EIDORS features.

After analyze the summarized information listed in Table 3-1, obtained from researching about EIT image reconstruction platforms, EIDORS is a software toolkit, that offers an open source tool and an active community that is continually working supporting and providing constant maintenance. Also it provides free software algorithms for forward and inverse problems modeling for EIT [32].

Table 3-1. Image Reconstruction software tool features

Platform	Description	License	Support	Environment
EIDORS	Electrical Impedance and Diffuse Optical Reconstruction Software	Open Source GNU General Public License. Free to use, modify, and distribute modifications. May be used in a commercial product	Yes, a specific group is responsible for this project. A big community is working with this platform	Windows, Linux. Works linked with MATLAB or Octave

3.13.3 Human forearm Image reconstruction methodology flow diagram using EIDORS

For a better explanation about how the image reconstruction platform works, the flow diagram in Figure 3-2 was created. Next, steps and details to generate a reconstructed image of the human forearm using EIT technique in EIDORS platform will be addressed.

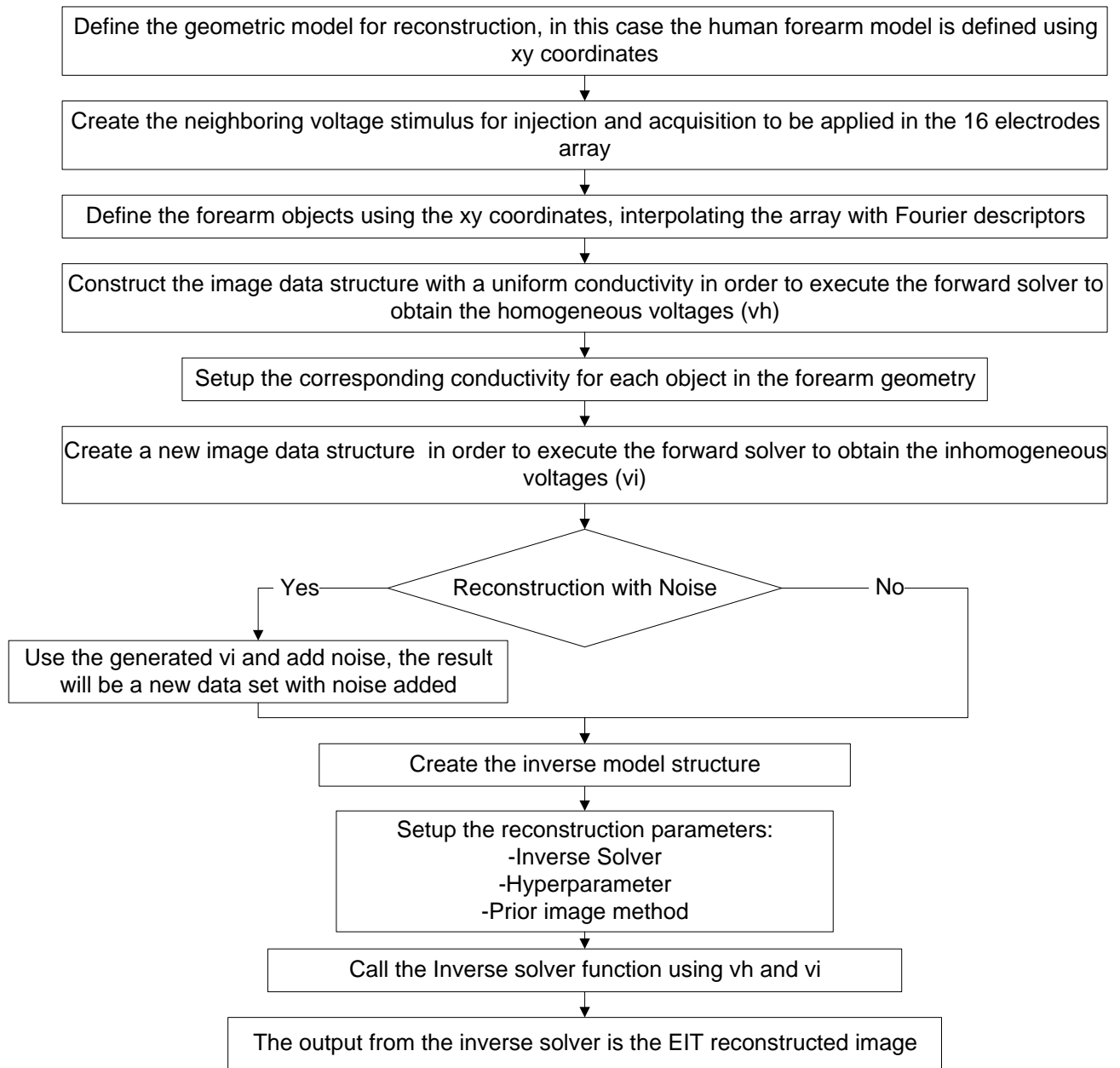


Figure 3-2. EIDORS Image reconstruction flow diagram.

In order to use EIDORS, it is necessary to install MATLAB or Octave, Appendix A shown the detail of EIDORS installation and the human forearm methodology implementation for image reconstruction. Appendix B contains the implementation of the methodology, showing the source code developed during this research.

The following information corresponds to a detailed description of each stage of the methodology for image reconstruction using EIDORS, using the flow diagram shown

in Figure 3-2. The detailed methodology is specifically for human forearm due to its complexity and geometry; however, it could be used as reference for other similar parts of the human body or industrial processes.

- Define the geometric model for reconstruction. In this case the human forearm model is defined using (x,y) coordinates.

A human forearm geometry was built in the previous work [1], where the forward problem was developed using the software platform COMSOL. Having that geometry as reference, a file exported from COMSOL (in mphtxt format) provides the (x,y) coordinates that describe the geometry components.

The exported file cannot be used directly, because it contains a lot of additional information, so the components (x,y) points were extracted and edited into an excel workbook. The information extracted to excel workbook is then plotted to check if the component is defined correctly according to coordinates contained in the exported file.

The mphtxt file organize the (x,y) points for each object, typically in several manifolds, depending of the component complexity. During this research the (x,y) points extraction was made manually, but for future work it is recommended to implement a conversion script. With the (x,y) points defined for each component, it is necessary to create the MATLAB variables in the workspace with the corresponding information. The created workspace is saved with the variables in a .m file.

- Create the neighboring voltage stimulus for injection and acquisition to be applied in the 16 electrodes array.

The current injection pattern, the current level, electrode array size and electrode ring should be defined, as well the voltage measurement pattern. In EIDORS. these definitions are made using the function called "mk_stim_patterns" and the function returns the stimulation pattern structure to form part of the forward problem implementation.

For this development, the following values were defined as default values: adjacent method for current injection and voltage acquisition, 2mA current level, electrode array

size of 16, 1 electrode ring, using as reference the parameters defined in previous work of [1]. In further sections more values and their effects will be evaluated.

- Define the forearm objects using the (x,y) coordinates, interpolating the array with Fourier descriptors

Object definition for geometry construction is generated using the (x,y) points as parameters for EIDORS function called "ng_mk_extruded_model". This function creates the extruded model using NetGen.

To create the model geometry, the "ng_mk_extruded_model" function interpolates the (x,y) points using the Fourier descriptors. Fourier descriptors need the specification of samples in order to create the desired figure and the sample value will vary depending on the object.

The sample value for each object should be defined after an analysis of the figure. If the figure is complex with irregular shapes, a higher sample value should be used.

Another limitation during object definition is the point density, if the object is too small compared with others objects, the mesh density may be out of the range for mesh creation and NetGen could crash during the process.

During the FEM model creation, the electrodes shapes and positions must be defined, as well as the maximum size of the mesh element. NetGen [33] is the mesh generator used by EIDORS, The FEM task definition could turn out a quite tedious, because if some parameters are out of the operational range, NetGen crashes or stop working while trying to generate the model. The general recommendation is, to start building the minimal model, and then to start adding internal shapes and the electrodes progressively.

- Construct the image data structure with a uniform conductivity in order to execute the forward solver to obtain the homogeneous voltages (V_h)

The platform provides structures to manage the image object definition. These data structures should be initialized with the function "mk_image" when the EIDORS

image object is created. During this creation, the complete model geometry is already defined and initialized with the same conductivity for all the internal objects.

At this point, some voltage measurements can be taken. These voltages are known as homogeneous voltages and will be used for the inverse solver function to guess the initial values for prior information definition.

- Setup the corresponding conductivity for each object in the forearm geometry

Once the homogeneous voltages are measured, the correspondence conductivity for each object should be defined; this definition is simple and it is done just with indexing the object matrix to setup the conductivity value.

- Create a new image data structure in order to execute the forward solver to obtain the inhomogeneous voltages (V_i).

Now we need to simulate the data obtained from electrodes with the defined conductivities. The simulated data is created by using the function "fwd_solve", where the forward solver is executed using the stimulus patterns and the conductivities previously defined; this data is known as the inhomogeneous voltage values.

- Reconstruction with noise: Use the generated V_i and add noise to get a new data set with noise added.

For EIT image reconstruction is a good practice to add some noise during development to evaluate the effect of non-idealities inherent to a practical implementation. Some other error sources, as the contact impedance and motion artifact, cannot be easily eliminated.

To add the Gaussian noise in the inhomogeneous voltages is used a pseudo random number generator with an identical variance.

- Create the inverse model structure

It is necessary to create the inverse model data structure to setup the corresponding parameters, this inverse model is created with the function "eidors_obj". Once the data structure has been created, the model parameters could be configured for the inverse solver function.

- Setup the reconstruction parameters

Image reconstruction is obtained by using the inverse solver function and some parameters should be configured in EIDORS before the inverse solver is executed. Among these configuration parameters, the inverse solver algorithm, the hyperparameter, and the prior regularization method are the most relevant. During the setup evaluation for this thesis research, these parameters have been swept to identify its contribution to EIT image reconstruction process, in order to define the best performance setup.

- Call the Inverse solver function using V_h and V_i

Finally, the inverse solver with the corresponding configuration is executed, with the homogeneous and the inhomogeneous voltage measurements as parameters. The inverse solver function is called "inv_solve" and returns the reconstructed image information in the model data structure.

- The output from the inverse solver is the EIT reconstructed image

To visualize the reconstructed image with the conductivities distribution it is required to execute the function called "show_fem" using the inverse model data structure as parameter. Some parameters could be set to modify the reconstructed image visualization, like the colors filtering, if the mesh is displayed or not, or the mesh color, for instance.

In the next chapter, the EIT reconstruction methodology for human forearm is analyzed and validated. All the analysis is illustrated with forearm reconstructed images, where the influence of the reconstruction parameters during the setup definition can be particularly relevant.

The developed methodology was defined after an intensive process of testing different configurations and parameters, due to the components, quantity and complexity.

Chapter 4 Analysis and validation of EIT image reconstruction methodology for human forearm

In this chapter, it is described the human forearm EIT image reconstruction methodology introduced in chapter 3. The different stages of that methodology and the effects of its parameters variation during the image reconstruction process are analyzed and validated. The best performance set up for nerve identification and the operational valid ranges for parameters used for forearm reconstruction are also evaluated.

Among the parameters validated in this chapter, the following ones can be mentioned: the forearm geometry, FEM, the mesh size, Fourier descriptors, current injection and voltage acquisition methods, hyperparameters, current injection level, noise, electrodes quantity and GN using different prior methods. In addition, the defined methodology feasibility to identify the forearm nerves will be confirmed or discarded.

4.14 Human forearm geometry

The forearm geometry implemented in COMSOL in the previous work explained in [1] is shown in Figure 4-1. This geometry is used as reference in EIDORS, but only the geometry is required as the mesh must be redefined in EIDORS.

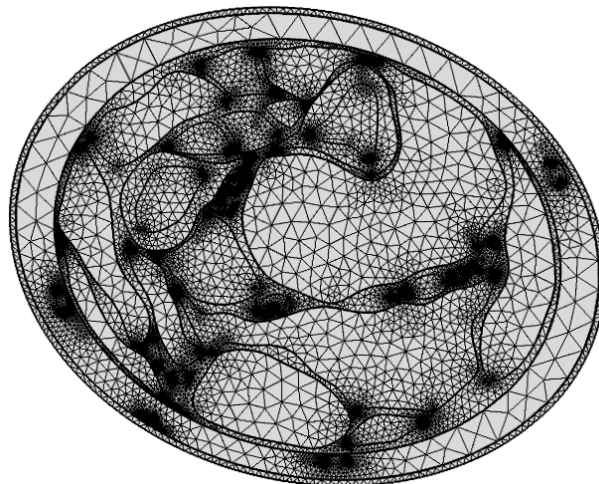


Figure 4-1. Forearm geometry and FEM used in COMSOL.

The (x,y) coordinates that describe the complete components of the geometry are extracted from the file exported from COMSOL. Then, Microsoft Excel is used to plot all the points in order to check the data obtained define properly the geometry components. That corresponds to the geometry as plotted using Excel. In this plot, it can be detected by visual inspection if any (x,y) point is out of the boundary. This is an important step to discard any missed or wrong coordinate due the conversion from COMSOL file to (x,y) coordinates that at this point needs to be performed manually.

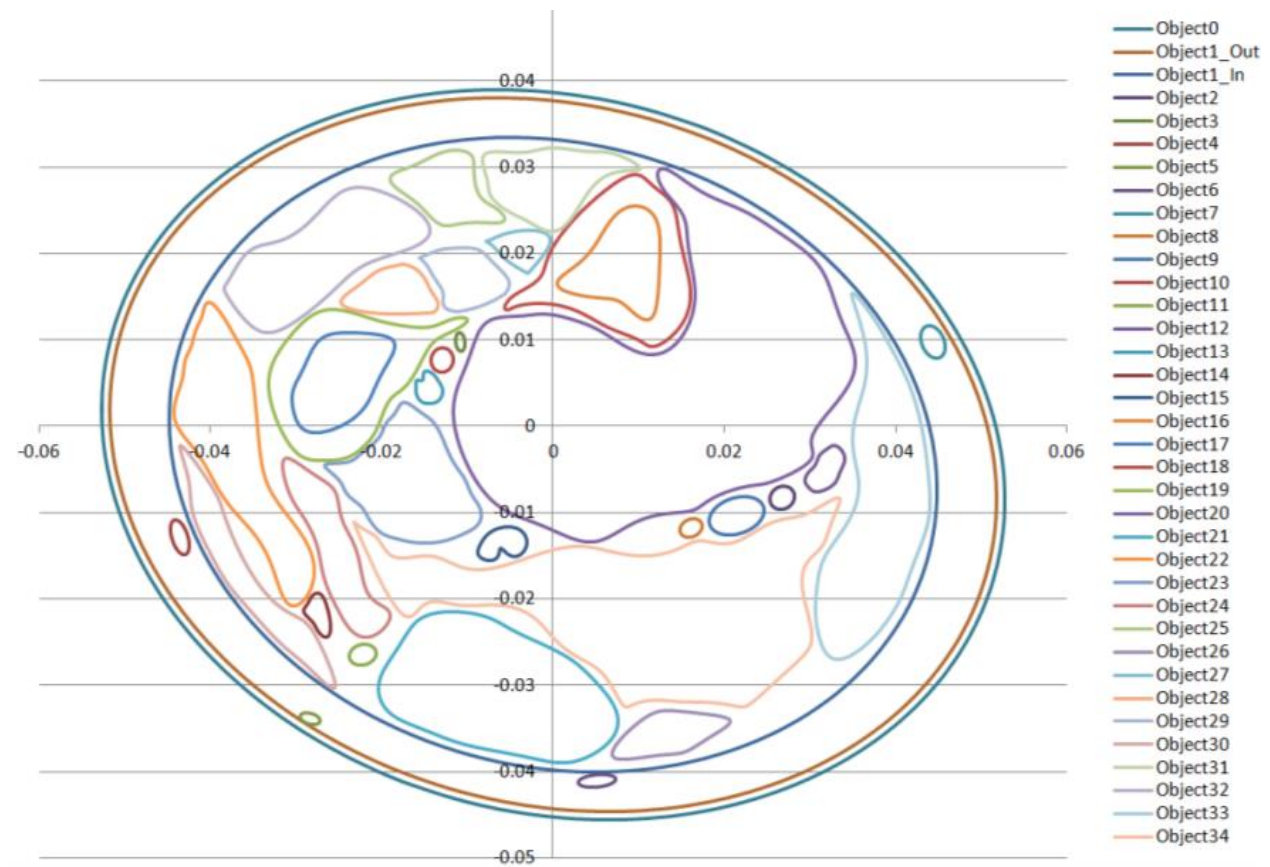


Figure 4-2. Geometry plotted using Microsoft excel and (X,Y) coordinates extracted from COMSOL file.

Having these (x,y) coordinates, the geometry is translated to EIDORS by means of variables matrices. The variables values are defined and saved in a file, this type of file is used by MATLAB to import values to its workspace. The values extracted from COMSOL are multiplied by 10000 to preserve the values in decimals places and the new values are divided by 100 in EIDORS for converting in a range from -5 to 5 in the (x,y) axis.

4.14.1 Fourier descriptors

EIDORS use (x,y) coordinates to generate the objects in the finite element model (FEM). In Figure 4-3 is shown the forearm boundary and the ulna bone; those objects have been generated interpolating the (x,y) coordinates using the Fourier descriptors.

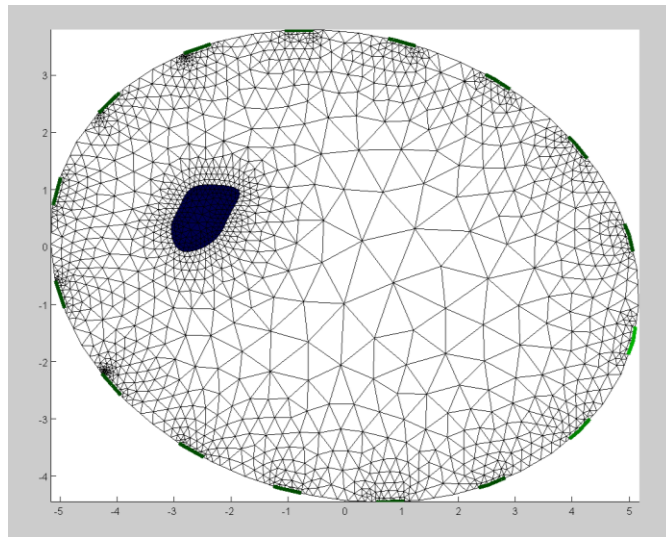


Figure 4-3. Forearm boundary and the ulna bone (object one) generated in the FEM.

The representation of this object in COMSOL is composed with 310 (x,y) points. Figure 4-4 and Figure 4-5 show a detailed view of the same object using different parameters; from (a) to (f) are the results different (x,y) samples quantity and different Fourier descriptors samples.

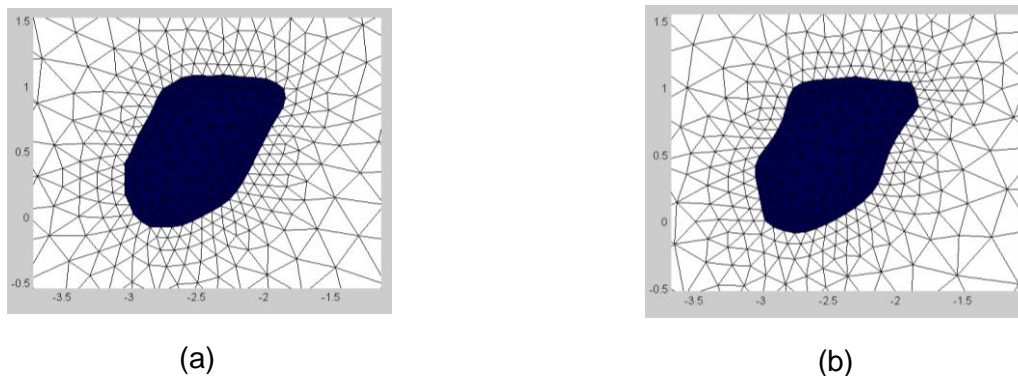


Figure 4-4. Object one model using different (x,y) samples and Fourier descriptors samples: (a) 31 Samples FD=47 and (b) 16 Samples FD= 47.

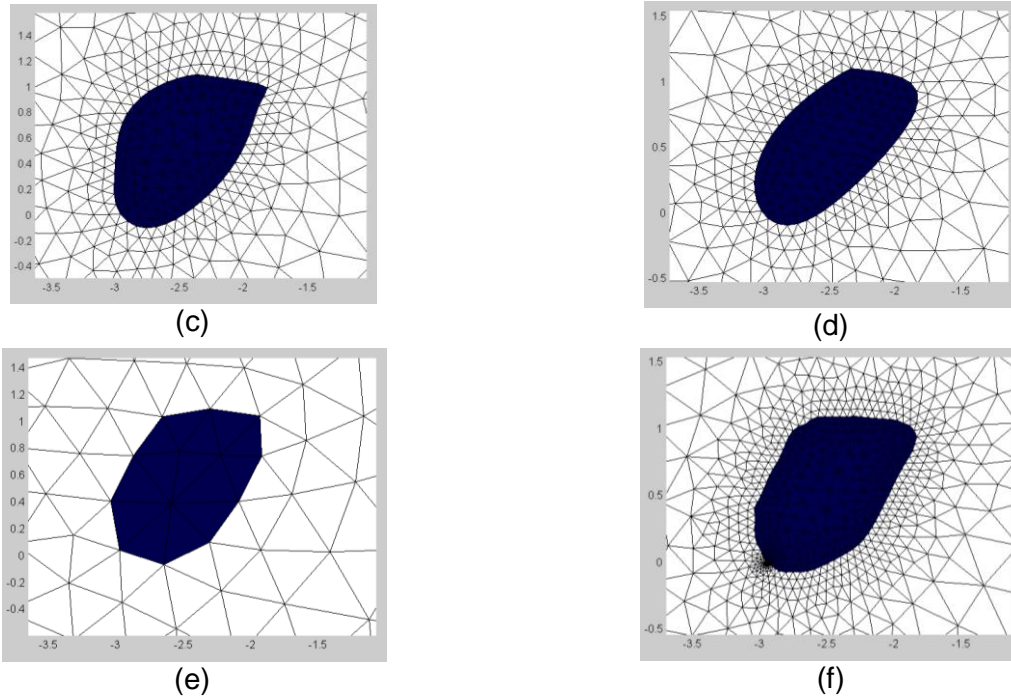


Figure 4-5. Object one model using different (x,y) samples and Fourier descriptors samples: (c) 11 Samples FD=47, (d) 6 Samples FD = 47 (e) 31 Samples FD=10 and (f) 31 Samples FD=70.

The object that preserves the original form with balanced size of elements is (f), using 31 samples and 70 FD samples. The final object implementation is detailed in Figure 4-6 (a) and it is generated using 310 samples and 20 FD samples. This definition was selected to conserve the object shape very close with respect to the original, but at the same time avoiding high element density in FEM. This analysis was done for each object in the model, in order to generate a complete FEM where the original object geometry is preserved with a reasonable accuracy compared with the reference geometry Figure 4-6 (b).

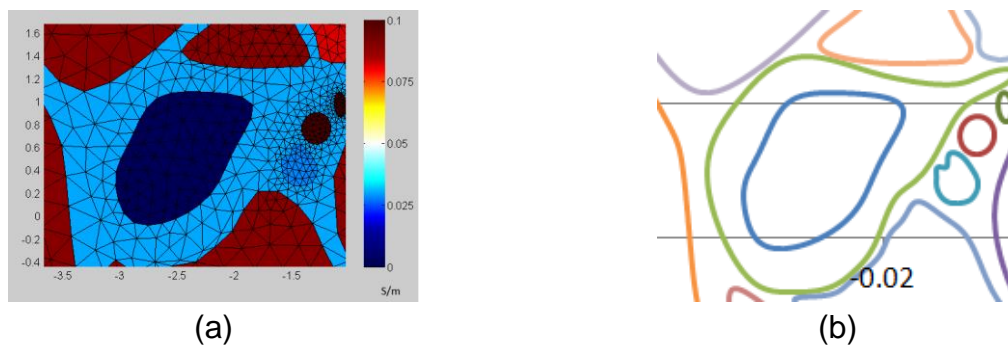


Figure 4-6. a) Object one model using 310 (x,y) samples and 20 Fourier descriptors samples and b) reference object plotted in excel.

4.14.2 Geometry with tissue conductivities

The human forearm geometry is extruded using the EIDORS function "ng_mk_extruded_model", after exporting all the objects using the (x,y) coordinates in Matlab and assigning the conductivities for the human forearm employing the values defined in Table 2-2. This result is shown in Figure 4-7, the colored bar at right side corresponds to the conductivity representation, units are S/m.

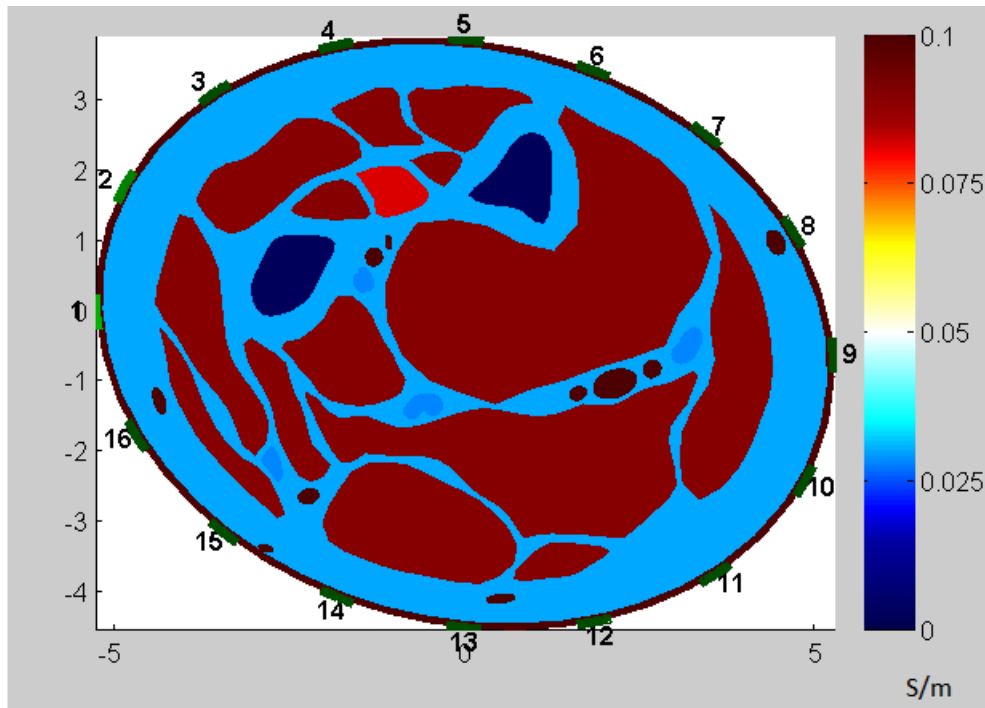


Figure 4-7. Human forearm geometry with conductivities definition.

Comparing the resultant geometry in Figure 4-7 with the one defined in Figure 2-20, it seems that the nerves, cortical bone, and some others object are missing; however, these objects are already defined. These tissues seem to be hidden due to the fact that their conductivities are similar for all of them, with a value of around 0.03 S/m.

The geometry imported to EIDORS from COMSOL after its processing, is congruent and therefore it is a suitable geometrical model to apply in / to the EIT image reconstruction process.

4.14.3 Finite Element Method (FEM)

In EIT the forward solution is determined with the knowledge of Newman and Dirichlet boundary conditions; since it cannot be obtained analytically for any random geometry, a numerical method such as the FEM is needed. The FEM for the human forearm with the maximum size of mesh elements configured in 0.11 is shown in Figure 4-8. This FEM is composed of 104466 elements and it requires a processing time of 85.197 seconds for meshing it with a computer Core i7 processor, 8GB of RAM memory. The RAM consumption during the FEM processing has reached the 100% of 8GB, to use EIDORS you will need at least 2GB RAM.

The FEM generator is the process that takes more time during EIT image reconstruction, the FEM generating time is directly proportional to the elements quantity.

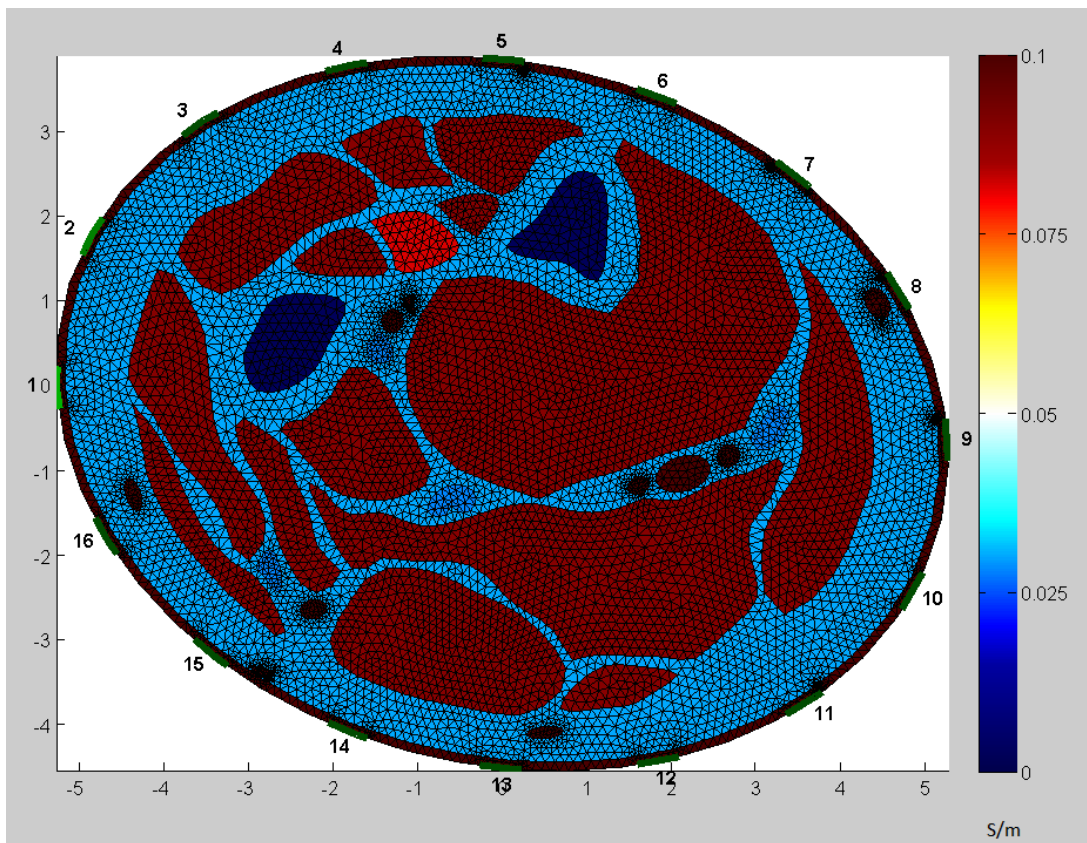


Figure 4-8. Human forearm FEM with maximum mesh size of 0.11.

Smaller elements can be defined in the FEM, as shown in for mesh size of 0.05 cm, but EIDORS platform is not capable of perform the image reconstruction and crashes while processing. For this reason, the minimum value for maximum mesh size is 0.11 cm.

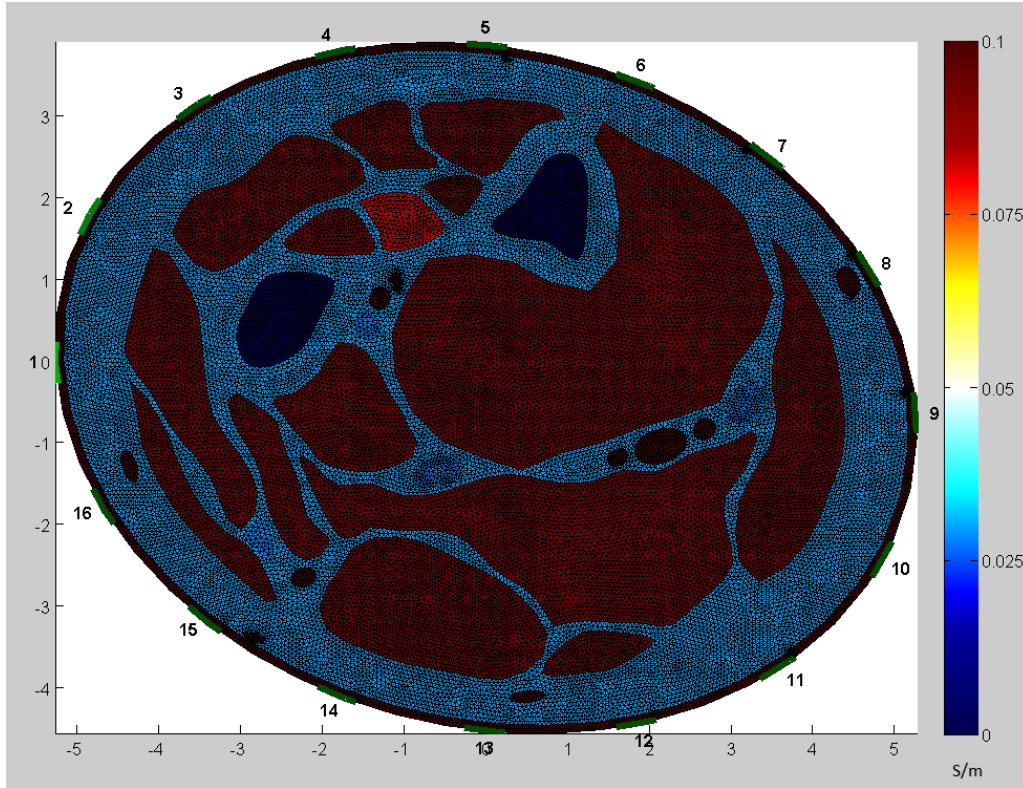


Figure 4-9. Human forearm FEM with mesh size of 0.05 cm.

4.15 Current injection and voltage acquisition method

A reference FEM with just two objects (the ulna and radius bone marrows) is shown in Figure 4-10. It is employed to evaluate the performance between current injection and voltage acquisition methods.

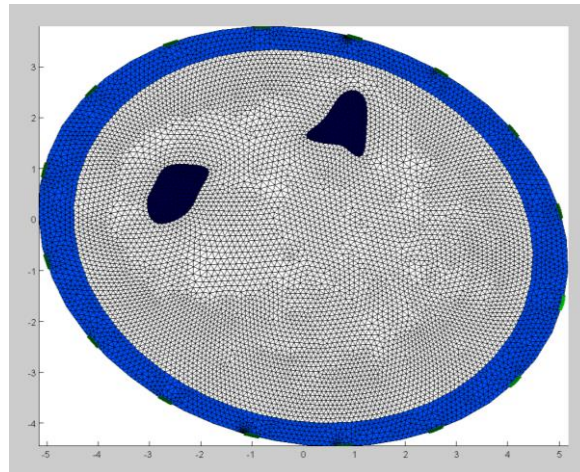


Figure 4-10. FEM with two objects, used as reference for evaluation of injection and acquisition methods.

Figure 4-11 corresponds to opposite and neighboring methods results for the FEM with the two objects. According to these figures, the best performance is obtained with the neighboring method. These results are congruent with the theory, because opposite method is preferred when the object is located in the center and neighboring method performance is higher in the areas located near to the boundaries. For this reason, the selected method for current injection and voltage acquisition is the neighboring method.

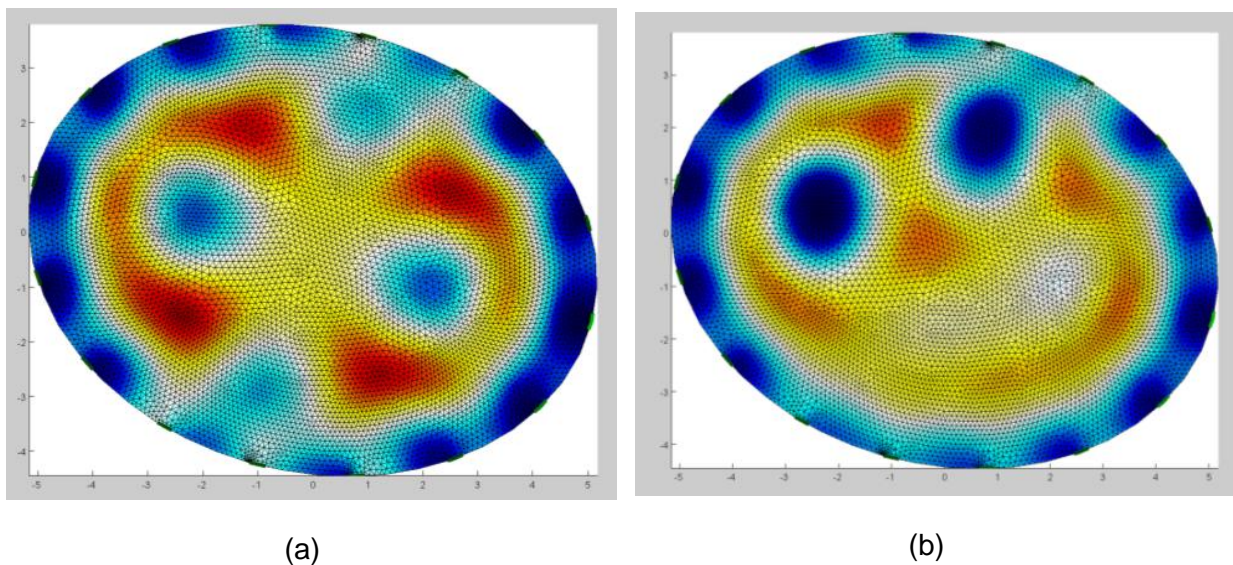


Figure 4-11. Current injection and voltage acquisition patterns: (a) Opposite method and (b) neighboring method

The first four injections stimulus for the neighboring injection pattern sequence in a 16-electrodes array is observed in Figure 4-12. From left to right the first current injection is through electrodes 1 and 2, then 2 through 3, so on until 16 through 1.

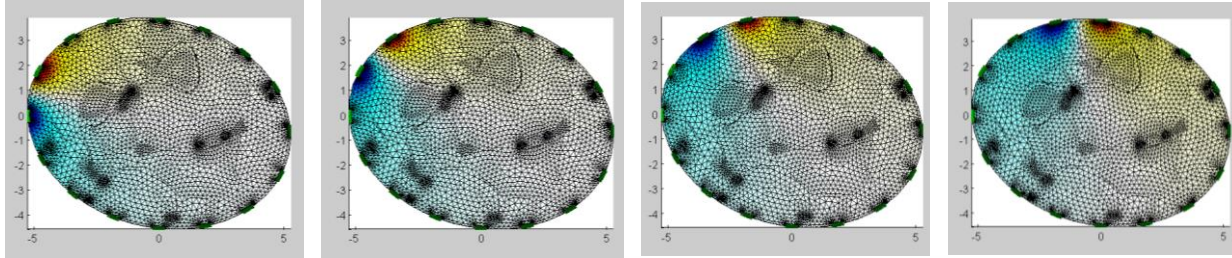


Figure 4-12. Current injection pattern for neighboring method.

The voltage measured in electrodes after current injection in the FEM without any object or inner conductivity definition is called homogeneous voltage. The voltage measured after object conductivity definition is called inhomogeneous voltage. In next figure homogeneous voltage, inhomogeneous voltage, and their difference is plotted.

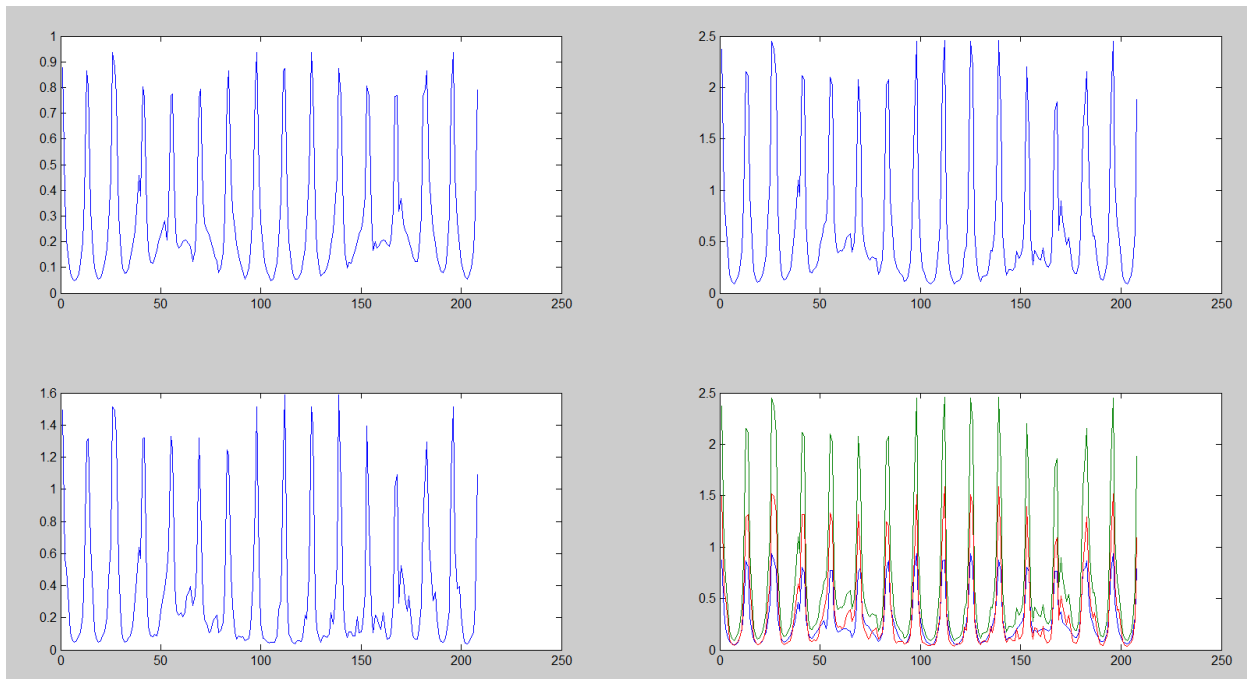


Figure 4-13. Homogeneous voltages (V_h) [Left-Top], Inhomogeneous voltages (V_i) [Right-Top], their difference ($V_i - V_h$) [Left-Bottom] and finally all plots in the same image [Right-Bottom].

From Figure 4-13 is observed that there is a difference of voltage between the homogenous voltage and the inhomogeneous. This difference confirms the change in the objects conductivity after object conductivity definition.

4.16 Current lines

The current lines during the current injection stimulus in electrode 1 and 2 are illustrated in Figure 4-14. Inside the image, it is detailed the objects with more conduction like the blood in veins.

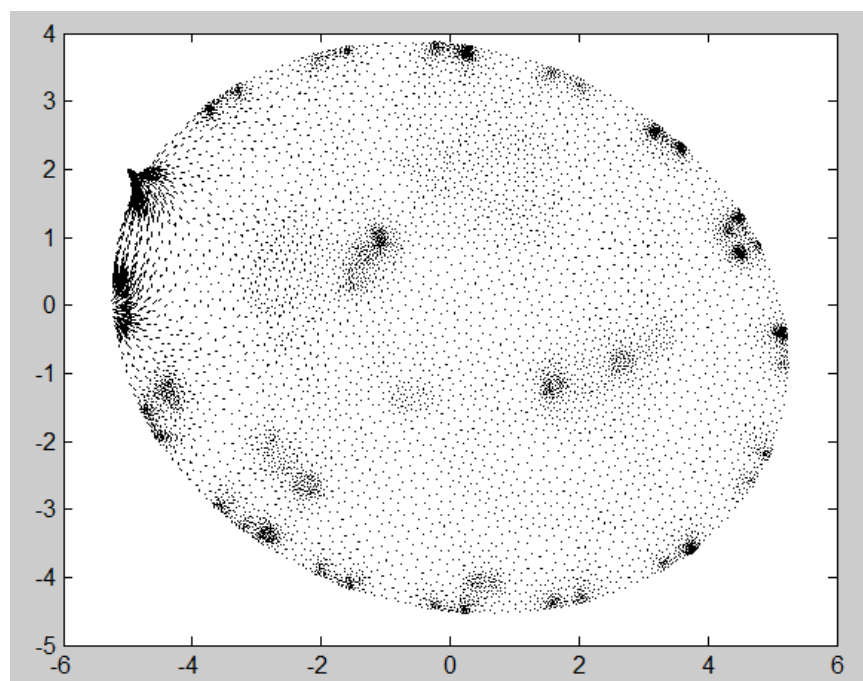


Figure 4-14. Current lines generated during injection in electrode 1 and 2.

Figure 4-15 presents a detailed view of electrodes 1 and 2 for better appreciation of current lines.

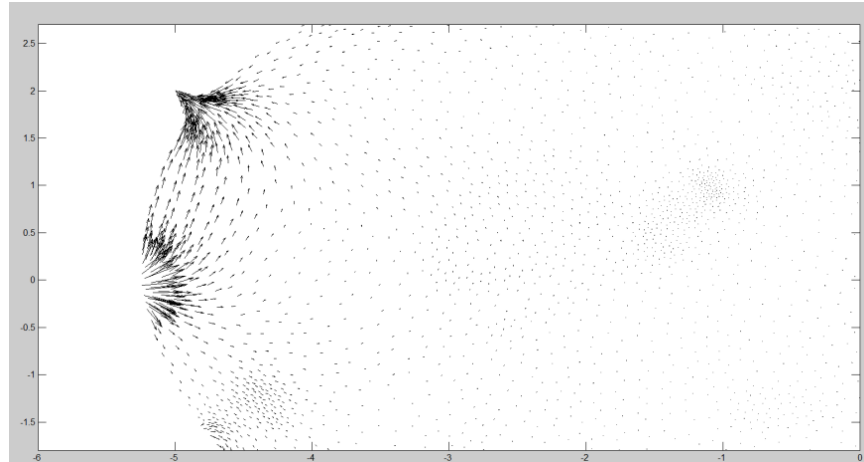


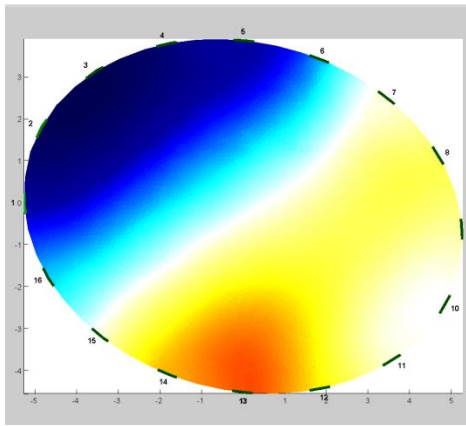
Figure 4-15. Detailed view of current lines focus in electrode 1 and 2.

As observed in Figure 4-15, the current lines flow goes from negative to positive as expected in direct current. The electrode with negative polarity is located in the lower area in the coordinate (-5,0) and the electrode with positive polarity is located in the coordinate (-5,2) approximately.

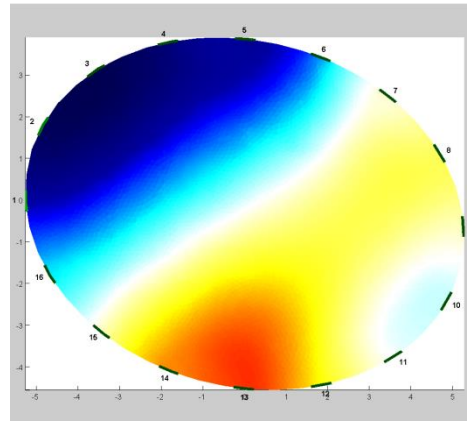
4.17 Image reconstruction

4.17.1 Hyperparameter selection

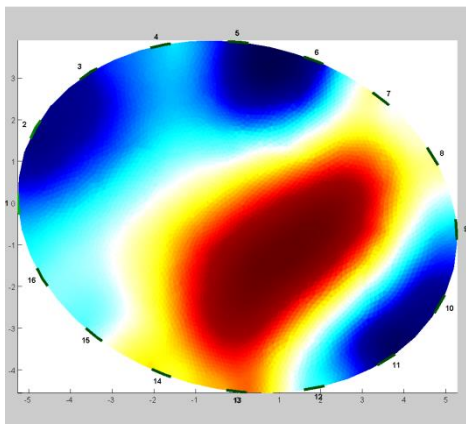
In image reconstruction, the hyperparameter is used for the regularization to calculate a stable and accurate solution. For this thesis the heuristic method was used and according to the images shown in Figure 4-16 and Figure 4-17, the best hyperparameter found was $2 \cdot 10^{-3}$ (shown in (g)) because allows to identify the position of the nerves, bones and muscles better than the others. The hyperparameter selected is $2 \cdot 10^{-3}$.



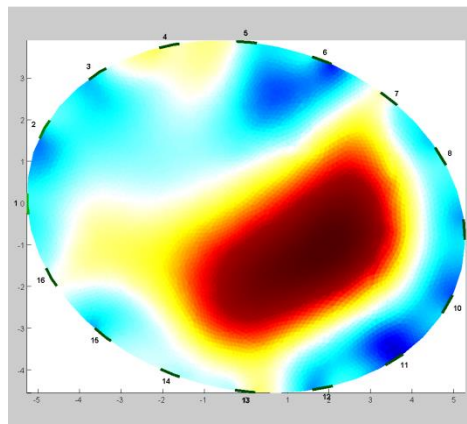
(a)



(b)



(c)



(d)

Figure 4-16. Image reconstructions using different hyperparameters: (a) hyperparameter = 3, (b) hyperparameter = 1, (c) hyperparameter = 0.1 and (d) hyperparameter = $2 \cdot 10^{-2}$. (1-2)

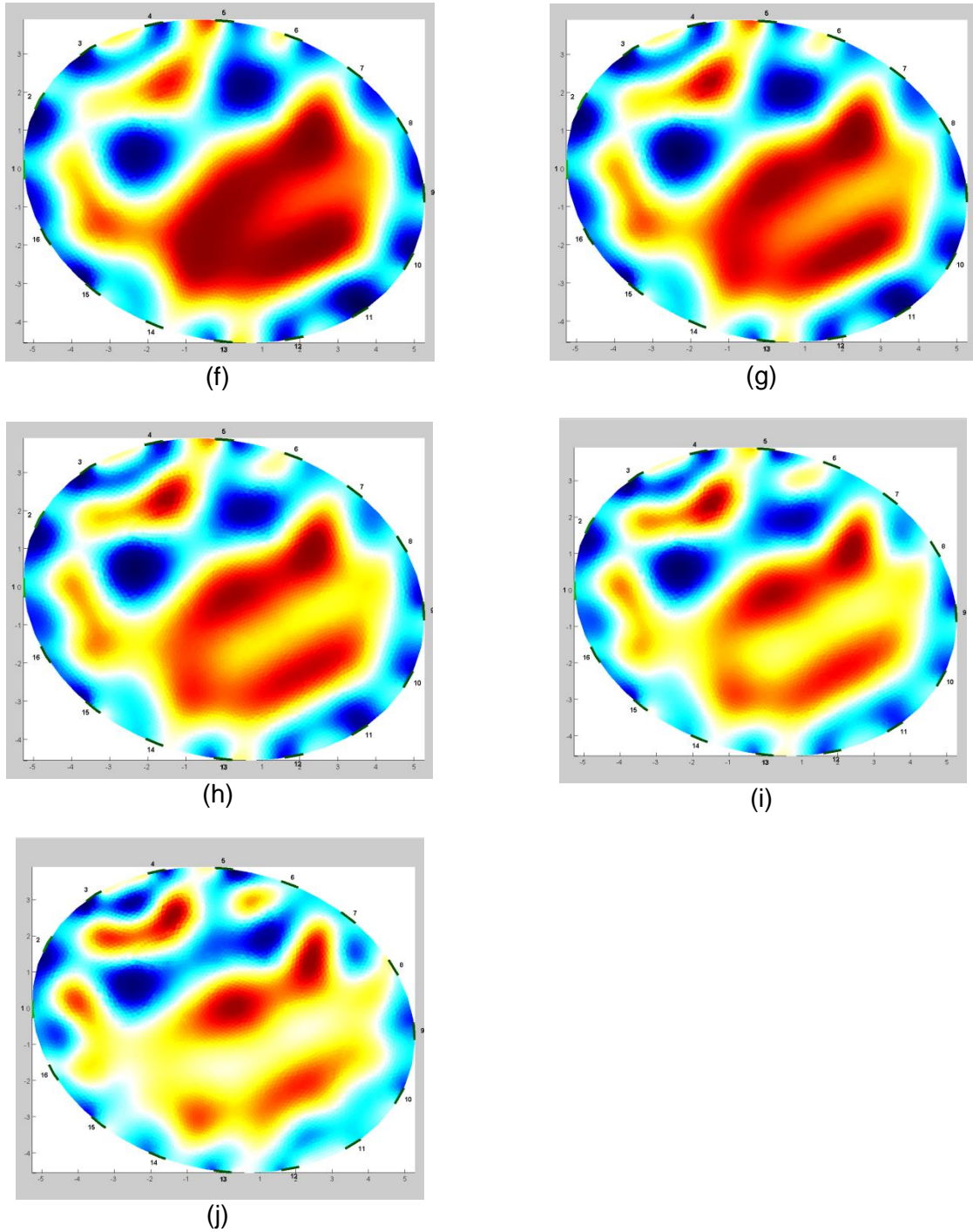


Figure 4-17. Image reconstructions using different hyperparameters: (f) hyperparameter = $3 \cdot 10^{-3}$, (g) hyperparameter = $2 \cdot 10^{-3}$, (h) hyperparameter = $1.5 \cdot 10^{-3}$, (i) hyperparameter = $1 \cdot 10^{-3}$ and (j) hyperparameter = $5 \cdot 10^{-4}$. (2-2)

4.17.2 Current level

For EIT, conducting electrodes are attached to the skin of the subject and a maximum current of 5mA can be applied within the safety limits. Images shown in Figure 4-18 have been generated injecting different currents from 0.1mA to 5mA. The best image reconstruction for nervous identification was reached using 1mA, as it is shown in image (c). Using a current of 0.1mA a poor reconstructed image is generated with not detail in components. With higher current level near to 5mA the reconstructed image performs a very low spatial resolution, since only the higher intensity points are distinguishable.

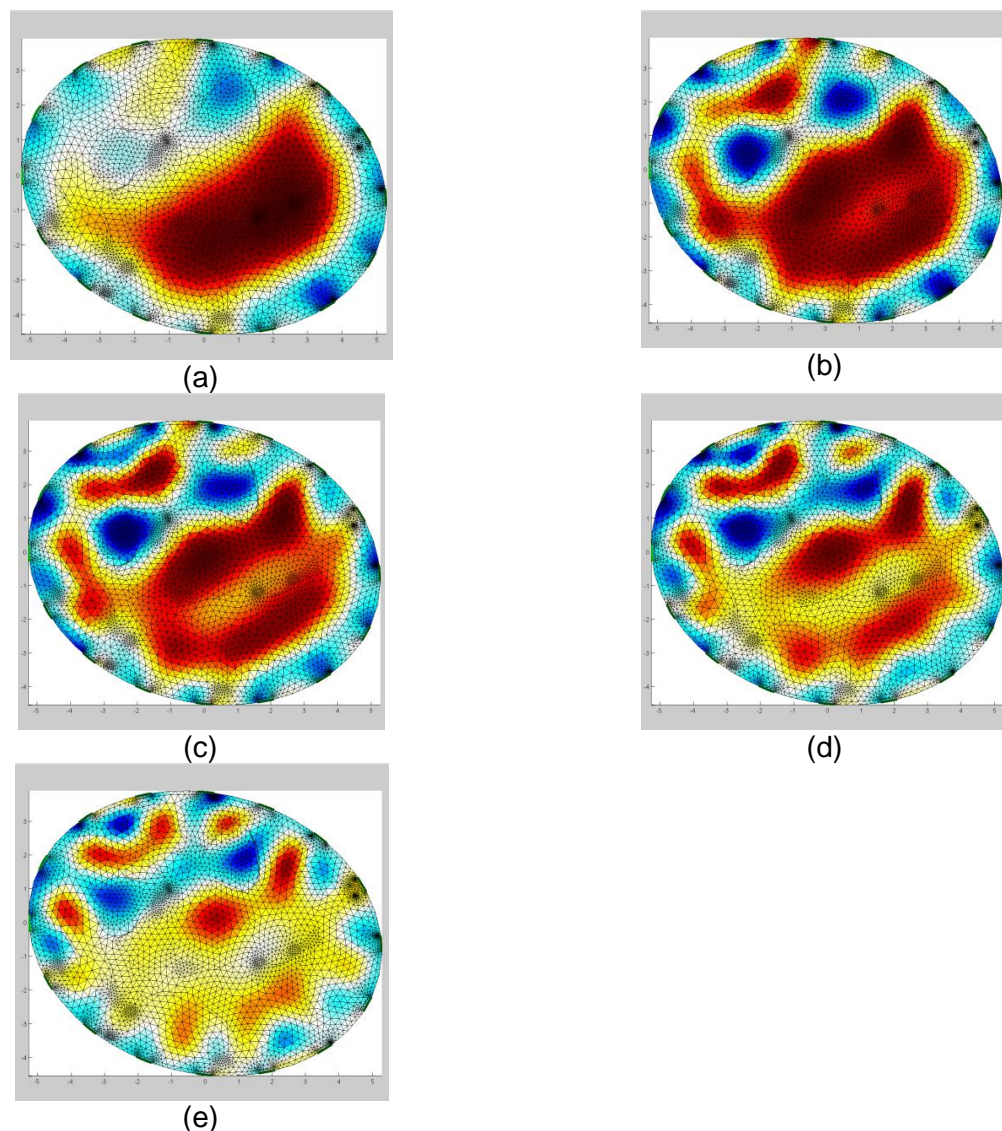


Figure 4-18. Image reconstructions using different current levels in injection: (a) 0.1mA, (b) 0.5mA, (c) 1mA, (d) 2mA and (e) 5mA.

4.18 EIT algorithm and prior information methods

For this thesis purposes Back-Projection and Gauss Newton algorithms were evaluated. Back-Projection was discarded to be implemented, because according to the theory the performance in Gauss Newton is better in boundaries due it uses the FEM allowing different shapes; while Back-Projection domain is for circular shapes mainly. Gauss Newton is mainly intended to find the lowest value between the predicted data and measured data. The predicted data or prior information can be calculated using different methods. Figure 4-19 and Figure 4-20 show the results of implementations using different prior methods as Tikhonov, NOSER, Laplace and Total Variation. The reconstruction without noise and with SNR of -25dB is also compared.

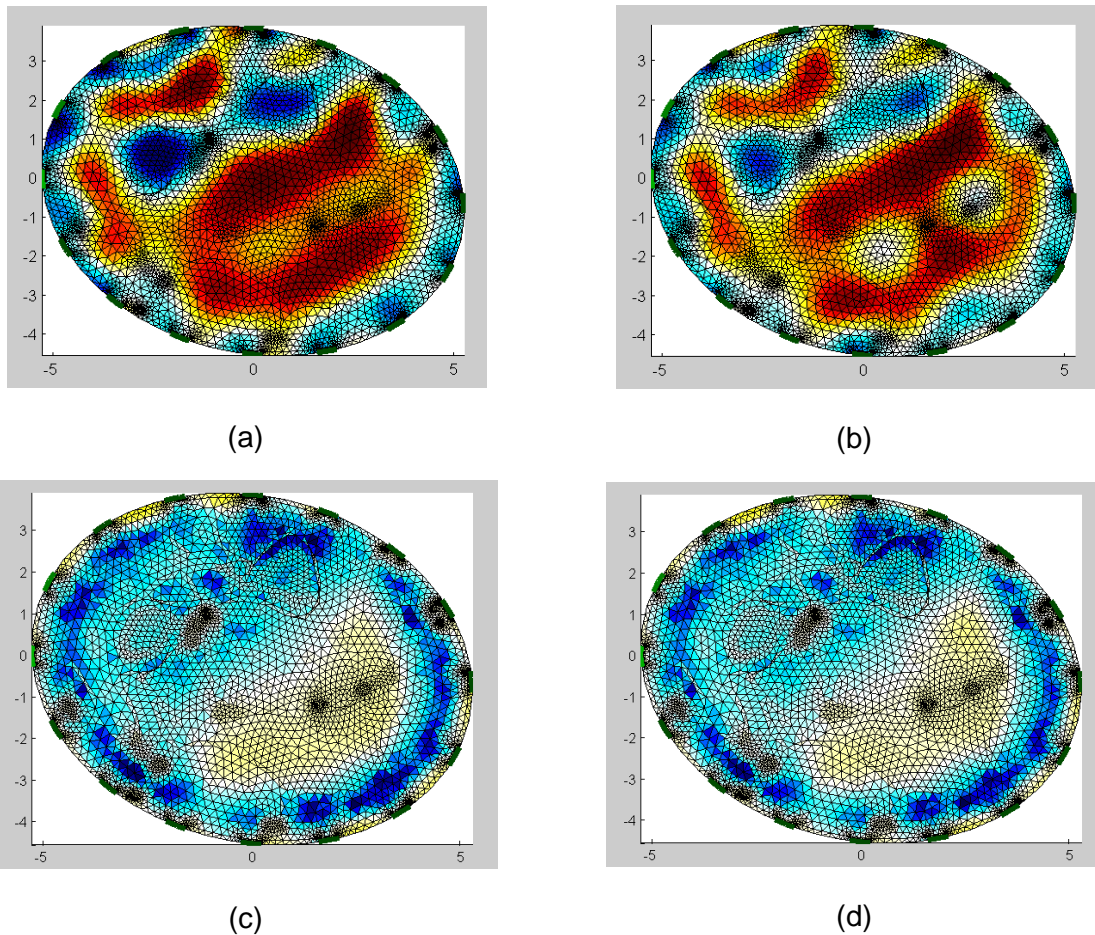
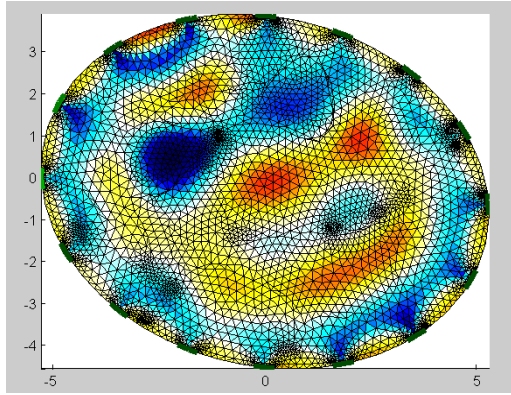
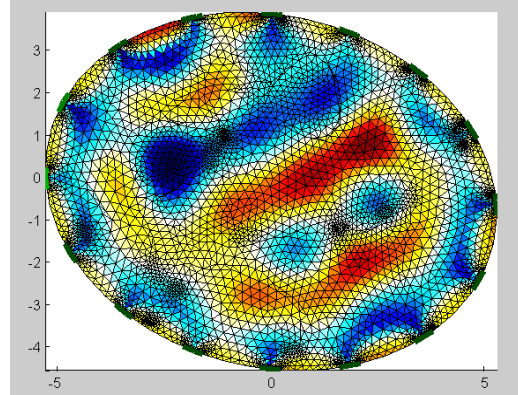


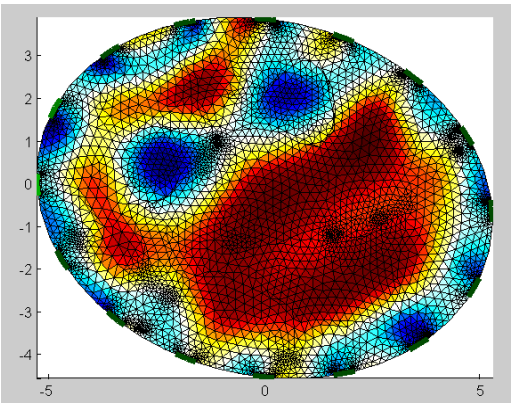
Figure 4-19. Image reconstructions using different prior information methods: (a) Default, (b) Default with 25dB SNR, (c) Tikhonov prior and (d) Tikhonov prior with 25dB SNR.



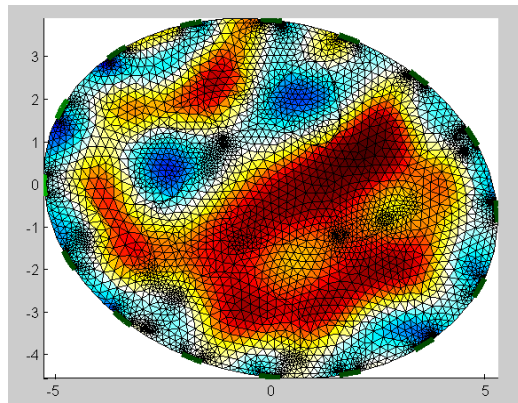
(e)



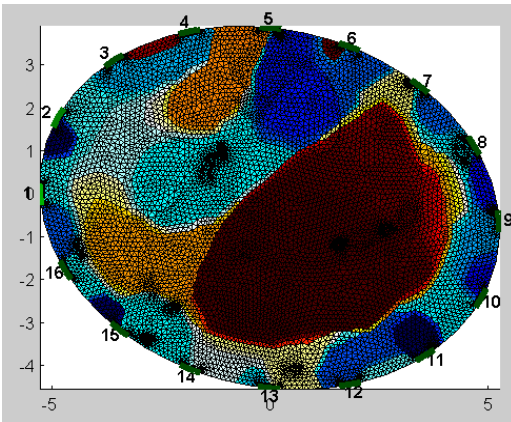
(f)



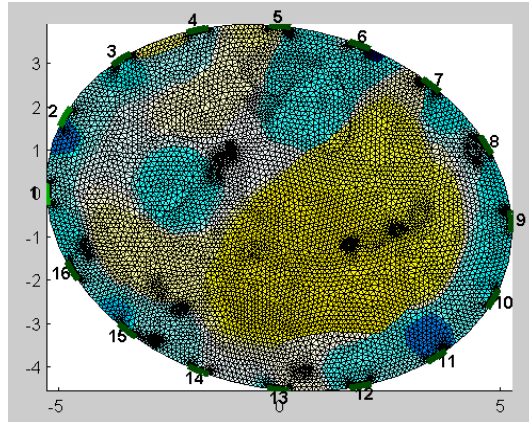
(g)



(h)



(i)



(j)

Figure 4-20. Image reconstructions using different prior information methods: (e) NOSER prior, (f) NOSER prior with 25dB SNR, (g) Laplace prior, (h) Laplace prior with 25dB SNR, (i) Total Variation prior and (j) Total Variation prior with 25dB SNR.

Contrasting ideal conditions with noisy and real environment, adding noise in the algorithm comparison, it gives a more realistic interpretation of results in order to select the best algorithm performance in a controlled environment. Noise effect change the image reconstruction results significantly.

As observed in Figure 4-19 and Figure 4-20, bones and muscle can be identified in the human forearm image reconstruction using Tikhonov, NOSER, Laplace and Total Variation. Tikhonov prior showed a similar image reconstruction with and without noise. Both of them identify the zone with muscles and the zone where the bones are located but the nerves or blood cannot be identified.

NOSER prior displays a poor image reconstruction in both with and without noise, bones are the only objects identified clearly. Laplace prior generates the most accurate image reconstruction, more accurate than Tikhonov, NOSER or Total Variation, in both conditions with noise and without, presenting a smoothed image where the bones, muscle, blood and the most important nerves are clearly identified. Total variation prior perform a very sharp image reconstruction, bones and muscles zones are very clear and the image reconstructed with noise is very different compared with the image without noise.

After comparing and analyzing the performance obtained with the different priors with and without noise, it is concluded that the best results for human forearm image reconstruction is obtained using Laplace prior information with the Gauss Newton algorithm to resolve the inverse problem.

4.18.1 Noise effect

In order to have a reliable human forearm image reconstruction, it is necessary to study the effect of noise in measurements to define the minimal signal to noise value (SNR) for a useful reconstructed image. For this research a pseudo random number generator is used to add Gaussian noise to each measurement. The results of image reconstruction with noise are shown in Figure 4-21, Figure 4-22 and Figure 4-23.

According to [34], the central limit theorem means that independent identical Gaussian noise is a good approximation to the true statistics of the data error. However, in electrical imaging, there are many sources of error including variable contact impedance, motion, variable surface geometry, etc.; all of which produce correlated errors in the data. These effects are out of the scope of this thesis.

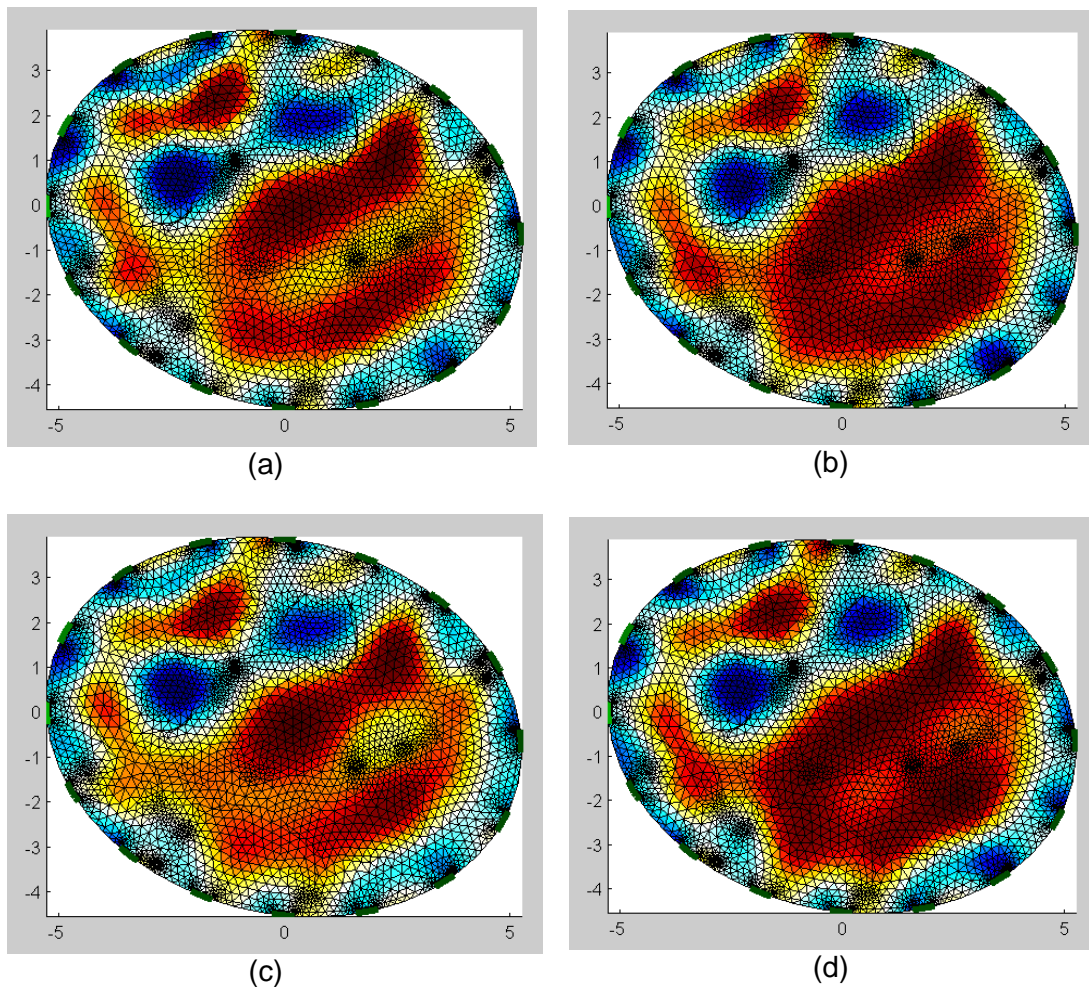


Figure 4-21. Image reconstructions using different signal to noise values with default and Laplace priors: (a) Default with SNR = 40dB, (b) Laplace with SNR = 40dB, (c) Default with SNR = 35dB, (d) Laplace with SNR = 35dB. (1-3)

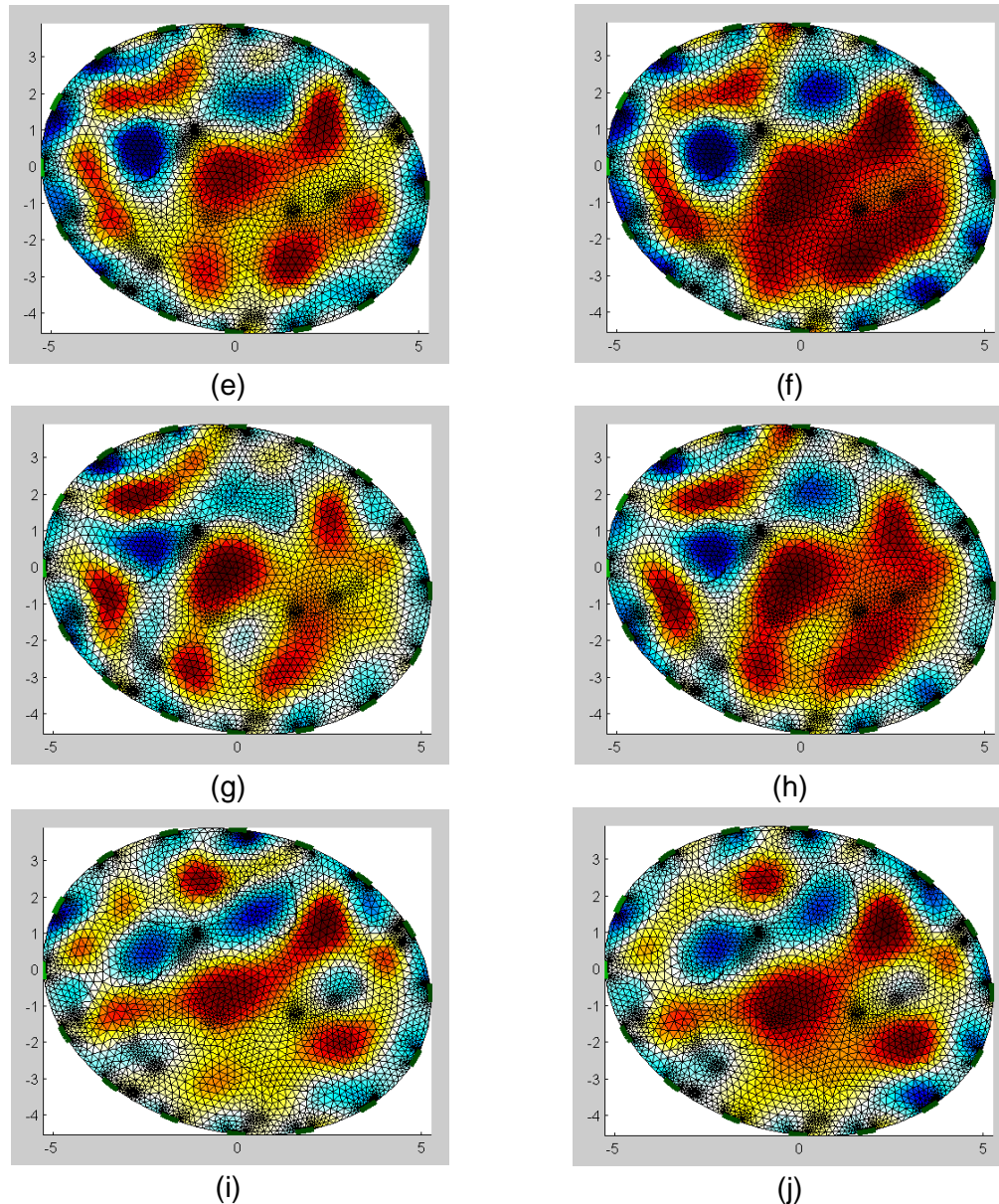


Figure 4-22. Image reconstructions using different signal to noise values with default and Laplace priors: (e) Default with SNR = 30dB, (f) Laplace with SNR = 30dB, (g) Default with SNR = 25dB, (h) Laplace with SNR = 25dB, (i) Default with SNR = 20dB and (j) Laplace with SNR = 20dB. (2-3)

Analyzing the obtained results in Figure 4-21, Figure 4-22 and Figure 4-23 the minimal SNR is defined as 30dB (image (e) and (f), for default and Laplace priors respectively). With Laplace prior and SNR lower than 30dB the reconstructed image is not useful because the spatial resolution is too low to identify forearm components using the conductivity distribution image.

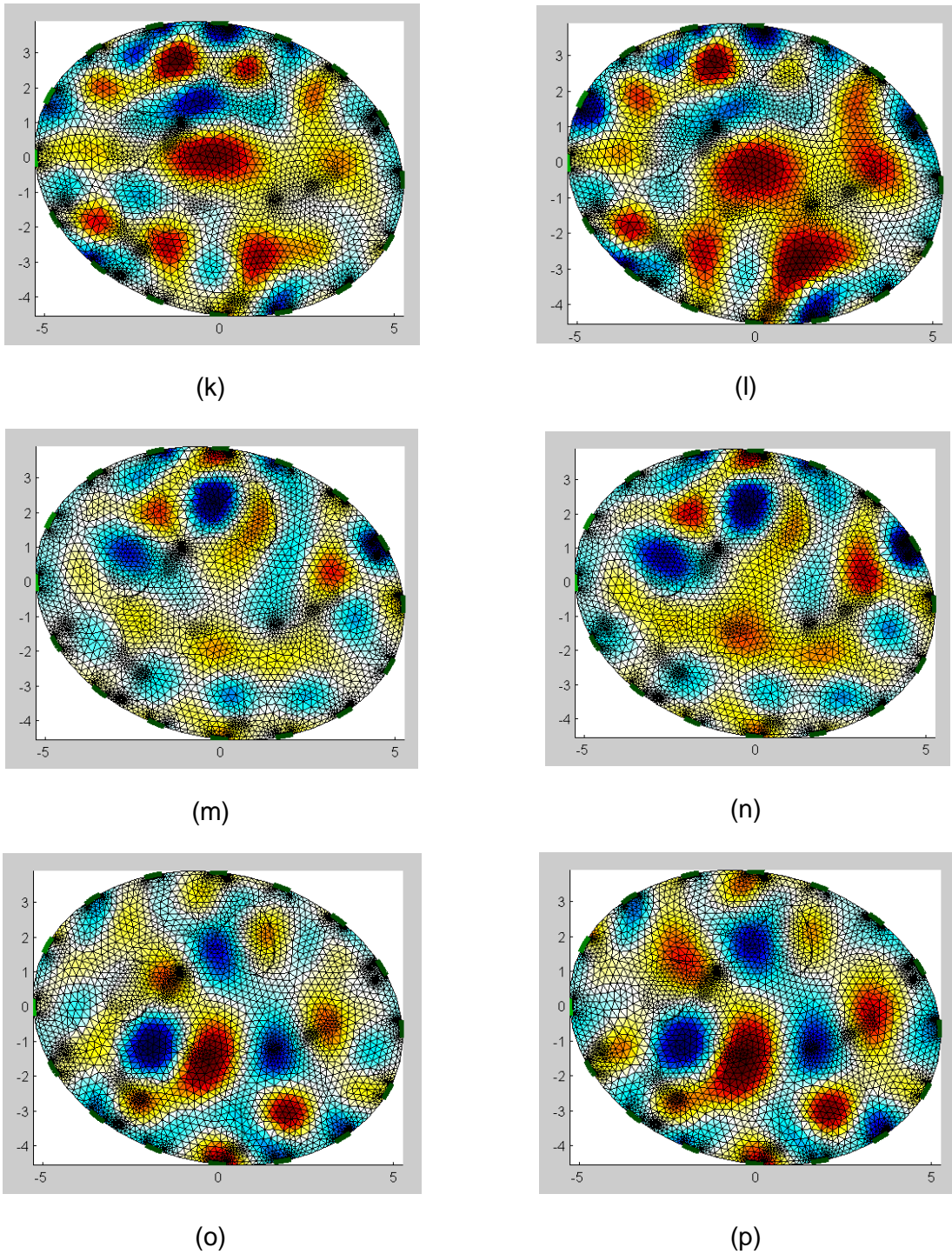


Figure 4-23. Image reconstructions using different signal to noise values with default and Laplace priors: (k) Default with SNR = 15dB, (l) Laplace with SNR = 15dB, (m) Default with SNR = 10dB, (n) Laplace with SNR = 10dB, (o) Default with SNR = 5dB and (p) Laplace with SNR = 5dB. (3-3)

4.19 Validation and evaluation of human forearm EIT methodology

4.19.1 Feasibility of EIT image reconstruction for nerve identification based on EIDORS toolkit

Once the best configuration for forearm EIT image reconstruction methodology is defined for 16 electrodes array (hyperparameter of $2 \cdot 10^3$, 1mA of current injection and Laplace prior information), it is necessary to evaluate the reconstructed images. In Figure 4-24 reconstructed output without noise (a) and with 30dB SNR (b) are shown. The reference forearm is depicted in (c) and the reconstructed image with the reference image superimposed in (d).

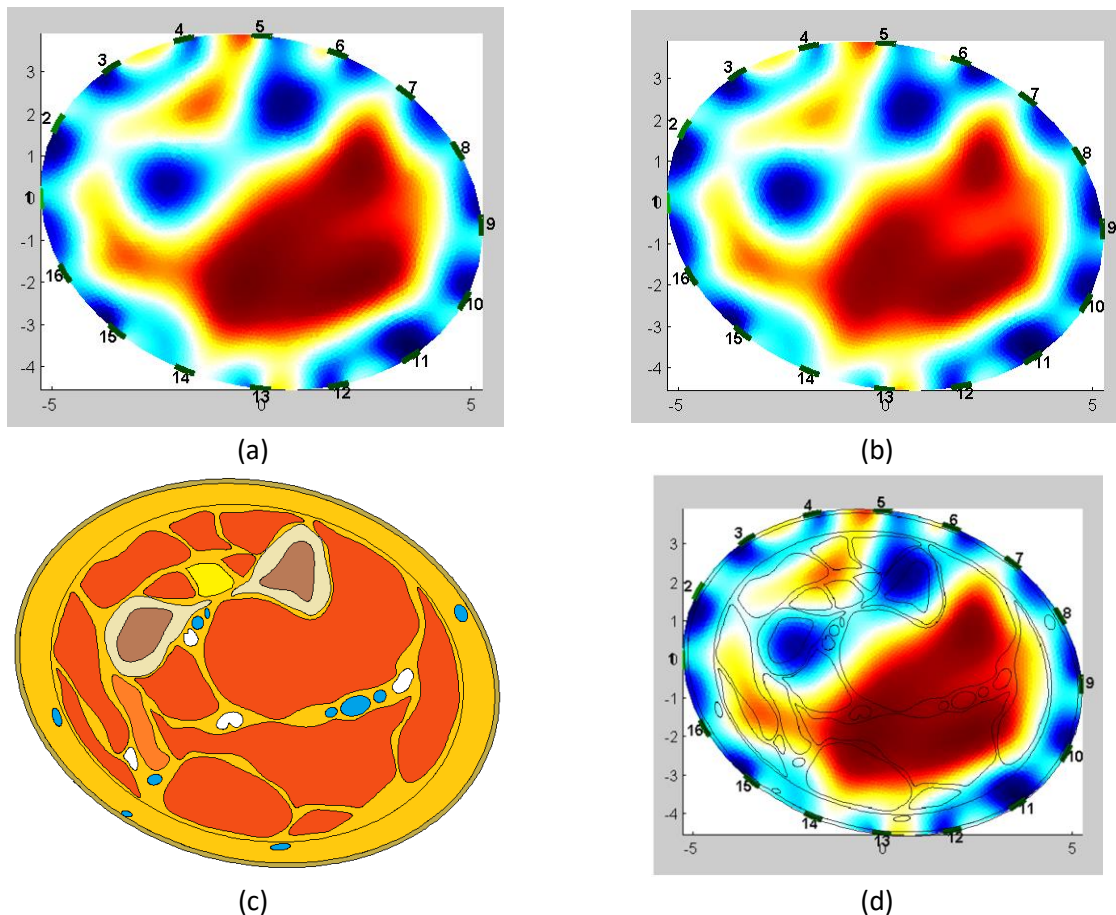


Figure 4-24. Human forearm EIT image reconstruction using the recommended parameters according with previous sections; (a) Image without noise, (b) Image with 30dB SNR, (c) human forearm reference image and (d) reconstructed image with forearm reference image superimposed.

In the reconstructed images shown in Figure 4-24 (d), two bones in blue color are clearly identified; the yellow, orange and red areas are associated with the muscular tissues; but the most important elements for the application target are the four nerves white colored in Figure 4-24 (c). Nerve location could be interpolated using the bones and muscles information, but using the impedance map, nerve identification was not feasible with the reconstructed image through the EIDORS toolkit.

In order to improve the reconstructed image spatial resolution, three parameter modifications were evaluated, although it do not necessarily resemble a reasonable practical implementation. The first is to increase the array electrode quantity; the second is to increase the injected current more than the safety range for medical applications and the last one is to apply some post processing by adding some filters for the reconstructed image.

4.19.2 Effect of increasing the electrode number

In this section, the effect of increasing the electrode number is evaluated. Using more electrodes would allow acquiring more information from subject under test, although the practical implementation would be very challenging because of the electrode sizes and the physical array. With 32 electrodes and more information, the spatial resolution is more accurate than using 16 electrodes. In Figure 4-25 are shown two different reconstructions using different electrodes quantity: (a) 16 electrodes and (b) 32 electrodes.

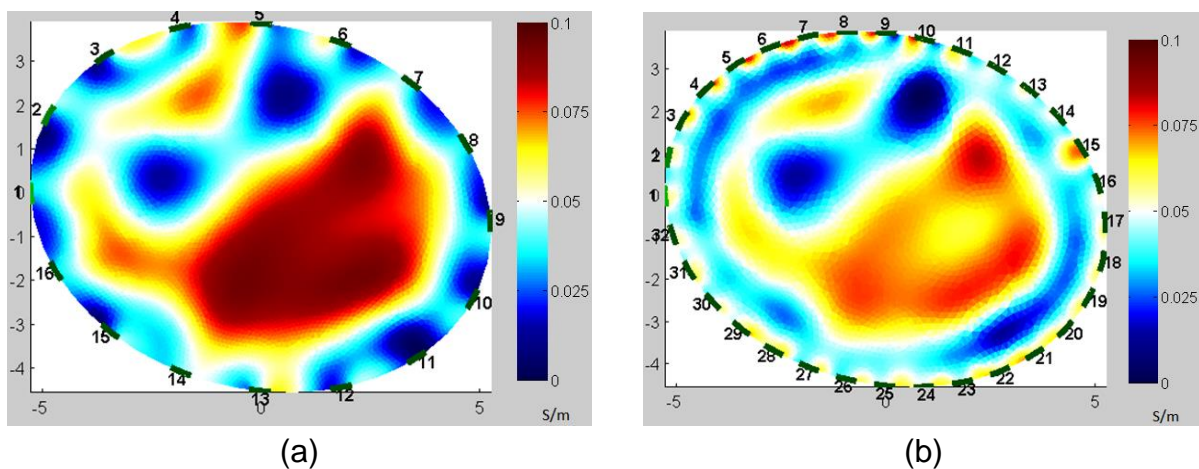


Figure 4-25. Human forearm EIT Image reconstruction using different electrode quantity in electrode array; (a) 16 electrodes and (b) 32 electrodes.

By increasing the electrodes quantity from 16 to 32, the spatial resolution will improve. This fact can be demonstrated and compared easily by observing the reconstructed image in Figure 4-25 (b), where a vein is exposed near o electrode 15, whereas in the reconstructed image in Figure 4-25 (a), the vein is not in the impedance map. However, increasing the electrode quantity still is not enough to identify the nerves in the reconstructed image.

A 32 electrodes array implementation is mechanically complicated for human forearm but it is not impossible. More than 32 electrodes would impose serious limitations, and for that reason further analysis with more electrodes was not conducted.

4.19.3 Effect of filtering the EIT output image

The main objective of this research is to define the best performance setup to obtain an EIT human forearm reconstructed image that allows to locate the nerves position. The previous images shown in Figure 4-25 are displayed with an impedance map centered in 0.05 S/m using a range from 0 to 0.1 S/m in a linear scale. In these images, different elements of the human forearm, such as muscles, bones, blood, fat can be identified, but not the nerves.

In order to identify nerves in the impedance map, it is necessary to evaluate the reduction of the display range. In Figure 4-26, four different images with a display filter are shown using a range from 0.04 to 0.06 S/m, where the nerves should be placed. The images where reconstructed using different current values and electrode quantity in order to compare the results. Nevertheless, nerve location is not clear in the reconstructed images. In the Figure 4-26 the blue color is for the tissues with a conductivity lower than 0.04 S/m and red color for conductivity higher than 0.06 S/m.

For images (c) and (d) in Figure 4-26, using 32 electrodes, a clear identification of muscles is obtained. Nerve location could be interpolated using the muscles information but the nerve itself is not identifiable in the impedance map. The two holes inside the muscles mark the zone where the inner nerves and some veins are located but is not possible to identify nerves and veins separately.

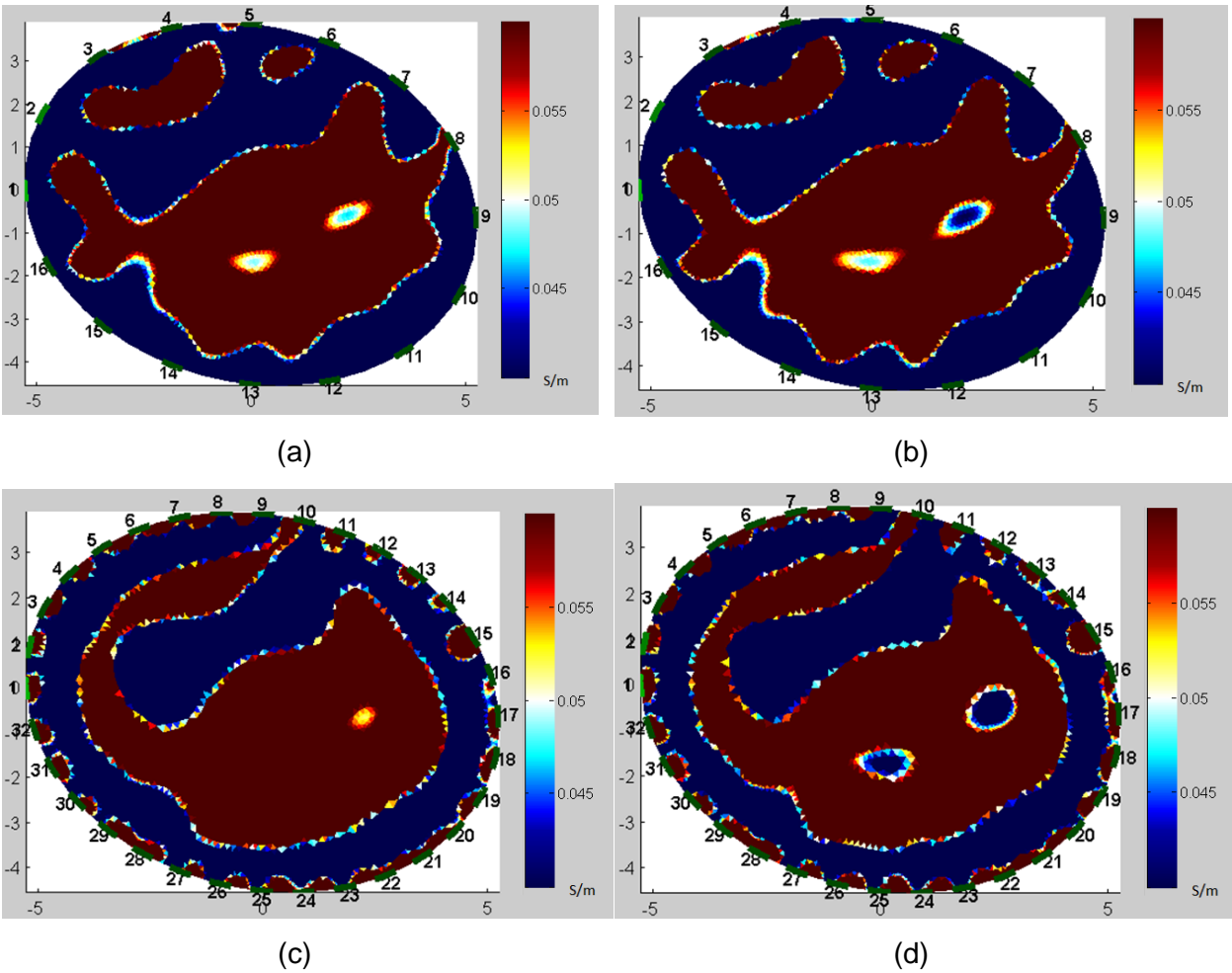


Figure 4-26. Human forearm EIT Image reconstruction using an image filter centered in -10 ± 1 ; (a) Injection current of 4mA using 16 electrodes, (b) Injection current of 5mA using 16 electrodes, (c) Injection current of 2mA using 32 electrodes, (d) Injection current of 5mA using 32 electrodes.

An alternative color scale is recommended to be evaluated in order to increment the contrast between different tissues conductivities in the reconstruction. For this purpose, a logarithmic scale for visualization may be useful.

4.19.4 Effect of a current value over the safety range

For medical applications, the human body current injection range should be limited. According to [1] the maximum current should not exceed 5mA. In this section, the setup for image reconstruction is set out of the safety range in order to explore the behavior of

the image reconstruction, keeping in mind that in a practical implementation the maximum range is 5mA, also nerve stimulation should be avoided and low currents should be used in final implementation.

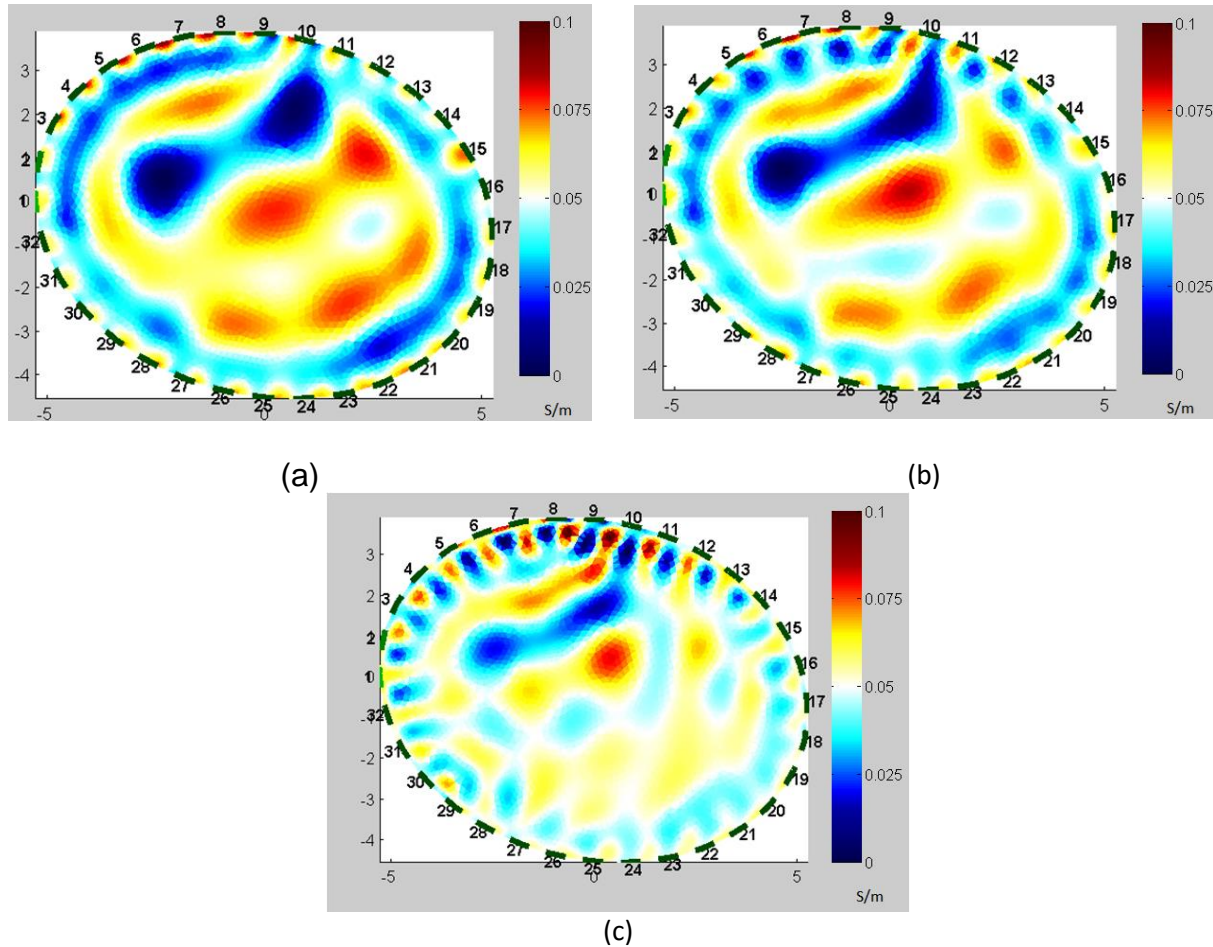


Figure 4-27. Human forearm EIT Image reconstruction using different currents; (a) Current of 3 mA, (b) Current of 10mA and (c) Current of 50mA

In Figure 4-27, the effect of using an injection current out of the safety range for human body is shown (greater than 5mA). When increasing the injection current in human forearm to 3mA, 10mA and 50mA parameters (images (a), (b) and (c), respectively), a poor impedance map is displayed. The results do not improve the reconstructed image spatial resolution in comparison with the images obtained using currents lower than 3mA. This may occur because the voltage level is increased and minor voltage changes are

not significant in measurement. Only the biggest areas with the same conductivities are shown in the reconstructed image.

4.20 Optimal setup for human forearm EIT image reconstruction

In this section, the best setup using 32 electrodes is presented, after evaluating different parameters for human forearm EIT image reconstruction across the development of this thesis. Table 4-1 lists the corresponding parameters or configuration for forearm image reconstruction.

Table 4-1. Best setup for human forearm EIT reconstruction image.

Description	Parameter or configuration
Maximum element mesh size in FEM	0.11
Reconstruction algorithm	Gauss-Newton
Prior information	Laplace
Hyperparameter	$9 \cdot 10^{-4}$
Current injection	2.5mA
Electrodes	32

Forearm tissues conductivities are plotted in Figure 4-28. This visual representation provides a clear idea about the magnitude differences between tissues conductivities. Filtering is applied to the reconstructed forearm images to differentiate the lower conductivities from the higher ones, in order to try to locate the nerves. The filter threshold is set in 0.05, as indicated with the green line; higher conductivities are colored in red and lower conductivities in blue using the same scale for the filtered reconstructed image.

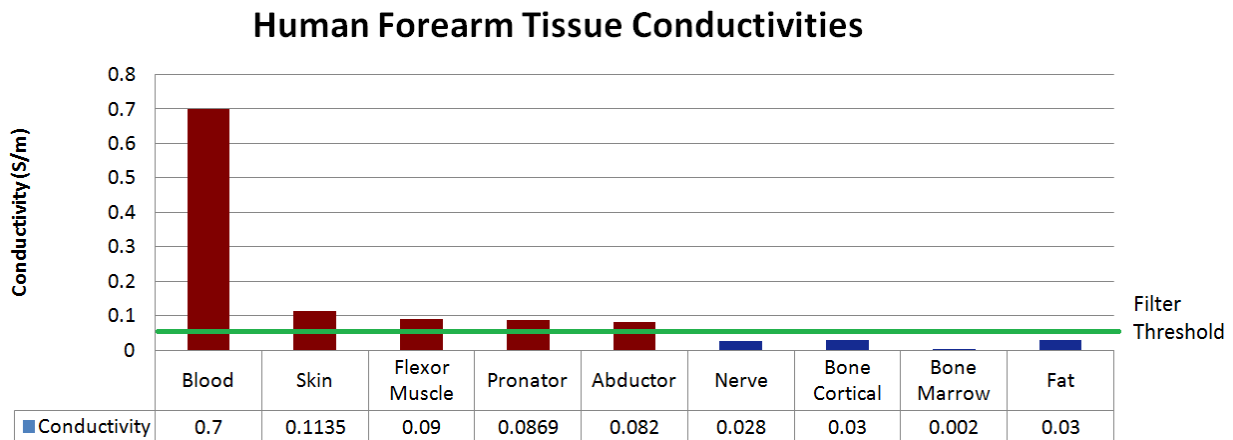


Figure 4-28. Tissue conductivity representation and filter threshold for filtering.

Images shown in Figure 4-29, Figure 4-30, Figure 4-31 and Figure 4-32 are the results after defining the image reconstruction environment with the parameters listed in Table 4-1, in order to obtain the best spatial resolution. The images identified with (a) are the reconstruction with a SNR of 30 dB and (b) are the images without noise.

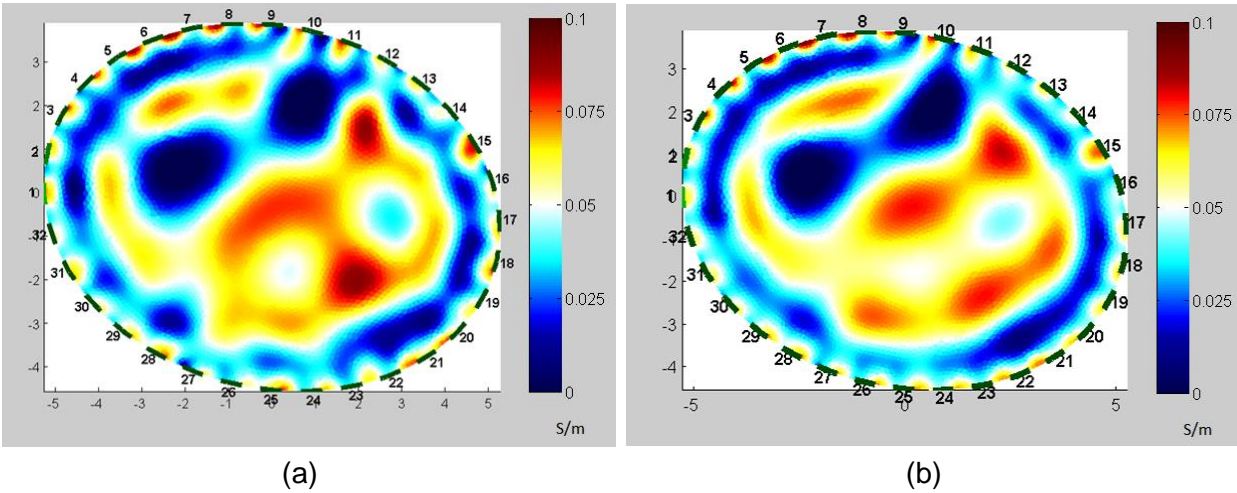


Figure 4-29. Human forearm EIT Image reconstruction; (a) 30 dB SNR, (b) without noise.

In Figure 4-30 the geometry is superimposed to evaluate the conductivity distribution in the reconstructed image and the components location. These reconstructions present a better definition in components boundaries; fat and bones are clearly identifiable.

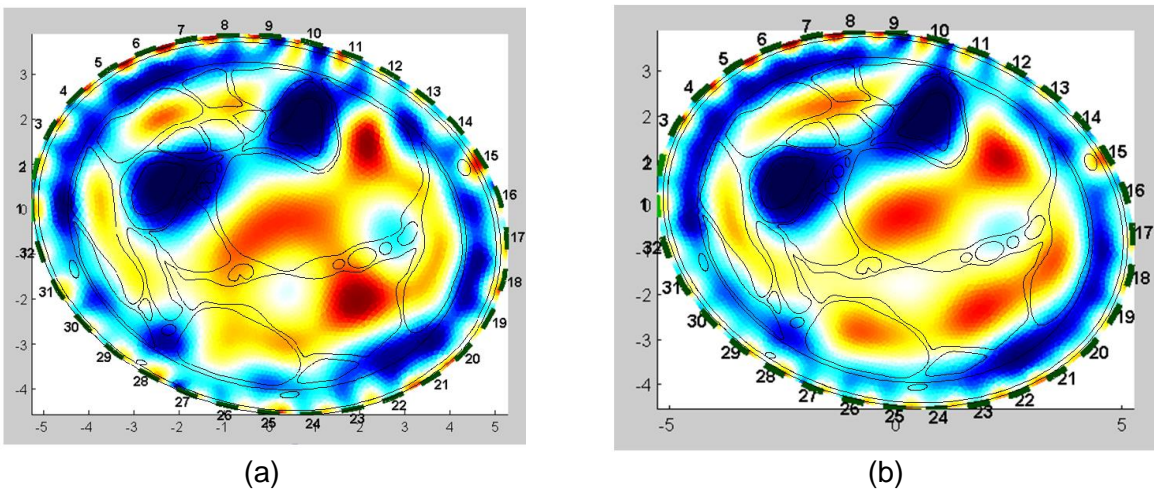


Figure 4-30. Human forearm EIT Image reconstruction with the geometry superimposed; (a) 30 dB SNR, (b) without noise.

Previous images are reconstructions with different conductivities but the main purpose of this research is to identify nerves for target application, for this reason a scale change is applied in order to filter high from low conductivities using as threshold a value of 0.05 S/m as depicted in Figure 4-28 by the green line.

Figure 4-31 shows the results after applying the filtering in the reconstructed image, two main colors are identified according to tissues conductivity, red color stands for tissues with higher conductive than the threshold and blue color for lower conductivities. A positive fact is that all the areas where muscles, veins and the skin with conductivities higher than 0.05 S/m are colored in red and fat, bones and nerves areas are colored in blue.

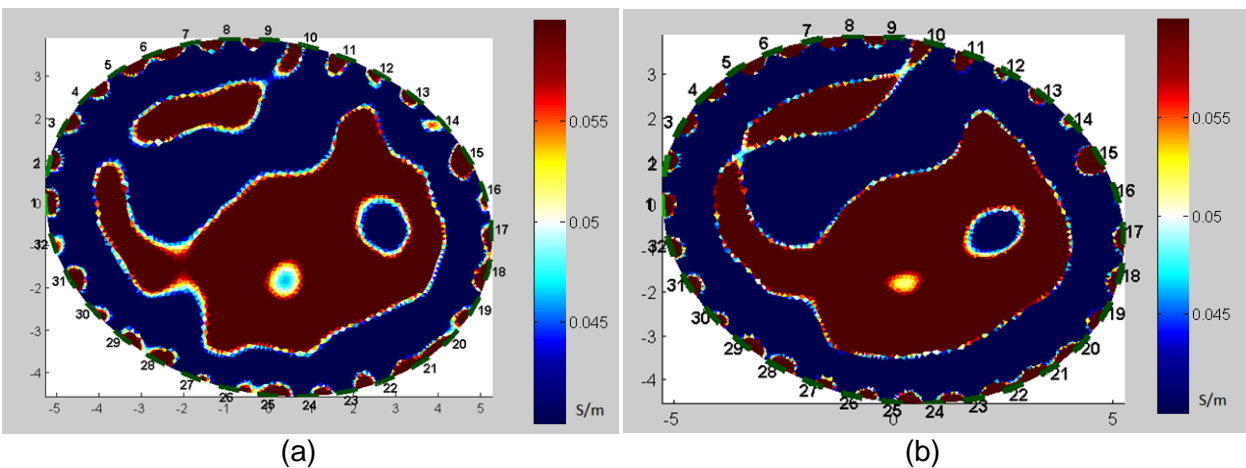


Figure 4-31. Human forearm EIT Image reconstruction with filtering; (a) 30 dB SNR, (b) without noise.

In order to evaluate the nerve position in the reconstructed image, Figure 4-32 shown a super imposed images in green color containing the four nerves location in white color.

Nerves are in the low conductivity zone and their conductivity is noted in the reconstructed image. However, its location is shifted respect to the reference geometry, this could be because of the influence of muscles and blood conductivity values, these mentioned tissues cover a big area around the nerves.

Using the super imposed image to evaluate the reconstructed image is notable that the reconstructed image keeps the shape of the biggest areas, the small areas with different conductivities are no reconstructed.

Analyzing these results about the reconstruction, its conclusive that the spatial resolution is not enough to identify the nerves location under the settings shown in Table 4-1, forearm muscles, fat and bones are very feasible to identify with EIT methodology. In Figure 4-32 the noise effect is also evident because in figure (b) the reconstructed shape in red is following the reference, however (a) shown more shape irregularities in the reconstructed image.

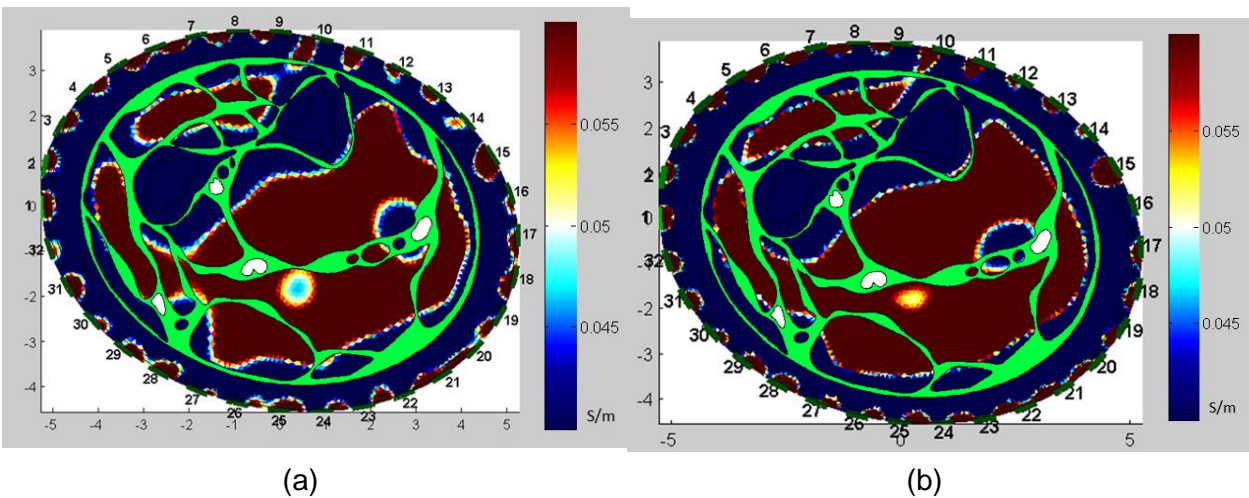


Figure 4-32. Human forearm EIT Image reconstruction with filtering and the geometry superimposed; (a) 30 dB SNR, (b) without noise.

4.20.1 Forearm geometry and reconstructed image area comparison

In order to evaluate the reconstructed image with the reference forearm geometry, the use of CAD tools is required as a follow due to the geometry complexity. Using the exported model from COMSOL and importing it in AutoCAD, dimensions and areas can be calculated with high accuracy as shown in Figure 4-33.

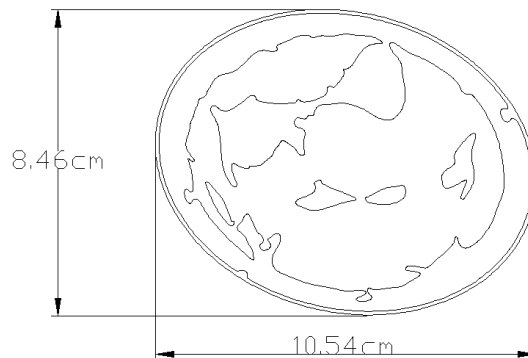


Figure 4-33. Forearm dimension image using the AutoCAD software.

The selected method to evaluate the forearm image reconstruction is comparing the reference forearm area for tissues with conductivities higher and lower than 0.05 S/m and the reconstructed image for the same range of conductivities. In Figure 4-34, (a) is the reference geometry but due to its complexity the figure (b) is created using AutoCAD, where the small areas between the muscles, veins and skin are not taken into consideration in order to simplify the error calculation.

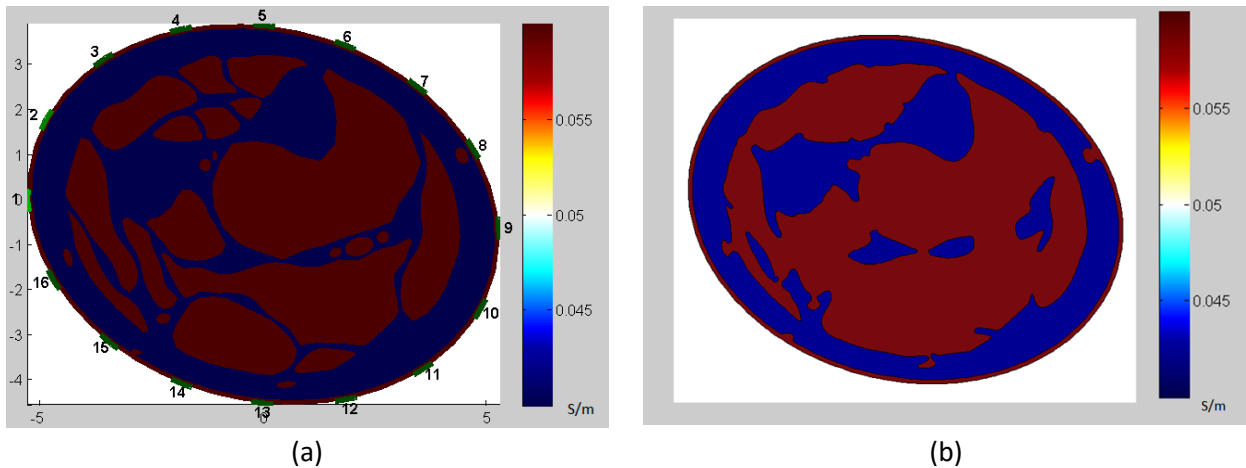


Figure 4-34. Human forearm geometry with tissues colored according to their conductivity (a) complex geometry, (b) simplified geometry.

Using the simplified forearm image as reference and comparing it with the reconstructed images after filtering high and low conductivities. The results are shown in Figure 4-35 (a) and (b) super-imposing the reconstructed the images colored in grey over the reference, where the first one is the reconstruction with 30dB SNR and the second one is without noise.

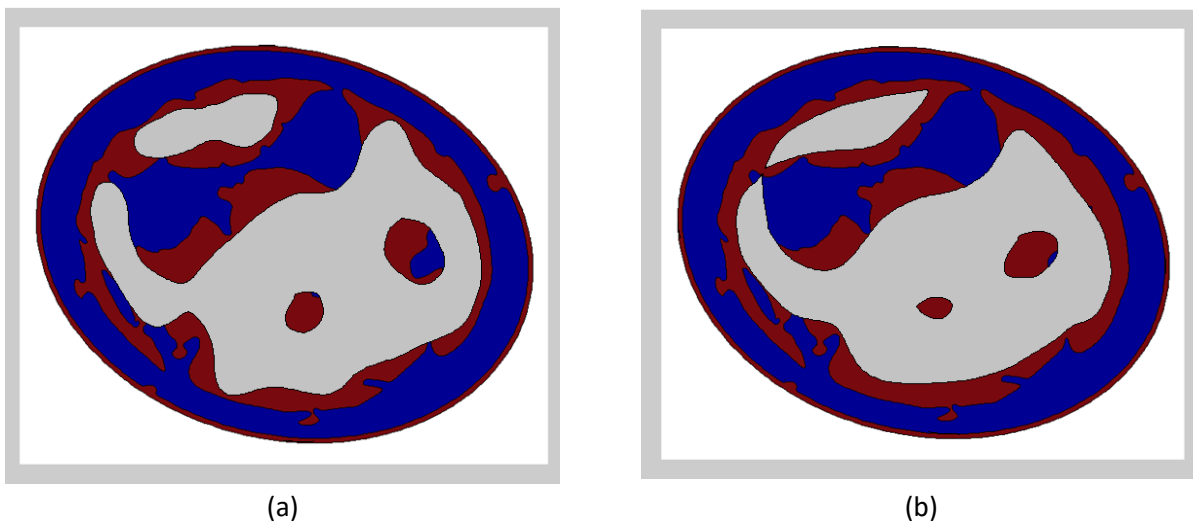


Figure 4-35. Human forearm simplified geometry with reconstructed image super imposed (a) with 30 dB SNR, (b) without noise.

4.20.2 Error calculation in reconstructed image

In order to calculate the error in the reconstructed image, the area for tissues with conductivities higher than 0.05 S/m is used as reference. Image shown in Figure 4-34 (a) is the target and in Figure 4-35 (a) with noise and (b) without noise are the images under evaluation.

Using the equation (4.1), the error in the human forearm reconstruction image using EIT is evaluated; the results of this evaluation are demonstrated in Table 4-2. The target image has an area with a conductivity higher than 0.05 S/m of 37.9431 cm^2 .

$$Error(\%) = \frac{(Target - reconstructed\ image) * 100}{Target} \quad (4.1)$$

Table 4-2. Comparison the area of reference geometry and reconstructed image for tissues conductivities higher than 0.05 S/m.

Image	High conductivity area (cm^2)	Error(%)
Reconstructed image without noise	25.8976	31.74
Reconstructed image with noise	26.9674	28.92

From Table 4-2, it can be extracted that the reconstructed human forearm image using EIT performs around a 30 % of error for tissues with a conductivity higher than 0.05 S/m from the reference forearm geometry, the difference from the image with noise versus the image without noise is 2.82% and it is not relevant due to the irregular shapes.

Chapter 5 Conclusions and recommendations

5.1 Conclusions

EIDORS was the only suitable open platform found available for this work, specialized on the EIT field. Its use is recommended for image reconstruction development since it offers a multi-platform open source tool. It also offers Licensing terms for commercial products and has an active community that is supporting and maintaining the code. Regarding its performance for image reconstruction, aspects as the reconstructed image complexity and the impedance difference between inner components should be taken into account in order to satisfy the expectations. Better results are obtained when the reconstructed image is made of simple shapes and the impedance contrast between components is higher.

For the purpose of this thesis, a complete human forearm EIT image reconstruction methodology was developed using the EIDORS with good results. To achieve this reconstruction, a complex human forearm geometry was imported using (x,y) coordinates and Fourier descriptors. The FEM model, tissues conductivities, hyperparameter, as well as the injection and measurement acquisition patterns were defined.

The image reconstruction of the human forearms is clear enough to recognize and identify the bones, muscles and blood. However, for practical setup scenarios, the spatial resolution seems to be not sufficient to identify finer structures such as nerves in the impedance map image. Therefore, the general objective of this thesis for determining the feasibility to develop a human forearm image reconstruction for nerve identification based on EIT technique was completed however the required resolution was not achievable based on the studies done using the EIDORS toolkit. EIDORS toolkit is oriented for diffuse images reconstruction and it is very useful for dynamics studies with impedance changes in time EIT can resolve the air changes in the distribution of lung volumes, for instance.

The main findings during the development of the processing methodology with EIDORS for the specific case of human forearm can be summarized as follows:

- Neighboring injection as acquisition method has a better performance than the opposite method.
- FEM forearm model shall use a maximum element mesh size lower than 0.11; otherwise, the image will not be reconstructed by EIDORS ending with a software crash.
- Using a maximum mesh size of 0.11, the FEM forearm model containing 122262 elements was generated in 108.327 seconds with a Sony Vaio computer with a Core i7 processor.
- The best image reconstruction obtained during this research for human forearm using the Gauss Newton reconstruction algorithm with Laplace prior information and the regularization hyperparameter of 9×10^{-4} with a current injection level of 2.5 mA in the 32 electrodes array is shown in Figure 4-32 with a 30% of error compared with reference geometry for conductivities higher than 0.05 S/m.
- 30dB of SNR is the lowest value acceptable in the voltage measurements in order to generate a clear and useful human forearm image reconstruction.

5.2 Recommendations

Due to the nature of EIT, image reconstruction methodology could face some limitations. The following recommendations could help to improve the results or increase the criteria for future work.

The research scope regarding EIT image reconstruction algorithms is limited to Gauss-Newton in EIDORS. Other algorithms should be evaluated and compared with the performance obtained. For this evaluation, other software may be used or developed to solve the inverse problem.

Additionally, trigonometric patterns for current injection and voltage acquisition should be evaluated. According to [35], good results have been obtained with these patterns. Also, it is recommended to evaluate the BestRes method for hyperparameter calculation. As shown in [36], BestRes method has a better performance than heuristic method.

In order to evaluate the estimated results during the development of the proposed methodology, it is recommended to setup a circuit to drive current through a human forearm and acquire the voltages to contrast it with the simulated values calculated in EIDORS toolkit. For experimental implementation, it should be considered that the data discretization may affect the results from the ones shown in this thesis, as well the image reconstruction performed using real electrodes because some source of errors may be added and their behavior must be analyzed. Most of the test cases evaluated in the developed methodology do not include the forearm shape variations or movement. The recommendation is to generate an image reconstruction with small changes in the forearm electrode position to simulate movement and analyze its effect.

Previous work in [37], where the forward problem is solved using the COMSOL Multiphysics platform, could be extended by benchmarking COMSOL results with the results obtained in this thesis based on EIDORS. This could help to improve the image reconstruction methodology for implementation without simulated values. This evaluation could help in fine tune parameters definition.

Bibliography

- [1] M. Vílchez, "Finite Element Method Simulation Study of Electrical Impedance Tomography (EIT) for the Human Forearm," pp. 1–6, 2015.
- [2] S. Bentolhoda Ayati, D. Bouazza-Maroufb, Kaddour Kerrc, and M. O'Tooled, "Performance evaluation if a digital electrical impedance tomography system," no. May, pp. 101–105, 2012.
- [3] "Electrical Impedance Tomography: The realization of regional ventilation monitoring." [Online]. Available: http://www.draeger.com/sites/assets/PublishingImages/Generic/UK/Booklets/rsp_eit_booklet_9066788_en.pdf. [Accessed: 26-Apr-2015].
- [4] J. Malmivuo and R. Plonsey, *Bioelectromagnetism - Principles and Applications of Bioelectric and Biomagnetic Fields*. 1995.
- [5] V. Sarode, P. M. Chimurkar, and A. N Cheeran, "Electrical Impedance Tomography using EIDORS in a Closed Phantom," *Int. J. Comput. Appl.*, vol. 48, no. 19, pp. 48–52, 2012.
- [6] R. H. Bayford, "Bioimpedance tomography (electrical impedance tomography).," *Annu. Rev. Biomed. Eng.*, vol. 8, pp. 63–91, 2006.
- [7] R. Harikumar, R. Prabu, and S. Raghavan, "Electrical Impedance Tomography (EIT) and Its Medical Applications : A Review," *Int. J. Soft Comput. Eng.*, vol. 3, no. 4, pp. 193–198, 2013.
- [8] F. Braun, "Systolic Time Intervals Measured by Electrical Impedance Tomography (EIT)," p. 96, 2013.
- [9] C. Gómez-Laberge and A. Adler, "Direct EIT Jacobian calculations for conductivity change and electrode movement.," *Physiol. Meas.*, vol. 29, no. 6, pp. S89–99, 2008.
- [10] K. H. Lim, J.-H. Lee, G. Ye, and Q. H. Liu, "An efficient forward solver in electrical impedance tomography by spectral element method.," *IEEE Trans. Med. Imaging*, vol. 25, no. 8, pp. 1044–51, Aug. 2006.
- [11] "Electrical impedance tomography - Wikiversity." [Online]. Available: https://en.wikiversity.org/wiki/Electrical_impedance_tomography. [Accessed: 29-Nov-2015].
- [12] E. G. Lucas, "USE OF AN ELECTRICAL IMPEDANCE TOMOGRAPHY METHOD TO DETECT AND TRACK FRACTURES IN A GELATIN MEDIUM," 2014.
- [13] S. I. Kabanikhin, "Definitions and examples of inverse and ill-posed problems," *J. Inverse Ill-Posed Probl.*, vol. 16, no. 4, pp. 317–357, 2008.
- [14] O. de Weck and I. Y. Kim, "Finite Element Method," *Eng. Des. Rapid Prototyp.*, vol. 810, 2004.
- [15] Carlos A. Felippa, "FEM Modeling: Introduction," *Introd. to FINITE Elem. METHODS*, pp. 1–15, 2004.
- [16] Y. Yoo, "Tutorial on Fourier Theory," *Retrieved June*, no. March, pp. 1–18, 2001.
- [17] B. S. Morse, "Lecture 7 : Shape Description (Contours)," *Small*, pp. 1998–2000, 2000.
- [18] P. C. Nan, "an Implementation of the Back-Projection Algorithm According To Santosa and Vogelius," *Symp. A Q. J. Mod. Foreign Lit.*, vol. 1, no. 2, pp. 1–6, 2006.
- [19] B. Soediono, "Electrical Impedance Tomography: The realisation of regional

- ventilation monitoring,” *J. Chem. Inf. Model.*, vol. 53, p. 160, 1989.
- [20] V. Sarode, S. Patkar, and A. N. Cheeran, “Comparison of 2-D Algorithms in EIT based Image Reconstruction,” *Int. J. Comput. Appl.*, vol. 69, no. 8, pp. 6–11, 2013.
- [21] M. Cheney, D. Isaacson, and J. Newell, “Electrical impedance tomography,” *SIAM Rev.*, vol. 41, no. 1, pp. 85–101, 1999.
- [22] M. Vauhkonen, D. Vadász, P. A. Karjalainen, E. Somersalo, and J. P. Kaipio, “Tikhonov regularization and prior information in electrical impedance tomography,” *IEEE Trans. Med. Imaging*, vol. 17, no. 2, pp. 285–93, 1998.
- [23] M. Cheney, D. Isaacson, J. C. Newell, S. Simske, and J. Goble, “NOSER: An Algorithm for Solving the Inverse Conductivity Problem,” *International Journal of Imaging Systems and Technology*, vol. 2, no. 2, pp. 66–75, 1990.
- [24] M. L. Fall and P. Set, “Slides: CS195-5: Introduction to Machine Learning,” *Mach. Learn.*, pp. 1–8, 2006.
- [25] A. Rochford, “Prior Distributions for Bayesian Regression Using PyMC.” [Online]. Available: <http://austinrochford.com/posts/2013-09-02-prior-distributions-for-bayesian-regression-using-pymc.html>. [Accessed: 14-Dec-2015].
- [26] T. F. Chan and S. Esedoglu, “TVL1 Models for Imaging: Global Optimization & Geometric Properties Part I,” *Optimization*, pp. 1–34.
- [27] “Underfitting vs. Overfitting — scikit-learn 0.17 documentation.” [Online]. Available: http://scikit-learn.org/stable/auto_examples/model_selection/plot_underfitting_overfitting.html. [Accessed: 14-Dec-2015].
- [28] F. Dieterle, “2.8.1. Overfitting, Underfitting and Model Complexity (Dr. Frank Dieterle).” [Online]. Available: http://www.frank-dieterle.de/phd/2_8_1.html. [Accessed: 14-Dec-2015].
- [29] “Forearm Anatomy, Definition & Definition | Body Maps.” [Online]. Available: <http://www.healthline.com/human-body-maps/forearm>. [Accessed: 30-Nov-2015].
- [30] A. Adler and W. R. B. Lionheart, “Uses and abuses of EIDORS: an extensible software base for EIT,” *Physiol. Meas.*, vol. 27, no. 5, pp. S25–S42, 2006.
- [31] T. Eidors, “Collaborative open scientific software: The EIDORS experience.”
- [32] N. P. and W. R. B. Lionheart, “A Matlab toolkit for three-dimensional electrical impedance tomography: a contribution to the Electrical Impedance and Diffuse Optical Reconstruction Software,” *Proj. Meas. Sci. Technol.* 13(12)1871-1883, 2002.
- [33] “NETGEN - automatic mesh generator.” [Online]. Available: <http://www.hpfem.jku.at/netgen/>. [Accessed: 09-Jan-2016].
- [34] W. R. B. Lionheart, “Developments in EIT Reconstruction Algorithms.”
- [35] A. Adler, P. O. Gaggero, and Y. Maimaitijiang, “Adjacent stimulation and measurement patterns considered harmful,” *Physiol. Meas.*, vol. 32, no. 7, pp. 731–744, 2011.
- [36] B. M. Graham and A. Adler, “Objective selection of hyperparameter for EIT,” *Physiol. Meas.*, vol. 27, no. 5, pp. S65–79, 2006.
- [37] M. E. Vilchez, “Finite Element Method Simulation Study of Electrical Impedance Tomography (EIT) for the Human Forearm,” pp. 1–6, 2015.

Glossary


Benchmark	It is usually associated with assessing performance characteristics.
Homogeneous	In EIT when outer geometry is defined without any conductivity.
Hyperparameter	Parameter of a prior distribution; the term is used to distinguish them from parameters of the model.
Ill-Posed Problem	A problem which may have more than one solution, or in which the solutions depend discontinuously upon the initial data.
Well-Posed Problem	A problem with a unique solution.
Inhomogeneous	Something that is not homogeneous or uniform, in EIT is when voltages are defined with inner conductivities.
Normalized	To bring some value back to a usual or expected state or condition.
Over-fitting	Occurs when a model is excessively complex, such as having too many parameters relative to the number of observations.
Regularization	Refers to a process of introducing additional information in order to solve an ill-posed problem or to prevent over-fitting
Tomography	Technique for displaying a representation of a cross section through a human body.
Under-fitting	When a model is not sufficient to fit.
Well-Posed Problem	A problem that has a unique solution which depends continuously on the initial data.

Appendix A EIDORS Quick Start Guide

A.1 Installing EIDORS

- 1) Make sure MATLAB or Octave is already installed. EIDORS is a toolkit linked to MATLAB.
- 2) Install Microsoft Windows SDK 7.1, requires .NET Framework 4.0
Download the SDK from:
<http://www.mathworks.com/support/compilers/R2015a/index.html>
- 3) Once the SDK 7.1 is installed, run the following command:
`mex -setup`
- 4) Download and install EIDORS and NetGen
 - a) Download EIDORS 3.8 from:
<http://prdownloads.sf.net/eidors3d/eidors-v3.8.zip>
 - b) Unzip the software in a directory such as /path/to/eidors(UNIX) or C:\path\to\eidors(Windows) (installation instructions for model_library are included in a README file).
 - c) Download NetGen 5.3 from:
<http://prdownloads.sf.net/eidors3d/eidors-v3.8-ng.zip>
- 5) Start MATLAB.
- 6) Once EIDORS is already installed, run the following command in a MATLAB(or Octave) session. The command should be executed each time to use EIDORS toolkit. If EIDORS is installed correctly, the output should be like the one shown in Figure A-1.

run C:\Eidors\eidors-v3.8\startup



```
Command Window
>> run C:\Eidors\eidors-v3.8\startup
EIDORS:[tested function eidors_var_id: OK]
EIDORS:[Setting Default Colours]
EIDORS:[Installed EIDORS (Ver: 3.8)]
EIDORS:[Parameter: cache_size=1024 MB]
EIDORS:[Parameter: mapped_colour=127]
EIDORS:[Default background colour: white]
EIDORS:[EIDORS mex folder: C:/Eidors/eidors-v3.8/arch/matlab]
EIDORS:[EIDORS cache folder: C:/Eidors/eidors-v3.8/models/cache (must be writable)]
EIDORS:[EIDORS model cache: C:/Eidors/eidors-v3.8/models/cache]
EIDORS:[New to EIDORS? Have a look at the Tutorials.]
>> |
```

Figure A-1. EIDORS output when startup script is executed.

A.2 EIDORS simulation guide

In this section, a simulation guide is presented to execute the human forearm EIT image reconstruction using EIDORS toolkit. In order to use EIDORS, it is necessary to launch MATLAB application and run the startup script.

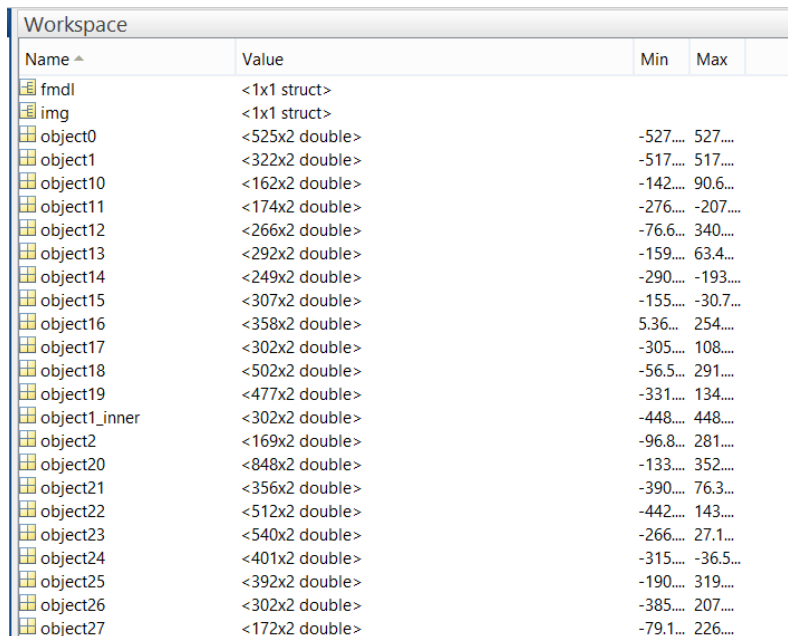
The source code shown in Appendix B contains the necessary setup defined in EIDORS to perform the human forearm EIT image reconstruction. A brief explanation of most important source code parts is detailed as follow:

A.2.1 Geometry definition

The forearm geometry is defined by a group of objects, which are defined by a set of (x,y) coordinates. The (x,y) coordinates should be saved as variables in the workspace, then workspace is saved as .mat file with objects definition. File with variables information is loaded in Matlab workspace using the following function:

```
load C:\Users\David\Forearm.mat;
```

Workspace with variables loaded successfully is shown in Figure A-2, matrix size is displayed as well the minimum and maximum values contained.



Name ^	Value	Min	Max
fmdl	<1x1 struct>		
img	<1x1 struct>		
object0	<525x2 double>	-527...	527...
object1	<322x2 double>	-517...	517...
object10	<162x2 double>	-142...	90.6...
object11	<174x2 double>	-276...	-207...
object12	<266x2 double>	-76.6...	340...
object13	<292x2 double>	-159...	63.4...
object14	<249x2 double>	-290...	-193...
object15	<307x2 double>	-155...	-30.7...
object16	<358x2 double>	5.36...	254...
object17	<302x2 double>	-305...	108...
object18	<502x2 double>	-56.5...	291...
object19	<477x2 double>	-331...	134...
object1_inner	<302x2 double>	-448...	448...
object2	<169x2 double>	-96.8...	281...
object20	<848x2 double>	-133...	352...
object21	<356x2 double>	-390...	76.3...
object22	<512x2 double>	-442...	143...
object23	<540x2 double>	-266...	27.1...
object24	<401x2 double>	-315...	-36.5...
object25	<392x2 double>	-190...	319...
object26	<302x2 double>	-385...	207...
object27	<172x2 double>	-79.1...	226...

Figure A-2. EIDORS workspace.

A.2.2 Model creation

Model creation use the (x,y) coordinates saved in the workspace and Fourier descriptors sample number for each object. Maximum element size for the mesh, number of electrodes and size are also defined in this function to create the FEM.

```
% Create FEM
fmd1 = ng_mk_extruded_model({0,{object0/100, object1/100, object2/100,object3/100,
object4/100,object5/100,object6/100, object7/100, object8/100, object9/100, object10/100,object11/100,
object12/100,object13/100, object14/100, object15/100, object18/100, object19/100 ,object16/100 ,object17/100
, object20/100,object21/100 ,object22/100 ,object23/100 ,object24/100 ,object25/100 , object26/100, object27/100
,object28/100 ,object29/100 , object30/100,object31/100 ,object32/100 ,object33/100 ,object34/100} , {[4,47] ,
[4,47],[4,20],[4,20], [4,20],[4,20],[4,20],[4,20], [4,20],[4,20],[4,20], [4,20],[4,20],[4,20],[4,20],
[4,20],[4,30],[4,30] ,[4,30],[4,30],[4,30], [4,25],[4,30],[4,25],[4,25], [4,25],[4,25], [4,25],[4,25],[4,25],
[4,25],[4,25],[4,25],[4,25], [4,70] } , 0.11} ,[32,1,0],[0.5, [0.15, 0, 0]]);
img = mk_image(fmd1,0.1135);
show_fem(img,[1,1]);
```

FEM created at this point is observed in Figure A-3, where all the objects are configured with the same conductivity.

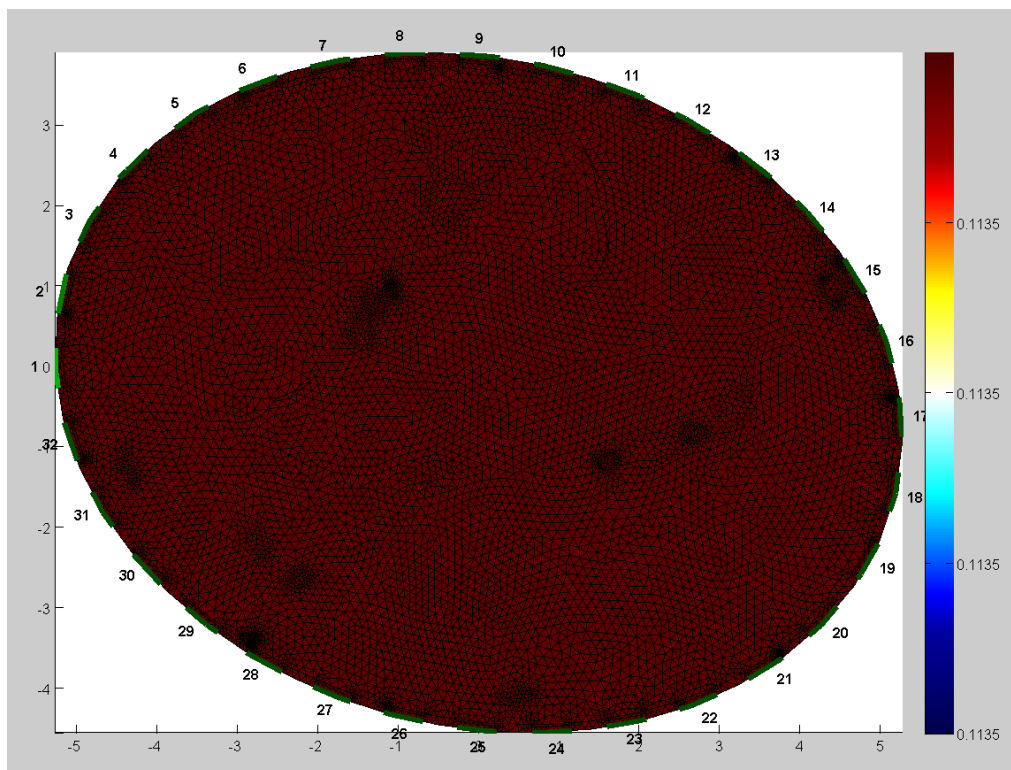


Figure A-3. FEM with homogeneous conductivities.

A.2.3 Stimulus definition

Current injection and acquisition voltage pattern, electrodes quantity and current amplitude is defined in the stimulus function as follow.

```
% Create Stimulation Patterns
[stim,mse1] = mk_stim_patterns(32 , 1 , '{ad}','{ad}',{ } ,2.5);
% [stim, meas_sel]=mk_stim_patterns(n_elec, n_rings, inj, meas, options, amplitude(mA))

fmdl.stimulation = stim;
fmdl.meas_select = mse1;
```

A.2.4 Forward solver used to calculate V_h and V_i

In order to simulate the homogenous voltage, it is necessary to execute the forward solver with homogenous conductivities.

```
%homogeneous voltage
vh = fwd_solve(img);
```

Then objects conductivities should be defined, setting the conductivity value in each object matrix.

```
%Object conductivity definition
img.elem_data(fmdl.mat_idx{2} ) = 0.03;
img.elem_data(fmdl.mat_idx{3} ) = 0.7;
img.elem_data(fmdl.mat_idx{4} ) = 0.7;
img.elem_data(fmdl.mat_idx{5} ) = 0.7;
img.elem_data(fmdl.mat_idx{6} ) = 0.7;
img.elem_data(fmdl.mat_idx{7} ) = 0.7;
img.elem_data(fmdl.mat_idx{8} ) = 0.7;
img.elem_data(fmdl.mat_idx{9} ) = 0.7;
img.elem_data(fmdl.mat_idx{10} ) = 0.7;
img.elem_data(fmdl.mat_idx{11} ) = 0.7;
img.elem_data(fmdl.mat_idx{12} ) = 0.7;
img.elem_data(fmdl.mat_idx{13} ) = 0.028;
img.elem_data(fmdl.mat_idx{14} ) = 0.028;
img.elem_data(fmdl.mat_idx{15} ) = 0.028;
img.elem_data(fmdl.mat_idx{16} ) = 0.028;
img.elem_data(fmdl.mat_idx{17} ) = 0.03;
img.elem_data(fmdl.mat_idx{18} ) = 0.03;
img.elem_data(fmdl.mat_idx{19} ) = 0.002;
img.elem_data(fmdl.mat_idx{20} ) = 0.002;
img.elem_data(fmdl.mat_idx{21} ) = 0.09;
img.elem_data(fmdl.mat_idx{22} ) = 0.09;
img.elem_data(fmdl.mat_idx{23} ) = 0.09;
img.elem_data(fmdl.mat_idx{24} ) = 0.09;
img.elem_data(fmdl.mat_idx{25} ) = 0.0869;
img.elem_data(fmdl.mat_idx{26} ) = 0.09;
img.elem_data(fmdl.mat_idx{27} ) = 0.09;
img.elem_data(fmdl.mat_idx{28} ) = 0.09;
img.elem_data(fmdl.mat_idx{29} ) = 0.09;
img.elem_data(fmdl.mat_idx{30} ) = 0.082;
img.elem_data(fmdl.mat_idx{31} ) = 0.09;
img.elem_data(fmdl.mat_idx{32} ) = 0.09;
img.elem_data(fmdl.mat_idx{33} ) = 0.09;
img.elem_data(fmdl.mat_idx{34} ) = 0.09;
img.elem_data(fmdl.mat_idx{35} ) = 0.09;
```


FEM model with conductivity defined is in each object as shown in Figure A-4. With the corresponding conductivities, it is necessary to execute the forward solver again, in order to calculate the inhomogeneous voltages required in the inverse solver.

```
show_fem(img,[1,1]);
%inhomogeneous voltage
vi = fwd_solve(img);
```

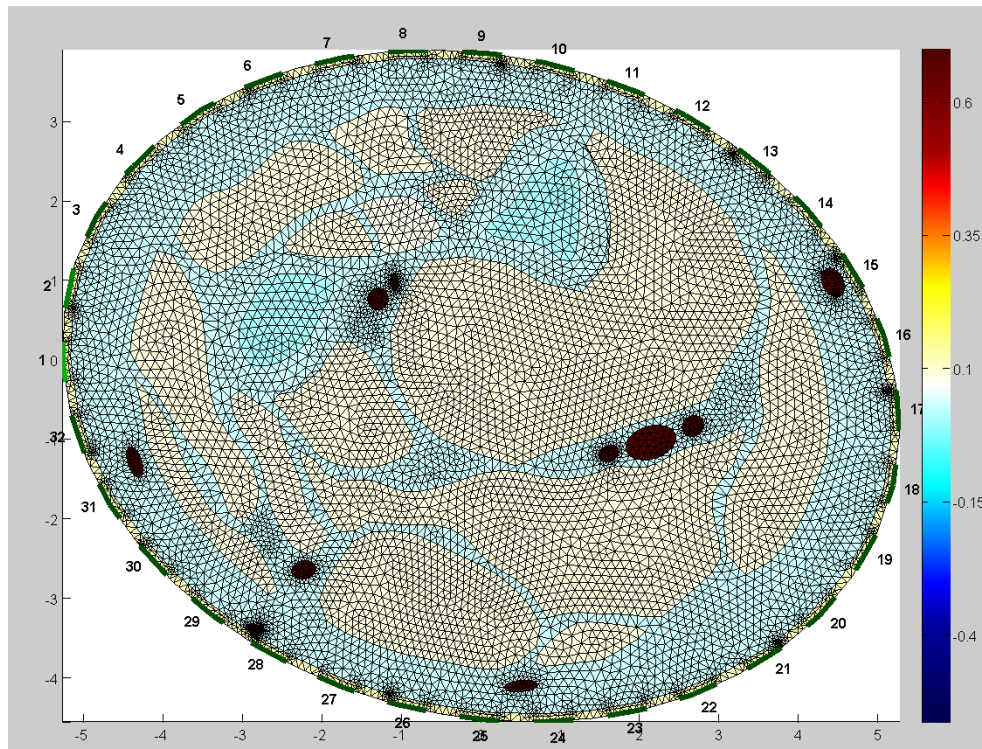


Figure A-4. FEM with inhomogeneous conductivities.

A.2.5 Noise addition

Using the inhomogeneous voltages values obtained previously, Gaussian noise is added with a random function.

```
% Add 30dB SNR
vi_n= vi;
namp1 = 0;
namp1= std(vi.meas - vh.meas)*10^(-30/20);
vi_n.meas = vi.meas + namp1 *randn(size(vi.meas));
```

A.2.6 Inverse solver configuration

Inverse solver requires the corresponding setup in order to solve the image reconstruction, prior information and hyperparameter is defined as follow.

```
inv2d= eidors_obj('inv_model', 'EIT inverse');           % Create Inverse Model
inv2d.reconst_type= 'difference';
inv2d.jacobian_bkgnd.value= 1;

imb= mk_common_model('b2c',16);
imb.fwd_model =img.fwd_model;
inv2d.fwd_model= imb.fwd_model;
inv2d.fwd_model.np_fwd_solve.perm_sym= '{y}';

inv2d.solve=      @inv_solve_diff_GN_one_step;         % Gauss-Newton solvers

inv2d.hyperparameter.value = 9e-4;                   % Laplace image prior
inv2d.RtR_prior=  @prior_laplace;

inv2d = inv_solve( inv2d, vh, vi);                   %inverse Solver
```

A.2.7 Conductivity distribution map

Reconstructed image with the conductivity distribution is displayed with the show_FEM function. Additionally, a filter could be configured in order to display the relevant information. In Figure A-5 the reconstructed images without and with filtering are reflected (a) and (b) respectively.

```
inv2d.calc_colours.ref_level = -8; % Applying the filter centered in -8
inv2d.calc_colours.clim = 1;

hh =show_fem(inv2d,[1,1]);
set(hh,'EdgeColor',[1,1,1]);
set(hh,'EdgeColor','none');
```

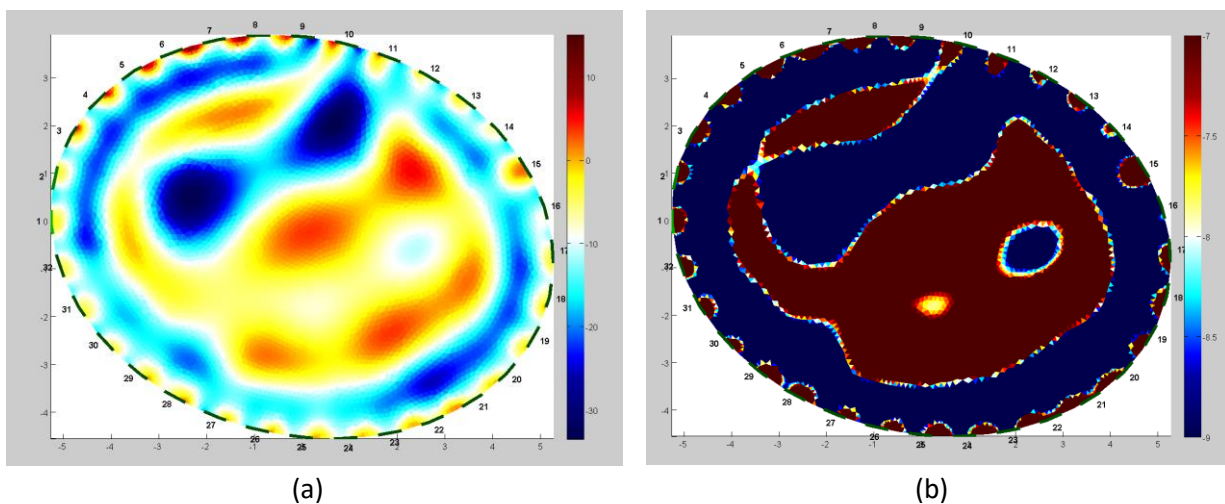


Figure A-5. Forearm reconstructed image (a) without filter and (b) with filter.

Appendix B EIDORS source code

In this section is the source code used to generate the FEM model, current injection stimulus, components conductivity definition and inverse solver parameters definition. The workspace variables definition are set in the file called Forearm.m which contains the x,y coordinates for each inner forearm component.

```
load C:\Users\David\Forearm.mat;

object0      = flipud(object0(1:1:end,:));
object1      = object1(1:1:end,:);
object2      = flipud(object2(1:1:end,:));
object3      = flipud(object3(1:1:end,:));
object4      = flipud(object4(1:1:end,:));
object5      = object5(1:1:end,:);
object6      = flipud(object6(1:1:end,:));
object7      = flipud(object7(1:1:end,:));
object8      = object8(1:1:end,:);
object9      = object9(1:1:end,:);
object10     = object10(1:1:end,:);
object11     = object11(1:1:end,:);
object12     = object12(1:1:end,:);
object13     = object13(1:1:end,:);
object14     = object14(1:1:end,:);
object15     = object15(1:1:end,:);
object16     = flipud(object16(1:2:end,:));
object17     = flipud(object17(1:2:end,:));
object18     = object18(1:1:end,:);
object19     = object19(1:1:end,:);
object20     = object20(1:2:end,:);
object21     = object21(1:2:end,:);
object22     = object22(1:2:end,:);
object23     = object23(1:2:end,:);
object24     = object24(1:2:end,:);
object25     = object25(1:2:end,:);
object26     = object26(1:2:end,:);
object27     = object27(1:2:end,:);
object28     = object28(1:2:end,:);
object29     = object29(1:2:end,:);
object30     = object30(1:2:end,:);
object31     = object31(1:2:end,:);
object32     = object32(1:2:end,:);
object33     = object33(1:2:end,:);
object34     = object34(1:2:end,:);

% Create FEM

fmd1 = ng_mk_extruded_model({0,{object0/100, object1/100, object2/100,object3/100,
object4/100,object5/100,object6/100, object7/100, object8/100, object9/100, object10/100,object11/100,
object12/100,object13/100, object14/100, object15/100, object18/100, object19/100 ,object16/100 ,object17/100
, object20/100,object21/100 ,object22/100 ,object23/100 ,object24/100 ,object25/100 , object26/100, object27/100
,object28/100 ,object29/100 , object30/100,object31/100 ,object32/100 ,object33/100 ,object34/100} , {[4,47]
,[4,47],[4,20],[4,20], [4,20],[4,20],[4,20],[4,20], [4,20],[4,20],[4,20], [4,20],[4,20],[4,20],[4,20] ,
[4,20],[4,30],[4,30] ,[4,30],[4,30],[4,30], [4,25],[4,30],[4,25],[4,25], [4,25],[4,25], [4,25],[4,25],[4,25],
[4,25],[4,25],[4,25],[4,25], [4,70] } , 0.11} , [32,1,0],[0.5, [0.15, 0, 0]]);

% Create Stimulation Patterns
[stim,mse1] = mk_stim_patterns(32 , 1 , '{ad}','{ad}',{ } , 2.5);
% [stim, meas_sel]=mk_stim_patterns(n_elec, n_rings, inj, meas, options, amplitude(mA))

fmd1.stimulation = stim;
fmd1.meas_select = mse1;

img = mk_image(fmd1,0.1135);
show_fem(img,[1,1]);

%homogeneous voltage
vh = fwd_solve(img);
```

```

img.elem_data(fmdl.mat_idx{2}) = 0.03;
img.elem_data(fmdl.mat_idx{3}) = 0.7;
img.elem_data(fmdl.mat_idx{4}) = 0.7;
img.elem_data(fmdl.mat_idx{5}) = 0.7;
img.elem_data(fmdl.mat_idx{6}) = 0.7;
img.elem_data(fmdl.mat_idx{7}) = 0.7;
img.elem_data(fmdl.mat_idx{8}) = 0.7;
img.elem_data(fmdl.mat_idx{9}) = 0.7;
img.elem_data(fmdl.mat_idx{10}) = 0.7;
img.elem_data(fmdl.mat_idx{11}) = 0.7;
img.elem_data(fmdl.mat_idx{12}) = 0.7;
img.elem_data(fmdl.mat_idx{13}) = 0.028;
img.elem_data(fmdl.mat_idx{14}) = 0.028;
img.elem_data(fmdl.mat_idx{15}) = 0.028;
img.elem_data(fmdl.mat_idx{16}) = 0.028;
img.elem_data(fmdl.mat_idx{17}) = 0.03;
img.elem_data(fmdl.mat_idx{18}) = 0.03;
img.elem_data(fmdl.mat_idx{19}) = 0.002;
img.elem_data(fmdl.mat_idx{20}) = 0.002;
img.elem_data(fmdl.mat_idx{21}) = 0.09;
img.elem_data(fmdl.mat_idx{22}) = 0.09;
img.elem_data(fmdl.mat_idx{23}) = 0.09;
img.elem_data(fmdl.mat_idx{24}) = 0.09;
img.elem_data(fmdl.mat_idx{25}) = 0.0869;
img.elem_data(fmdl.mat_idx{26}) = 0.09;
img.elem_data(fmdl.mat_idx{27}) = 0.09;
img.elem_data(fmdl.mat_idx{28}) = 0.09;
img.elem_data(fmdl.mat_idx{29}) = 0.09;
img.elem_data(fmdl.mat_idx{30}) = 0.082;
img.elem_data(fmdl.mat_idx{31}) = 0.09;
img.elem_data(fmdl.mat_idx{32}) = 0.09;
img.elem_data(fmdl.mat_idx{33}) = 0.09;
img.elem_data(fmdl.mat_idx{34}) = 0.09;
img.elem_data(fmdl.mat_idx{35}) = 0.09;

show_fem(img,[1,1]);

%inhomogeneous voltage
vi = fwd_solve(img);

% Add 30dB SNR
vi_n= vi;
namp1 = 0;
namp1= std(vi.meas - vh.meas)*10^(-30/20);
vi_n.meas = vi.meas + namp1 *randn(size(vi.meas));

fmdl= img;

% Create Inverse Model
inv2d= eidors_obj('inv_model', 'EIT inverse');
inv2d.reconst_type= 'difference';
inv2d.jacobian_bkgnd.value= 1;

% This is not an inverse crime; inv_md1 != fwd_md1
imb= mk_common_model('b2c',16);
imb.fwd_model =img.fwd_model;
inv2d.fwd_model= imb.fwd_model;
inv2d.fwd_model.np_fwd_solve.perm_sym= '{y}';

%Guass-Newton solvers
inv2d.solve= @inv_solve_diff_GN_one_step;

% Laplace image prior
inv2d.hyperparameter.value = 9e-4;
inv2d.RtR_prior= @prior_laplace;

inv2d = inv_solve( inv2d, vh, vi);
%inv2d = inv_solve( inv2d, vh, vi_n);

inv2d.calc_colours.ref_level = -8; % centered in -8
inv2d.calc_colours.clim = 1;

hh =show_fem(inv2d,[1,1]);

set(hh,'EdgeColor',[1,1,1]);
set(hh,'EdgeColor','none');

```